REPORT DOCUMENTATION PAGE

Form Approved
OMB No. 0704-0188

1. AGENCY USE ONLY *(Leave blank)*	2. REPORT DATE	3. REPORT TYPE AND DATES COVERED
	14.Jul.03	DISSERTATION

4. TITLE AND SUBTITLE
THE PRODUCTION AND FATE OF ANIONS FROM LOW ELECTRON AFFINITY MOLECULES IN THE GAS PHASE

5. FUNDING NUMBERS

6. AUTHOR(S)
MAJ SALYARDS MICHAEL J

7. PERFORMING ORGANIZATION NAME(S) AND ADDRESS(ES)
MONTANA STATE UNIVERSITY

8. PERFORMING ORGANIZATION REPORT NUMBER
CI02-992

9. SPONSORING/MONITORING AGENCY NAME(S) AND ADDRESS(ES)
THE DEPARTMENT OF THE AIR FORCE
AFIT/CIA, BLDG 125
2950 P STREET
WPAFB OH 45433

10. SPONSORING/MONITORING AGENCY REPORT NUMBER

11. SUPPLEMENTARY NOTES

12a. DISTRIBUTION AVAILABILITY STATEMENT
Unlimited distribution
In Accordance With AFI 35-205/AFIT Sup 1

DISTRIBUTION STATEMENT A
Approved for Public Release
Distribution Unlimited

12b. DISTRIBUTION CODE

13. ABSTRACT *(Maximum 200 words)*

20030731 071

14. SUBJECT TERMS

15. NUMBER OF PAGES
121

16. PRICE CODE

17. SECURITY CLASSIFICATION OF REPORT	18. SECURITY CLASSIFICATION OF THIS PAGE	19. SECURITY CLASSIFICATION OF ABSTRACT	20. LIMITATION OF ABSTRACT

THE VIEWS EXPRESSED IN THIS ARTICLE ARE THOSE OF THE AUTHOR AND DO NOT REFLECT THE OFFICIAL POLICY OR POSITION OF THE UNITED STATES AIR FORCE, DEPARTMENT OF DEFENSE, OR THE U.S. GOVERNMENT

ABSTRACT

Resonance electron capture and thermal electron detachment rate constants have been determined for several low electron affinity (EA) compounds, including anthracene, benzophenone, quinoxaline. These measurements were taken by comparing the molecule of interest with SF_6 using pulsed high pressure mass spectrometry (PHPMS) to evaluate the time profiles for the relevant anions. These measurements were affected by re-capture of detached electrons as well as loss of these electrons by diffusion to the walls of the ion source. This dissertation also explains why these low EA molecules are not seen at atmospheric conditions. Using the PHPMS, the reactions of the molecular anions of anthracene, quinazoline, benzophenone, quinoxaline and azulene with oxygen and water have been studied. In the simultaneous presence of oxygen and water, these molecular anions, M^-, are rapidly destroyed and the ion, $(O_2 \bullet H_2O)^-$, is rapidly formed. The high rate with which this transition occurs cannot be explained by the simplest model envisioned that is based on well-known ion molecule reactions. These results can be explained, however, by inclusion into the model of a previously uncharacterized reaction between the molecular ion-oxygen complex, $(M \bullet O_2)^-$, and water. The results reported here explain why the molecular anions of compounds that have lower EA's than that of azulene are not readily observed in electron capture ion sources of one atmosphere buffer gas pressure. In addition, it is shown that the reactions characterized here lead to a state of chemical equilibrium between the M^- and $(O_2 \bullet H_2O)^-$ ions within the PHPMS ion source from which the EA values of the low-EA compounds can be determined. By this method the electron affinities of anthracene, quinazoline, benzophenone and quinoxaline are found to be 0.54, 0.56, 0.61 and 0.68 eV, respectively.

THE PRODUCTION AND FATE OF MOLECULAR ANIONS FORMED BY ELECTRON ATTACHMENT TO LOW ELECTRON AFFINITY COMPOUNDS

by

Michael Jeffrey Salyards

A dissertation submitted in partial fulfillment
of the requirements for the degree

of

Doctor of Philosophy

in

Chemistry

MONTANA STATE UNIVERSITY
Bozeman, Montana

June 2003

APPROVAL

of a dissertation submitted by

Michael Jeffrey Salyards

This dissertation has been read by each member of the dissertation committee and has been found to be satisfactory regarding content, English usage, format, citations, bibliographic style, and consistency, and is ready for submission to the College of Graduate Studies.

Dr Eric P. Grimsrud _____ _____
(Signature) Date

Approved for the Department of Chemistry and Biochemistry

Dr Paul A. Grieco _____ _____
(Signature) Date

Approved for the College of Graduate Studies

Dr Bruce R. McLeod _____ _____
(Signature) Date

STATEMENT OF PERMISSION TO USE

In presenting this dissertation in partial fulfillment of the requirements for a doctoral degree at Montana State University, I agree that the library shall make it available to borrowers under rules of the Library. I further agree that copying of this paper is allowable only for scholarly purposes, consistent with the "fair use" as prescribed in the US Copyright Law. Request for the extensive copying or reproduction of this dissertation should be referred to Bell & Howell Information and Learning, 300 North Zeeb Road, Ann Arbor, Michigan 48106, to whom I granted "the exclusive right to reproduce and distribute my dissertation in and from microform along with the non-exclusive right to reproduce and distribute my abstract in any format in the whole or in part."

Signature _____

Date _____

TABLE OF CONTENTS

TABLE OF CONTENTS – CONTINUED

LIST OF TABLES

LIST OF FIGURES

Figure Page

LIST OF FIGURES continued

LIST OF FIGURES continued

INTRODUCTION AND LITERATURE REVIEW

One of the most fundamental processes in chemistry, especially analytical chemistry, is the capture of an electron by a neutral molecule to form the parent anion. This process, often referred to as resonance electron capture (REC), can be naively written as Reaction 1-1:

$$M + e^- \underset{k_{det}}{\overset{k_{ec}}{\rightleftharpoons}} M^- \qquad (1\text{-}1)$$

where k_{ec} is the electron capture rate constant, and k_{det} is the thermal electron detachment rate constant. Some of the sections that follow will show that this reaction also involves an intermediate. The importance of electron capture and negative ion formation to analytical chemistry has its roots in the 1948 discovery of a young English scientist. At that time, James Lovelock was commissioned by the British Medical Research Council to study the common cold. Specifically, he was asked to investigate the popularly held notion that colds are caught by being exposed to a cold draft. Lovelock's efforts, which included using radioactive α particle emitting paint from WWII aircraft gauges, to measure changes in the density of air led to the invention of an ionization apparatus. He did not learn anything useful about the common cold, but he did succeed in making a device that was especially sensitive to halocarbon gases [1]. Eventually the ionization source was changed to a β emitter, and the electron capture detector (ECD) was born. ECD use in the next 10 years moved to biochemistry and then to the detection of environmentally dangerous molecules [2] .

In 1962, Rachel Carson published Silent Spring [3]. Writing somewhat poetically about the environment, she described an impending chemical apocalypse. The ECD had proven so sensitive that researchers reported finding trace levels of pesticides in samples ranging from penguin fat to mother's milk. Carson's work thrust the ECD into the scientific limelight, and the study of electron capture and the formation of gaseous ions became popular. Presently, the study of electron capture is important in a wide range of disciplines including gaseous dielectrics [4], excimer lasers [5], discharges used for etching [6], and atmospheric chemistry [7].

The sections that follow will provide a discussion and review of: a) the pulsed high pressure mass spectrometer (PHPMS) which was used to collect data for all of the experiments in this dissertation, and b) relevant theories and literature surrounding the phenomenon of electron capture and its opposite, thermal electron detachment. Chapter 2 describes experiments that were designed to measure resonance electron capture and thermal electron detachment rate constants for several low electron affinity (EA) molecules. Finally, Chapter 3 presents a series of experiments that explain why these low EA molecules are difficult to detect at atmospheric conditions.

Pulsed High Pressure Mass Spectrometry

Kebarle developed the PHPMS during the late 1960's, and its construction and operation have been fully described previously [8]. This section is not intended to repeat the details of construction provided in this reference. However, brief descriptions of the

physical apparatus, the ionization source, the electron optics, and the types of data that can be collected, may be helpful for understanding the experiments in Chapters 2 and 3.

Hardware

Figure 1-1 is a schematic of the PHPMS. The gas handling plant is a 6.5 liter glass bulb. It is typically pressurized to approximately 800 torr with a buffer gas.

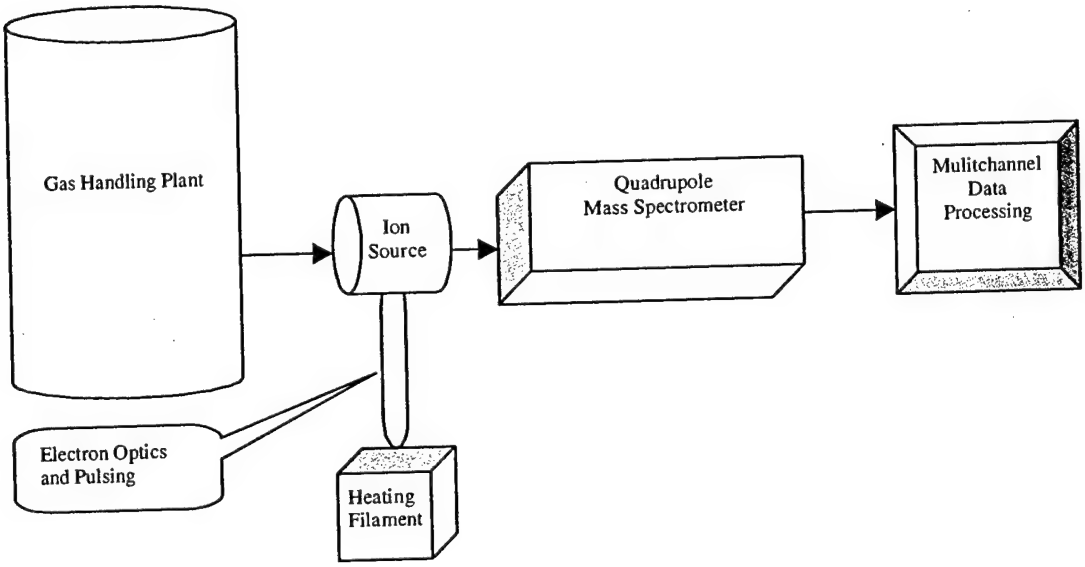

Figure 1-1. A schematic representation of the PHPMS hardware and main components.

For all of the experiments in this dissertation, methane was used as the buffer gas. Other gases including helium, nitrogen, oxygen, and argon with 15% methane have been used in previous experiments [9]. The gas handling plant is fitted with an injection port that allows introduction of both gas and liquid samples. Solid samples are dissolved in a suitable solvent (toluene was often used for the experiments in this dissertation) and the solution is injected. The gas handling plant is typically heated to about 120°C to ensure

complete volatilization of sample molecules that often have relatively low vapor pressures.

Once the gas handling plant is loaded with the desired analytes, a valve is opened, and the mixture flows through a heated transfer line into the ion source as shown in Figure 1-2.

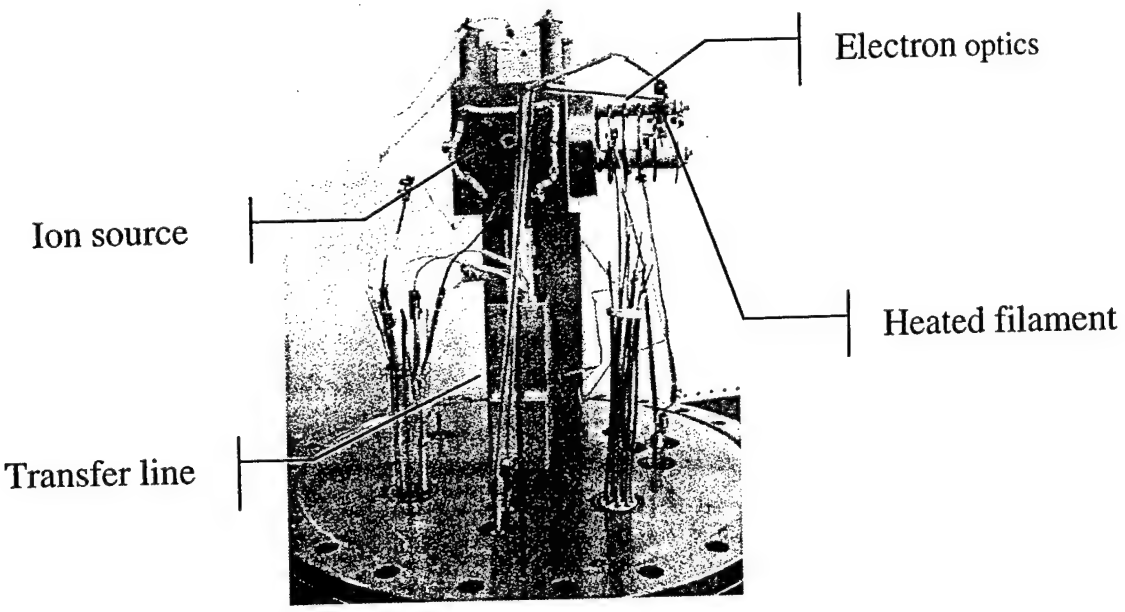

Figure 1-2. A photograph of the front flange of the PHPMS revealing the transfer line, ion source and the electron filament and pulsing optics. In this orientation, the gas mixture would flow from the bottom of the picture frame to the top. The electron optics are 90° off axis to the right at the top of the picture. For reference, the flange circumference is 10 inches.

The pressure in the ion source is controlled by the amount of gas flowing out of the gas handling plant. Typical ion source pressures are between 1-5 torr, and the ion source is heated between 30-150°C. Both of these parameters are adjusted as dictated by a given experiment.

Electrons are produced from a heated filament that is –2.95 kV relative to the ion source. A gate lens is approximately 0.75 cm in front of the filament. The gate lens is held at –3.0 kV. Approximately every 75-100 msec the gate lens potential is pulsed to – 2.90 kV for about 20 μsec. This voltage change sends a pulse of 2.95 keV high energy electrons through a stack of focusing lenses into the ion source via a small entrance aperture. Because the number density of the buffer gas is about 7-9 orders of magnitude greater than the number density of the sample molecules, these high energy electrons are believed to interact primarily with the buffer gas. The chemical cascade that follows was first described by Munson and Field in their seminal paper on chemical ionization [10]. Basically, a whole host of positive methane and ethane related ions are formed as well as a complementary population of thermal electrons. In methane buffer gas, each high energy electron produces about 85 thermal electrons. If the sample molecules have a positive EA, they will capture some of these thermal electrons and form anions. Depending on their proton affinity, sample molecules may also form cations by interacting with the positively charged buffer gas related ions. As will be detailed in the next section, these newly formed ions diffuse to the wall of the ion source. A representative population of these ions passes through an exit slit into a quadrupole mass spectrometer. By narrowing the exit slit, the ion source can be operated in the 10-20 Torr region. However, the narrow slit decreases the ion signal. Ions are detected using an electron multiplier and an ion counting channeltron.

Types of Data Collected

The electron pulsing and related detection hardware and software are what make the PHPMS unique. Multichannel scalar software allows discrete channels of data to be collected after the electron pulse event. The time length of the channels can be varied from 5 μsec to several hundred msec. By selecting long channel times (≈160 msec) and scanning the quadrupole, typical mass spectra are obtained. However if much shorter channel times (≈ 100 μsec) are used and the appropriate m/z is selected on the quadrupole, the population of a given ion in the source can be tracked in time as it is formed and diffuses to the wall. As might be expected, the diffusion of ions to the wall is a first order loss process and indicated in Figure 1-3.

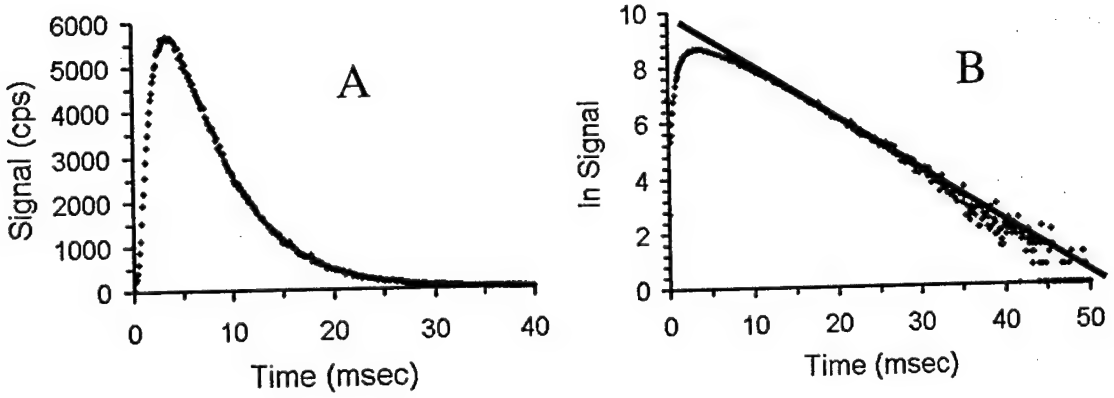

Figure 1-3. Standard time profile of SF_6 anion. The ion source pressure is ≈ 3.0 Torr. The ion source temperature is 60°C. (A) is the standard plot of signal versus time. (B) is the same data plotted as the ln of the signal versus time. A line as been superimposed on the data to highlight the linear relationship.

The diffusion rate constant, k_{diff}, is approximately 150 sec^{-1} at 3 torr and 60°C. Diffusion of ions depends primarily on three variables, the temperature squared, the inverse of pressure, and the reduced mobility of the ion. Equation 1-2 can be derived from equations provided by McDaniel and Munson [11].

$$k_{diff} \propto \frac{T^2}{P} K_0 \qquad (1\text{-}2)$$

In this equation, the reduced mobility term, K_0, contains information about the reduced mass of the ion of interest as well as a term that describes how strongly the ion interacts with the buffer gas [12]. For all the experiments in this dissertation, ions were considered to have the same mobility to a first approximation. Therefore, diffusion is treated as a function of inverse pressure and temperature squared.

In addition to diffusion, ions can be lost if they react with a neutral molecule or another ion. Further, the diffusional loss of other ions may be partially offset if they are being produced by a chemical reaction. Sometimes it is helpful to compare the time profiles of two ions as in Figure 1-4. Close examination of the logarithmic plot in Figure 1-4 (A) reveals that the population of the ion represented by the circles is disappearing faster than the population of the ion represented by the squares. Because these ions are both being lost to diffusion, sometimes these other loss and production terms are subtle and difficult to see on a logarithmic plot. The normalized plot in Figure 1-4 (B) is prepared by dividing a given ion signal by the total ion signal. The inference from Figure 1-4 (B) is that the circle ions are reacting away and the square ions are being produced.

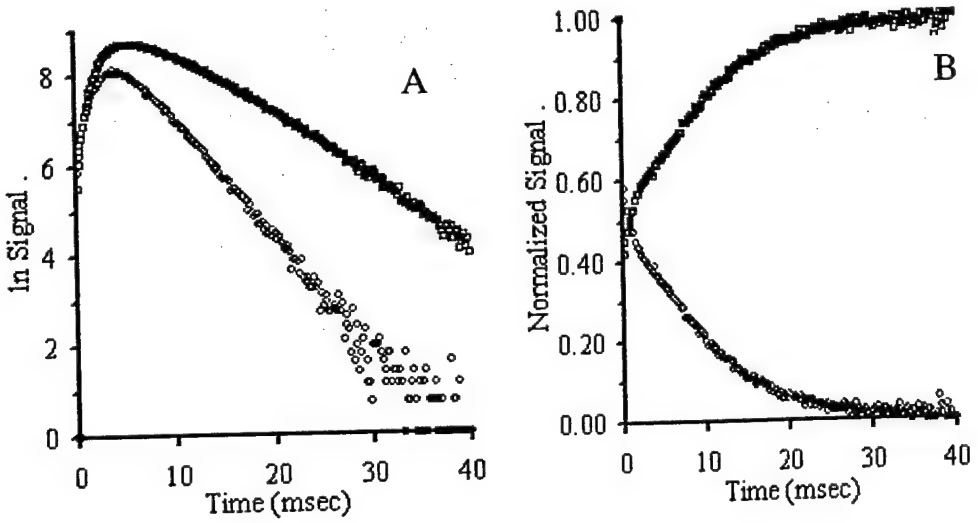

Figure 1-4. (A) A logarithmic plot similar to Figure 1-3 (B) but of two ions, (o), and ( ). (B) The same data shown as a normalized plot. The normalized plot demonstrates how each ion population is changing relative to the total population. In effect, this type of graph removes diffusion and (assuming ions are not diffusing at different rates) emphasizes any ion molecule chemistry that may be occurring.

Normalized time profiles may also reveal if two or more ions have come into equilibrium as shown in Figure 1-5. During the first 5 msec of this experiment, the ions represented by (x) appear to be reacting away while the ions represented by (o) and (Δ) are being produced. After about 5 msec, the relative concentrations become constant in time. This type of profile is strongly suggestive of chemical equilibrium. However, it should be noted that this steady state condition would also be observed for two ions with similar diffusion coefficients that are not reacting with each other at all. As shown in detail in Chapter 3, verifying equilibrium involves varying concentrations of reactants and products and comparing observed equilibrium constants with expected values.

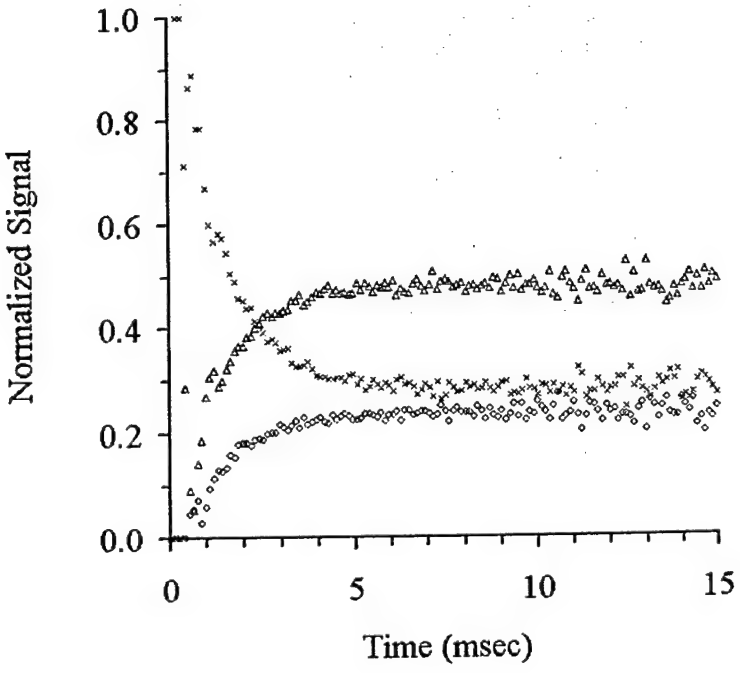

Figure 1-5. Normalized time profiles of several different ions showing what equilibrium typically looks like.

Plasma Conditions in the Ion Source

After the initial pulse of high energy, 2.95 keV, electrons enter the source, a weak plasma is created. Initially, the positive charge carriers are primarily ions materially related to the methane buffer gas (i.e. CH_5^+, and $C_2H_5^+$) and, the negative charge carries are thermal electrons. Several events happen rapidly. First, anions can be formed if some of the electrons are captured by sample molecules with a reasonable EA and a high enough electron capture rate constant. None of the experiments in this dissertation deal directly with positive ion chemistry, but it should be noted that the buffer gas related cations will also charge transfer to molecules with suitable proton affinities. The resulting plasma contains positive ions, negative ions and thermal electrons.

Both Kregel and McDaniel have eloquently described how this type of plasma behaves as the charged species diffuse to the wall of the ion source [13, 14]. Most recently, Franklin provided an outstanding review of electronegative plasmas [15]. A qualitative review of these works follows. Initially, the electrons diffuse much faster than the ions due to their high mobility. Biondi reports the mobility of an electron to be 1000 times that of a negative ion [16]; however, Franklin states the mobility of an electron to be 300 times that of a negative ion [15]. Neither author provides data or theory to support their reported electron mobility. However, it is generally accepted that mobility of an electron is high compared to an anion. This high mobility is the result of the electron's mass (it is ≈275,000 times smaller than a 150 amu anion) offset by inelastic collisions and interactions with the buffer gas. Electrons and all charged particles are neutralized at the wall. So, a charge imbalance develops. The plasma by definition maintains charge neutrality. As a result the diffusion of positive ions becomes coupled to the diffusion of electrons. The net effect is that the diffusion rate of the positive ions is doubled and the diffusion rate of the electrons is retarded to match the positive ions. This condition is often called ambipolar diffusion, and this type of plasma is referred to as electron dominated or an electron/positive ion plasma. The negative ions are, as Kregel states, "bottled" in the ion source and their diffusion rate is ≈ 0. This electron dominated plasma persists until the electron density is ≤ 10% of the negative ion density. As the electrons are depleted, the nature of the plasma changes to a negative ion dominated or negative ion/positive ion plasma, and the negative and positive ions begin to diffuse at their

normal rates. Miller provides a good mathematical summary of the ambipolar diffusion in an electron dominated plasma, listed here as equations 1-3, 1-4 and 1-5 [17]:

$$D_{a+} = 2D_{+} \tag{1-3}$$

$$D_{a,e^-} = 2D_{+}(1+\frac{n_-}{n_{e^-}}) \tag{1-4}$$

$$D_{a,-} = 2D_{+}(1+\frac{n_-}{n_{e^-}})(\frac{D_-}{D_{e^-}}) \tag{1-5}$$

where $D_{a,x}$ is the ambipolar diffusion coefficient of x, and D_x is the free diffusion coefficient of x (i.e. in the absence of a space charge), and n_x is the number density of x. Note that Equations 1-3 – 1-5 are in terms of a diffusion coefficient, D, instead of a diffusion rate constant, k_{diff}. These terms are linearly related as in Equation 1-6:

$$k_{diff_x} = \frac{D_x}{\Lambda^2} \tag{1-6}$$

where Λ is the characteristic diffusion length. If the ion source is a sphere, Λ = the radius of the sphere divided by π. McDaniel provides more details about how to calculate Λ for ion sources with atypical geometries [11, 14].

The ambipolar diffusion coefficient of negative ions, $D_{a,-}$, is ≈ 0 because $(D_- / D_e) \approx 0.001 - 0.003$ (the mobility of an electron is 300 - 1000 times greater than the mobility of an ion as previously mentioned). For a more rigorous treatment that describes both

electron dominated and ion dominated ambipolar diffusion see Rogoff [18]. Lineberger and Puckett reported this type of behavior in a stationary after glow instrument (similar to the PHPMS) in 1969 [19]. They used nitric oxide to make a plasma that contained $(NO{\bullet}NO)^+$, NO_2^- and free electrons as the charge carriers. Figure 1-6 is a recreation of their data.

At about 150 msec, a transition occurs. Before this point, the positive ions are diffusing approximately twice as fast as they are after the transition. The negative ions are not diffusing at all before the transition. After the transition both the positive and

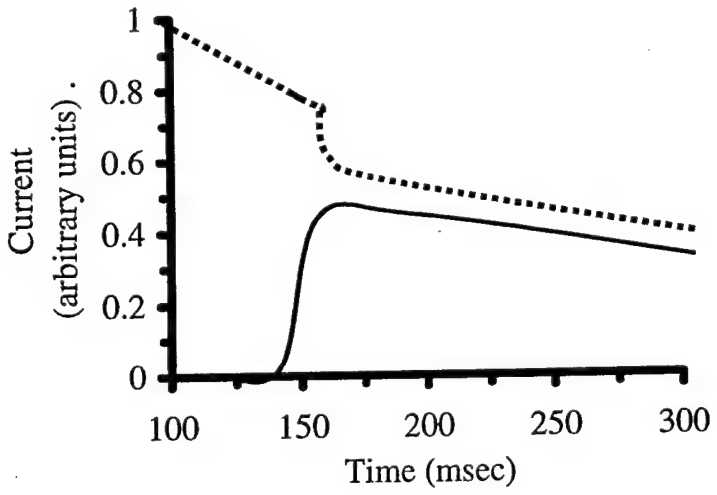

Figure 1-6. A recreation of Lineberger's nitric oxide data. The positive ions are represented by the dotted line; the negative ions are represented by the solid line. Electrons are not shown directly in this graph, but their effect is clearly seen at 150 msec where the plasma changes from electron dominated to ion dominated. The positive ion signal has been translated up to make it easier to see. After the transition point it should lay on top of the negative ion signal.

negative ions are diffusing at the same rate. Reviewing the logarithmic plots in Figures 1-3 (B), and 1-4 (A) shows that during the first few msec these anions are "bottled" inside the source.

When the number of charged particles becomes sufficiently small, the plasma condition breaks down, and the diffusion rates of electrons, negative ions, and positive ions are no longer coupled. This condition is often referred to as an ionized gas, and diffusion coefficients are referred to as free to distinguish them from ambipolar.

Data collected from the PHPMS for experiments in this dissertation are taken in the ion dominated ambipolar diffusion and the ionized gas free diffusion regions. If the behavior of two ions is being compared, it is not critical that the experiment be carefully limited to one type of diffusion as long as both ions are being affected equally by changes in the diffusion. As will be seen when thermal electron detachment is discussed in Chapter 2, the transition from an ion dominated plasma to free diffusion can have a huge effect on the recapture of detached electrons.

Electron Capture Cross Section, Feshbach States, and M^{*-} Lifetimes

The term resonance electron capture rate is rather unfortunate for two reasons. First, it is also used to describe the completely unrelated nuclear reaction where an inner shell electron is captured by the nucleus as a proton is transformed into a neutron. Second, the term has a connotation that is not obvious. It is often used by gas phase ion chemists to describe electron capture reactions, like Reaction 1-1, where a molecular

anion is formed. In contrast, the term dissociative electron capture is used to describe an electron capture event where a fragment ion is formed.

The concept of resonance electron capture is deceptively complex. Electron capture rates are a seemingly fundamental property. And, one might expect a molecule with a positive EA to capture electrons at some collisional rate analogous to Langevin or ADO theory in ion molecule chemistry. Even if electron capture rates differ for each molecule, shouldn't the typical junior level physical chemistry text have catalogue of electron capture rate constants for common molecules? Unfortunately, measuring electron capture rates is not easy. The theory is complicated and involves a failure of the Born-Oppenheimer approximation. Further, as shown by Knighton et al [20], electron capture rates do not seem to be a function of any standard thermodynamic properties. The first step to understanding resonance electron capture involves moving beyond Reaction 1-1 and writing the more complete Reaction 1-7:

$$M + e^- \underset{k_{-1}}{\overset{k_1}{\rightleftharpoons}} M^{*-} \underset{k_{-2}[B]}{\overset{k_2[B]}{\rightleftharpoons}} M^- \qquad (1\text{-}7)$$

This section will focus on the formation and lifetime of the excited intermediate, M^{*-} or the first half of this reaction. The following section will focus on the interaction of the excited intermediate with the buffer gas, or the second half of the reaction.

The initial formation of a temporary or transient negative ion (TNI) is most often described in the literature in terms of an electron capture cross section, σ_{cap}. This cross section, first given by Vogt and Wannier [21], is Equation 1-8:

$$\sigma_{cap} = 4\pi a_0^2 \sqrt{\alpha / 2E} \tag{1-8}$$

where a_0^2 is the Bohr radius, and α and E are the polarizabilty and the electron energy respectively (in atomic units). This equation is thought to be valid for very low electron energies, $E \approx 0$. As electron energy increases, the de Broglie s-wave cross section (given in Equation 1-9) may be more appropriate [22]:

$$\sigma_{cap} = \frac{\pi a_0^2}{2E} \tag{1-9}$$

Equation 1-10, from Klots' highly referenced 1976 paper [23], is an analytical form of this equation that describes the cross section in terms of the electron energy:

$$\sigma_{cap} = \pi\lambda^2 (1 - e^{[-4\gamma^2 E)^{\frac{1}{2}}]}) \tag{1-10}$$

where λ is the de Broglie wavelength of relative motion. The Langevin parameter, γ, is given by equation 1-11:

$$R\gamma^2 = (\frac{2\mu}{m})^2 (\frac{\alpha}{a_0^3}) \tag{1-11}$$

where μ is the mass, m is the mass of an electron, R is the Rydberg constant, α the polarizability, and a_0 the Bohr radius. Equation 1-12, provided by Dunning, is a more convenient version of Equation 1-10:

$$\sigma_{cap} = \frac{\pi a_0^2}{2E} (1 - e^{[-4(2\alpha E)^{\frac{1}{2}}]}) \tag{1-12}$$

The electron capture cross section is believed to be related to k_1 from Reaction 1-7 by Equation 1-13:

$$k_1 = \int_0^\infty v\sigma_{cap}(v) f(v) dv \tag{1-13}$$

where f(v) is the electron velocity distribution as given by Compton et al [24] in Equation 1-14:

$$f(v) = \left(\frac{m}{2kT}\right)^{\frac{3}{2}} e^{-\left(mv^2/2kT\right)} 4\pi v^2 \tag{1-14}$$

Perhaps the most simple and intuitive form of Equation 1-13 comes from Hahndorf and Illenberger [25] in Equation 1-15:

$$k_1 = \overline{\sigma_{cap} v} \tag{1-15}$$

where the right hand side of the equation is given in terms of the product of the average cross section and the average electron velocity for a given temperature.

Because the cross section term decreases with electron velocity, these terms off set each other, and electron capture rates are believed to be insensitive to temperature over a large range, 25-145°C in one study [25] and 25-325°C in another [26].

Once the electron is initially captured, an excited M^{*-} is formed. If the neutral molecule has a positive EA, the M^{*-} species has an excess energy which is equal or greater to the EA. The lifetime of this intermediate is described by Equation 1-16:

$$\tau = \frac{1}{k_{-1}} \qquad (1\text{-}16)$$

where k_{-1} is the first order autodetachment rate constant from Reaction 1-7.

This lifetime appears to depend on how the electron is bound and where the excess energy is stored. Different authors describe M^{*-} with different levels of complexity. In the most simple model, the M^{*-} is considered to be one of two types, short lived or long lived. The so called long lived species is often termed a Feshbach resonance [27]. Christophorou describes four different negative ion resonant states for the M^{*-} species: a) shape or single particle resonances, b) core excited shape resonances, c) nuclear excited Feshbach resonances, and d) electron excited Feshbach resonances [4].

Both types of shape resonances result when the incident electron is trapped by the centrifugal motion that arises from the relative motion of the electron and the neutral molecule. The trapped electron, in this case, will have a certain angular momentum (i.e. $\ell \geq 1, 2,$). As a result, this channel for anion formation is sometimes called p-wave attachment for $\ell = 1$. Barsotti et al recently (2002) published a paper showing evidence of p-wave electron attachment to Cl_2 [28]. The core excited shape resonance involves the same concept but begins with the molecule in an excited electronic state.

The nuclear excited Feshbach resonance involves coupling of the kinetic energy of the electron with rotational and vibrational motion of the molecule. This obvious

violation of the Born-Oppenheimer approximation makes actual calculations of the potential energy surfaces not possible with currently accepted theories.

The electron excited Feshbach resonance happens when the incoming electron electronically excites the molecule as it is captured. The electronically excited, M^{*-}, offers less shielding of the nucleus, and the incoming electron experiences a slightly positive charge that can temporarily bind it to the nucleus.

Another way of discussing electron molecule interactions is in terms of the lifetime of M^{*-}. In unpublished lecture notes, Reddish [29] describes three different scenarios in terms of the lifetime of M^{*-}, versus a typical vibrational period, $\approx 10^{-14}$ sec: a) impulse limit where $\tau << 10^{-14}$ sec, b) shape resonance where $\tau \approx 10^{-14}$, and c) Feshbach resonance where $\tau >> 10^{-14}$.

The impulse limit applies to the case where the electron is almost elastically scattered. The negative ion decays before a complete vibration occurs; the molecule can be rotationally and or vibrationally excited depending on how much energy the electron lost during the interaction.

Reddish describes the shape resonance similar to Christophorou (above) noting that the linear momentum of the electron is transferred into angular momentum. Reddish adds that the incoming electron attaches to the ground state molecule by entering the lowest unoccupied molecular orbital. Reddish does not address the electron excited shape resonance.

The Feshbach resonance, according to Reddish, is similar to the electron excited Feshbach resonance as described by Christophorou. The incident electron electronically

excites the molecule and then becomes bound to the molecule. The result is a negative ion with two excited electrons and an inner hole. The decay of this ion is believed to be a concerted process where both electrons have to change states simultaneously (one is ejected while the other returns to the ground state.) Reddish does not address the nuclear excited Feshbach resonance.

Most researchers agree that long lived M^{*-} Feshbach resonance species exist because most detection schemes require the M^{*-} species to live long enough to be detected or (as will be presented in the next section) stabilized by collisions with a buffer gas. But, how researchers describe the Feshbach resonance varies between the nuclear excited and the electron excited definitions provided above. Thoss and Domcke have put forth a theory about vibrational relaxation that is similar to Christophorou's nuclear excited Feshbach resonance with one complexity as shown in Reaction 1-17:

$$M + e^- \underset{k_{-1}}{\overset{k_1}{\rightleftharpoons}} M^{**-} \underset{k_{IVE}}{\overset{k_{IVR}}{\rightleftharpoons}} M^{*-} \underset{k_{-2}[B]}{\overset{k_2[B]}{\rightleftharpoons}} M^- \qquad (1\text{-}17)$$

where IVR refers to intramolecular vibrational relaxation, and IVE refers to intramolecular vibrational excitation. In this model, the incoming electron vibrationally excites the molecule. But, (possibly based on symmetry selection rules) only a few vibrational modes can be excited by the electron. These active modes are coupled to all of the other vibrational modes. As a result, vibrational energy that was initially concentrated in the active modes can be redistributed among the other inactive modes. In the parlance

of Reaction 1-17, M^{**-} relaxes into M^{*-}. In order for the excited anion to autodetach, the energy has to be collected back into the active modes, a process that is not entropically favored. Many researchers referenced by Thoss and Domcke [30] adhere to this intramolecular vibrational relaxation model. Table 1-1 summarizes how various researchers have defined the excited state of the Feshbach resonance (electronic, vibrational, combination, or undetermined).

Table 1-1. Review of Feshbach resonance descriptions in the literature

Researcher	Molecules Studied	Feshbach Resonance Description
Dessent et al [31]	Nitromethane halide clusters	Vibrational
Leber et al [32, 33]	Nitrous oxide clusters and carbon dioxide	Vibrational for both and but mentions electronic for $(N_2O)_N$
Tulej et al [34]	Porpadienylidene anion	Electronic
Miller et al [35, 36]	SF_5CF_3, PCl_3, and $POCl_3$	Undetermined
Miller et al [37]	SF_4 and SF_6	Electronic
Hahndorf and Illenberger [25]	CF_3I, CF_3Cl, CF_2Cl_2, C_6F_5Cl, and C_6F_5CN	Vibrational
Suess et al [38]	SF_6, C_6F_6, $C_{10}F_8$, and c-C_7F_{14}	Vibrational
Michaud et al [39]	Oxygen	Combination
Compton et al [24]	SF_6, and $C_6H_5NO_2$	Vibrational
Naff et al [40]	Alicyclic and aromatic fluorcarbons	Vibrational
Klots [41]	Theoretical treatment	Vibrational

Table 1-1 continued.

Researcher	Molecules Studied	Feshbach Resonance Description
Hadjiantoniou et al [42, 43]	Benzene derivatives, various other organic molecules	Vibrational
Collins et al [44]	p-benzoquinone	Combination,
Johnson et al [45]	NO_2 benzene derivatives	Vibrational
Horacek et al [46]	Hydrogen iodide	Vibrational
Garrett [47]	Theoretical treatment	Undetermined
Tobita et al [48]	Polycylic aromatic hydrocarbons	Combination
Thoss and Domcke [30]	Theoretical treatment	Vibrational

The most compelling evidence for the vibrational Feshbach resonances comes from data collected by Naff et al [40] shown here as Figure 1-7. However, Johnson et al directly referenced this data and pointed out:

> τ is affected by a number of other factors besides N, such as the internal energy of the ion (itself a function of electron affinity, incident electron energy, and the thermal and zero-point energies), geometry, and configurational changes which may take place upon capture. If for a group of molecules these other factors are approximately the same, then it is possible to see an increase in τ with increasing N. [45].

In this quotation, N refers to the number of vibrational degrees of freedom for a given molecule.

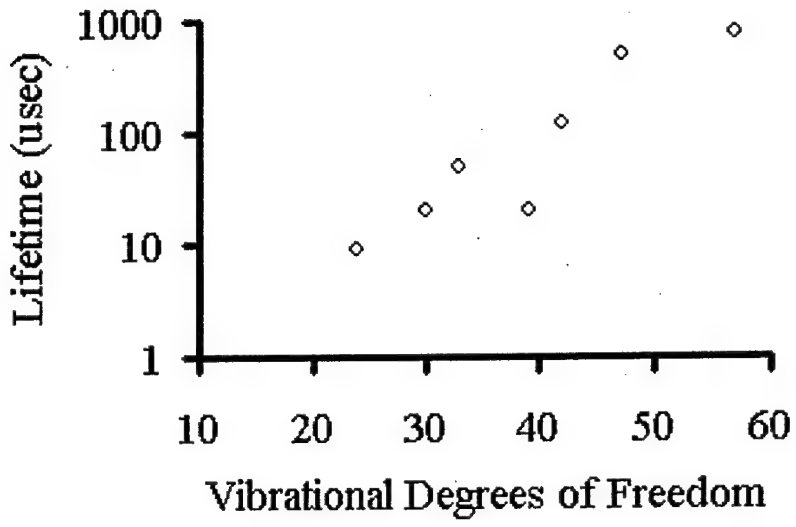

Figure 1-7. A recreation of data from Naff and Cooper on alicyclic and aromatic fluorocarbons, showing the increasing lifetime of temporary negative ions from 7 different molecules as a result of increasing vibrational degrees of freedom.

Tulej et al provides spectroscopic data of the popadienylidene anion that supports the electronic Feshbach resonance [34], and Miller et al suggest that SF_6^{*-} is formed by an electronic Feshbach resonance [37].

Garret (and references within) [47] and Dessent et al [31] discuss the need for the neutral molecule to have a dipole moment above a critical value, $\mu_c \approx 2$ debye, in order to initially bind the electron. The dipole bound electron orbital is believed to be very diffuse (> 30 Angstroms). The lingering dipole bound electron is then thought to be captured into the lowest unoccupied molecular orbital to form the vibrational Feshbach resonance.

As will be seen in Chapter 2, the molecules in the present study are benzophenone, anthracene, quinoxaline, and quinazoline. The experiments in this dissertation were not designed to determine what type of Feshbach resonances these

molecules form. However, based on previous experiments on similar molecules [42, 43, 49], it is very likely that the molecules in the present study form vibrationally excited Feshbach resonances.

The magnitude of k_1 and k_{-1} cannot be predicted for any molecule, but Compton et al proposed a way to predict the ratio $\frac{k_1}{k_{-1}}$ from first principles as indicated in Equation 1-18 [24]:

$$\frac{k_1}{k_{-1}} = \frac{\rho^-}{\rho^0} = \frac{2\pi^2 h^3 (EA + a\beta_z)^{N-1}}{m^2 v (N-1)! \prod_{i=1}^{N} h\nu_i} \qquad (1\text{-}18)$$

where ρ^- is the density of states for the anion, and ρ^o is the density of states for the neutral plus the electron. The variables on the far right hand side of the equation are as follows: m is the mass of the electron; v is the velocity of the electron; N the number of vibrational degrees of freedom; EA is the electron affinity; β_z is the zero point energy; ν_i the i^{th} vibrational frequency of the anion, and the variable a is an empirical correction factor that would need to be evaluated for each molecule. Knighton et al provides a helpful review of Equation 1-18 and the previous attempts to use known $\frac{k_1}{k_{-1}}$ values to estimate EA values (note that Equation 1-18 has a typographical error in the Knighton paper – the Π term in the denominator has been replaced by a Σ term) [20].

Interactions of Anions with a Buffer Gas

The ideas in this section should be intuitive to even the most casual observer, for we have all experienced ordinary gases and liquids coming into thermal equilibrium. Every day research is conducted in this regard as cold milk is poured into hot coffee and air conditioners are adjusted to make a room more comfortable.

The intermediate, M^{*-}, formed in Reaction 1-7 faces two different outcomes. It can autodetach the electron as governed by k_{-1}, or it can be stabilized by collisions with the buffer gas as governed by $k_2[B]$, where B is the concentration or pressure of the buffer gas. Further, the stable M^- can be excited back to M^{*-} by collisions with the buffer gas as governed by $k_{-3}[B]$. Both the forward and reverse step will be explained here in turn.

Stabilizing Collisions and the High Pressure Limit

The Lindemann–Hinshelwood mechanism dating back to 1921 is the starting point in most text books for unimolecular reactions [50]. These reactions are often written as Reaction 1-19:

$$A + B \underset{k_{-a}[B]}{\overset{k_a}{\rightleftharpoons}} A^* \overset{k_b}{\rightharpoonup} \text{Products} \qquad (1\text{-}19)$$

where B is a buffer gas molecule. Note that Reaction 1-19 is essentially the reverse of the last part of Reaction 1-7. By making a steady state assumption for the $[A^*]$, the reaction rate can be written as Equation 1-20.

$$\frac{d[\,Products\,]}{dt} = [\,A\,]\frac{k_a k_b [\,B\,]}{k_{-a}[\,B\,] + k_b} \tag{1-20}$$

This equation is often given in terms of a unimolecular rate constant as in Equation 1-21:

$$\frac{d[\,Products\,]}{dt} = k_{uni}[\,A\,];\;\; k_{uni} = \frac{k_a k_b [\,B\,]}{k_{-a}[\,B\,] + k_b} \tag{1-21}$$

The result of the Lindemann–Hinshelwood mechanism is a reaction that behaves one way at low [B] and another way at high [B]. This behavior becomes intuitive by evaluating the two extremes: a) the limit of k_{uni} as [B] goes to zero, and the limit of k_{uni} as [B] goes to infinity. The former case, sometimes called the low pressure limit, is shown here as Equation 1-22:

$$\lim_{[\,B\,]\to 0} k_{uni} = k_a [\,B\,] \tag{1-22}$$

and the latter case, sometimes called the high pressure limit, is shown here as Equation 1-23.

$$\lim_{[\,B\,]\to\infty} k_{uni} = \frac{k_a k_b}{k_{-a}} \tag{1-23}$$

Note that in the low pressure limit the reaction behaves like a second order process (i.e. the reaction rate depends on both [A] and [B]). However in the high pressure limit, the reaction behaves like a first order process (i.e. the reaction rate depends only on [A]). Graphically, Reaction 1-19 would behave as indicated by Figure 1-8.

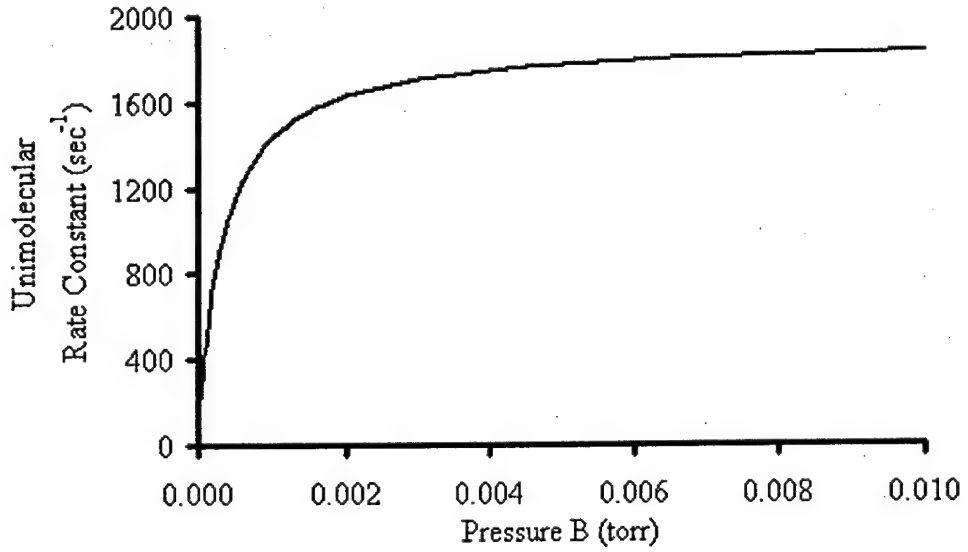

Figure 1-8. A representation of the Lindemann–Hinshelwood mechanism showing both the high and low pressure regions. The following parameters were used for this figure: $k_a = 2.0 \times 10^{-10}$ cc sec^{-1}, k_{-a}, 2×10^{-9} cc sec^{-1}, and $k_b = 1.8 \times 10^{4}$ sec^{-1}.

As a historical aside in the early 1920's, Professor J. Perrin examined data from a unimolecular dissociation reaction that, unbeknownst to him, was in the high pressure limit. Clearly, the reaction rate seemed independent of [B], and Perrin extrapolated these results to very low pressures, and he began to ponder. If the reaction proceeds at the same rate regardless of [B], and perhaps in the absence of [B], what outside agency is causing the reaction to happen? Perrin soon after put forth his theory that electromagnetic

radiation was responsible for creating the excited intermediate. In 1922, a discussion was published in which a remarkable group of scientists, Lindemann, Arrhenius, Langmuir and Dhar, rebutted this theory [51]. Lindemann was especially articulate pointing out that the unimolecular inversion of sucrose proceeds at the same rate in the sunlight as it does in total darkness. He also pointed out that the incident sunlight probably only penetrates the first 1mm of the solution. Lindemann then remarked, "After all this criticism, I suppose I had better put forward a constructive suggestion intended to meet Professor Perrin's difficulty." In summary, Lindemann's suggestion was that the population of A^* versus A is brought into thermal equilibrium with B. The time for this equilibrium to be established is directly related to the pressure of [B]. When [B] is high enough, this equilibrium is rapidly reestablished after $A^* \rightarrow P$. In this case, the rate limiting step, for a given temperature, is governed by k_b. On the other hand, if [B] is small, thermal equilibrium is established slowly compared to $A^* \rightarrow P$, then the rate limiting step is governed by the formation of A^*, or $k_a[B]$.

In 1927-8, Rice, Rampsberg, and Kessel, proposed more detailed theories for unimolecular reactions [52]. Their combined theory often goes by the eponym, RRK. In summary, RRK theory states that for a unimolecular reaction to occur certain critical vibrations and rotations must be excited. These critical modes are treated statistically by attempting to answer the question: what is the probability that collision will result in an A^* that has the critical modes excited? Later, Marcus added his thoughts, "I blended statistical ideas from the RRK theory of the 1920s with those of the transition state theory of the mid-1930s [53]." And, the theory is sometimes called RRKM in its complete form.

For the experiments in this dissertation, the Lindemann-Hinshelwood treatment is adequate. Williamson et al recently conducted experiments on the unimolecular thermal electron detachment of the azulene anion [9]. These experiments were conducted at Montana State University on the same PHPMS used for the experiments in this dissertation. Williamson found that the transition for low pressure to the high pressure region occurred at about 1 Torr. This result is unfortunate because the PHPMS has a pressure range from about 1-5 Torr. Therefore, ideal experiments, like comparing 1, 10 and 100 Torr results, could not be conducted. To determine if our experiments were in the high pressure limit, data from buffer gas pressures varying from 1-3 Torr were frequently compared. Because the measured rate constants in Chapter 2 and the equilibrium constants in Chapter 3 did not change at different buffer gas pressures, we can infer the experiments were conducted in the high pressure limit.

Comparing Reaction 1-1 with Reaction 1-7, it useful to ask how do k_{ec} and k_{det} relate to k_1, k_{-1}, k_2, and k_{-2} in the high pressure limit? The detailed answer to this question is contained in Appendix A. The final results are presented here as Equations 1-24 and 1-25.

$$k_{ec} = k_1 \tag{1-24}$$

$$k_{det} = k_{-1}\frac{k_{-2}}{k_2} \tag{1-25}$$

Excitation and Thermal Electron Detachment

In a 1999 personal correspondence regarding thermal electron detachment, Miller noted: "I've been thinking about this off and on for a long time with no obvious answer...for molecules whose k_{ec} and EA are known, isn't the k_{det} rate preordained by the thermodynamics equations? [54]." Indeed, the laws of thermodynamics govern the ratio of the electron capture rate constant and the thermal electron detachment rate constant, but, the magnitude of these individual terms is independent of thermodynamic quantities like electron affinity.

In 1985, Kebarle proposed an equation for predicting thermal electron detachment rate constants as a function of temperature, EA, entropy upon negative ionization, and k_{ec} [55]. As will be shown below, Kebarle's equation contains an assumption that may be in error. More recently, Miller proposed an equation using different assumptions [17, 56]. Kebarle's equation is based upon transition state theory as in Equation 1-26:

$$K = \frac{Q_{M^-}}{Q_M Q_{e^-}} e^{\frac{EA_M}{RT}} \qquad (1\text{-}26)$$

where K is the equilibrium constant for Reaction 1-1, Q_{M^-} and Q_M are the partition functions for M^- and M respectively, EA_M is the electron affinity for M, R is the molar gas constant, and Q_e is the partition function for an electron. Kebarle treats the electron as a monatomic gas with $\pm\frac{1}{2}$ spin degeneracy. Therefore Q_e is given by twice the translational partition function as in Equation 1-27:

$$Q_{e^-} = 2V\left(\frac{2\pi m_e kT}{h^2}\right)^{\frac{3}{2}} \tag{1-27}$$

where V is a volume term (1 m^3 for standard conditions), and m_e is the mass of an electron. Kebarle's assumption comes when he states Equation 1-28:

$$\frac{Q_{M^-}}{Q_M} = e^{\frac{\Delta S^0_{ni}}{R}} \tag{1-28}$$

where ΔS^0_{ni} is defined as the entropy of negative ionization given as ($S^0_{anion} - S^0_{neutral}$). Kebarle asserts this to be true because of the microcanonical treatment in Equation 1-29:

$$S = k \ln \Omega \tag{1-29}$$

where Ω is the number of microstates in a given macrostate. Although Ω is related to the partition function, they are not the same thing, and the more appropriate relationship, often referred to as the canonical ensemble, is given in Equation 1-30 [57]:

$$A = -kT \ln Q \tag{1-30}$$

where A is the Helmholtz free energy, and Q is the partition function for the whole system (i.e. $Q = Q_{translational} + Q_{electronic} + Q_{vibratiotal} + Q_{rotational}$). Therefore, the relationship in Equation 1-28 could be given as Equation 1-31:

$$\frac{Q_{M^-}}{Q_M} = e^{\frac{\Delta A^0_{ni}}{RT}} \tag{1-31}$$

where ΔA is defined ($A^0_{anion} - A^0_{neutral}$). Kebarle then invokes the simple relationship of forward and reverse rate constants to K as in Equation 1-32:

$$K = \frac{k_{ec}}{k_{det}} \tag{1-32}$$

Combining Equations 1-26, 1-27, 1-31, and 1-32 gives a canonical form of Kebarle's work as Equation 1-33

$$k_{det} = 4.8\times10^{15} T^{\frac{3}{2}} k_{ec} e^{\left(\frac{\Delta A^0_{ni} - EA_M}{RT}\right)} \tag{1-33}$$

where k_{ec} is given in cc sec^{-1} and k_{det} is calculated in sec^{-1}. The microcanonical form of Kebarle's equation with ΔS_{ni} instead of ΔA_{ni} in the exponential is shown here as Equation 1-34.

$$k_{det} = 4.8\times10^{15} T^{\frac{3}{2}} k_{ec} e^{-\left(\frac{\Delta S^0_{ni}}{R} + \frac{EA_M}{RT}\right)} \tag{1-34}$$

This equation has been used at least twice in the literature [58, 59], and it will be used in this dissertation so data can easily be compared with the previous publications.

Miller's treatment starts with the familiar relationship in Equation 1-32 and then adds another basic concept in Equation 1-35.

$$\Delta G^0 = -RT\, lnK = \Delta H^0 - T\Delta S^0 \tag{1-35}$$

Miller combines the relationships in Equations 1-32 and 1-35 to develop Equation 1-36:

$$k_{det} = k_{ec} L_0 \frac{273.15}{T} e^{[-\frac{EA}{kT} - \frac{\Delta S}{k} - \frac{(H_T - H_0)}{kT}]} \quad (1\text{-}36)$$

where L_o is Loschmidt's number (2.687×10^{19} cc^{-1}); EA is the electron affinity; ΔS entropy change as outlined below, and $(H_t - H_0)$ is a temperature correction for the enthalpy term as defined below.

The ΔS entropy term is given below in Equation 1-37.

$$\Delta S = S_{anion} - S_{neutral} - S_{electron} \quad (1\text{-}37)$$

The entropy of the electron is estimated by treating it as a monatomic gas with $\pm\frac{1}{2}$ spin degeneracy and applying the Sackur-Tetrode equation as in equation 1-38 [17, 60]:

$$S^0_{electron} = k\, ln[\, 2(2ekT)^{\frac{5}{2}} (2\pi m_e)^{\frac{3}{2}} (p^0 h^3)^{-1}\,] \quad (1\text{-}38)$$

where e is the base of the natural logarithm, m_e is the mass of an electron, and p^o is a reference pressure (101.3 kPa). The $S_{anion} - S_{neutral}$ portion of the equation can be calculated with ab initio methods or estimated with commercially available software. For the experiments in Chapter 2, reported entropy terms were adjusted until the prediction fit the data.

The $(H_t - H_0)$ term in Equation 1-36 is given here as Equation 1-39.

$$H_t - H_T = \int_0^T C_p(anion)\,dT - \int_0^T C_p(neutral)\,dT - \int_0^T C_p(electron)\,dT \quad (1\text{-}39)$$

The anion and neutral terms are approximately the same. Therefore, Equation 1-39 can be simplified to just the electron term which is given in Equation 1-40 [17, 61].

$$H_t - H_T \approx -\int_0^T C_p(electron)\,dT = -\frac{5}{2}kT \qquad (1\text{-}40)$$

Using the values in Table 1-2, thermal electron detachment rate constants can be calculated as a function of temperature for both the Miller and Kebarle Equation as in Figure 1-9.

Table 1-2. Thermodynamic and kinetic properties of a typical molecule

Property	Value	Equation
Electron Affinity	0.68 eV = 65.6 kJ mol^{-1}	Both
k_{ec}	2.23 x 10^{-9} cc sec^{-1}	Both
$S_{anion} - S_{neutral}$	+39 J mol^{-1} K^{-1}	Miller
ΔS_{ni}	-3 J mol^{-1} K^{-1} (-0.71 e.u.)	Kebarle

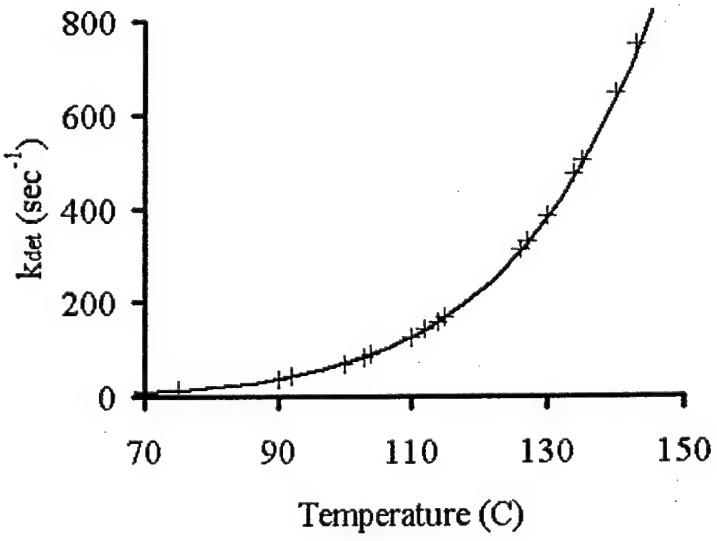

Figure 1-9. The solid line represents the values predicted by the Equation 1-36 (Miller); the (+) represents values predicted by Equation 1-34 (Kebarle).

As can be seen in Figure 1-9, both predictive equations could be used to model the same data. Ultimately, Miller's work in Equation 1-36, may prove more useful because of the possible confusion regarding the microcanonical treatment of Kebarle's work in Equation 1-34.

Methods for Measuring Resonance Electron Capture Rates

Electron capture rates can be studied under single or multiple collision conditions [62]. Examples of single collision experiments include electron transfer from Rydberg atoms, rare gas photoionization, reversal electron attachment, and crossed beam studies. Theses types of experiments involve the sample molecule interacting only with the incoming electron or Rydberg atom. On the other hand, multiple collision experiments involve the sample molecule reacting first with the incoming electron followed by numerous collisions with a third body. The PHPMS is a multiple collision experiment. Other examples of multiple collision experiments include electron swarm, Cavelleri electron density sampling, flowing afterglow, and pulsed radiolysis.

The Flowing afterglow with Langmuir Probe (FALP) has been used to successfully measure dissociative electron capture rates for some halogenated alkanes as well as resonance electron capture for SF_6 and Cl_2 [36, 37, 62-68].

In 1994, Knighton et al reported an innovative experiment using the PHPMS to measure electron capture rates for many substituted nitrobenzenes [20]. This study involved using a reference compound, R, and comparing it to the sample molecule, S, as in Equations 1-41 - 1-45:

$$R + e^- \xrightarrow{k_R} R^- \quad (1\text{-}41)$$

$$S + e^- \xrightarrow{k_S} S^- \quad (1\text{-}42)$$

$$I_{R^-} \propto k_R[R] \quad (1\text{-}43)$$

$$I_{S^-} \propto k_S[S] \quad (1\text{-}44)$$

$$k_s = k_R \frac{I_{S^-}[R]}{I_{R^-}[S]} \quad (1\text{-}45)$$

where I_x is the integrated mass spectrometry signal for compound X. Knighton used CH_3I for his reference compound. There are two requirements for a good reference compound. First it must have a well studied and accepted electron capture rate constant. Second, it must not react with the sample molecule in any way (i.e. no transfer of electrons from anions to neutrals). CH_3I has been well studied by FALP [64]. Further, the EA for CH_3I is ≈ 0.11 eV, well below the substituted nitrobenzene sample molecules which have EAs ranging from 0.92- 2.00 eV [20]. CH_3I undergoes dissociative electron capture to form I^-, and atomic iodine has an electron affinity ≈ 3.0 eV [69]. The electron affinity differences mean that no ion molecule electron transfer reactions should happen for the molecules in this experiment.

The experiments in Chapter 2 of this dissertation follow the same competitive model as Knighton et al used. However, SF_6 was used as the reference compound for reasons that are explained below.

The Suitability of SF_6 as a Surrogate

SF_6 is a truly unique molecule. It is thought to almost perfectly capture s-wave electrons [23]. It is a gas at room temperature, and experimentally, it is easy to work with. As a result, SF_6 has been extensively studied. Its electron capture rate constant is well known, $\approx 2.6 \times 10^{-7}$ cc sec^{-1} [24, 26, 37, 38, 63, 65, 70-72]. Its EA, ≈ 1.0 eV, is also well studied [73]. Also SF_6 seems to have a barrier to electron transfer reactions. This behavior was first reported by Grimsrud in 1985 [74]. In this PHPMS study, time profiles of SF_6^- were compared to time profiles of anions from various molecules with higher EAs than SF_6. Although electron transfer from SF_6^- to the higher EA molecule should occur on every collision (i.e. $k_c \approx 2.0 \times 10^{-9}$ cc sec^{-1}), Grimsrud noted these rate constants were $\leq 10^{-13}$ cc sec^{-1}. Recently, Neumaier reported, in a personal communication, the reverse of this phenomenon [75]. Anions and dianions from fullerenes like C_{76}, C_{78}, and C_{60} were trapped in an ion cyclotron mass spectrometer (ICR) with approximately 2×10^{-8} mTorr SF_6. The electron transfer to SF_6 was thermodynamically favored in each case, but no SF_6^- was seen. Reaction 1-46 is a typical example.

$$C_{78}^{2-} + SF_6 \rightharpoonup C_{78}^{1-} + SF_6^- \quad \Delta H \approx -0.8 \text{ eV} \qquad (1\text{-}46)$$

If the fullerene ions were accelerated in the ICR, the electron transfer reaction would eventually take place. But, the threshold was at about 2.0 eV.

Conclusion

Understanding the experiments that follow requires knowledge of several key points. First, the PHPMS was explained with special emphasis on how data are collected and examined. The plasma formed in the ion source complicates the behavior of ions and electrons as they diffuse to the walls. A discussion of ambipolar diffusion and the different types of plasmas, (i.e. electron dominated and ion dominated) was presented to clarify these issues. Various researchers have examined electron capture and the formation of long lived intermediates. Their work has been summarized to provide an introduction to the vocabulary and formalisms of this field. Finally, the role of the buffer gas and the high pressure limit has been explained both from a historic and a mathematical perspective. The next two chapters will present original research. In Chapter 2, electron capture rate constants and thermal detachment rate constants have been measured for several low EA molecules. Chapter 3 will answer a 30 year old mystery about why anions from these molecules are not seen at atmospheric conditions.

RESONANCE ELECTRON CAPTURE AND THERMAL DETACHMENT

Resonance electron capture and thermal electron detachment rate constants have been successfully measured of benzophenone, quinoxaline and anthracene. Typical of chemistry literature, these measurements will be presented in two sections: a) experimental, and b) results and discussion. The benzophenone discussion will chronicle the faulty assumptions that were overcome to successfully understand the data. The main results with less detailed discussions will follow for quinoxaline and anthracene. Finally, experiments on quinazoline will be presented showing the types of problems caused by background O_2. The quinazoline/O_2 problem will lead nicely into the experiments in Chapter 3.

Benzophenone

Benzophenone has a reported electron affinity of 0.61 eV [76]. Throughout this chapter the benzophenone anion will be abbreviated as BP^-. Benzophenone has a mass of 182 amu, and its structure is depicted in Figure 2-1.

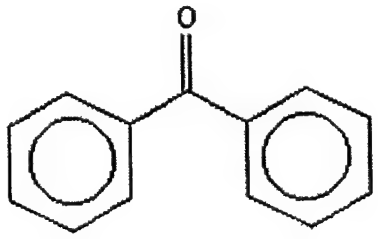

Figure 2-1. The molecular structure of benzophenone.

Experimental

The PHPMS was used for all experiments. The gas handling plant was prepared by injecting a solution of benzophenone in toluene. Injection amounts ranged from 1.31 x 10^{-5} – 1.73 x 10^{-4} moles of benzophenone which resulted in mixing ratios of 64.1 – 843 ppm in the buffer gas. The Clasius-Clapyeron equation was used to estimate vapor pressure limits for benzophenone in the gas handling plant, transfer line, and the ion source; injection amounts were limited to stay below the vapor pressure limit. Pure SF_6 was injected in amounts ranging from 2.10 x 10^{-7} – 1.11 x 10^{-4} moles which resulted in mixing ratios of 1.7 – 565 ppm in the buffer gas. SF_6 injection amounts were generally governed by the goals of each individual experiment.

Data were collected at source pressures ranging from 2-4 torr. All experiments involved taking mass spectra to determine which ions were present. Then, time profiles were taken for each ion present. Two types of experiments were conducted. The first type involved setting the ion source temperature and the benzophenone concentration and adding successive SF_6 injections. The second type involved setting the SF_6 and benzophenone concentrations and varying the ion source temperature.

Results and Discussion

The initial goal of this experiment was to duplicate the Knighton study [20] (detailed in Chapter 1), and mass spectra were recorded for a mixture of benzophenone and SF_6 as in Figure 2-2.

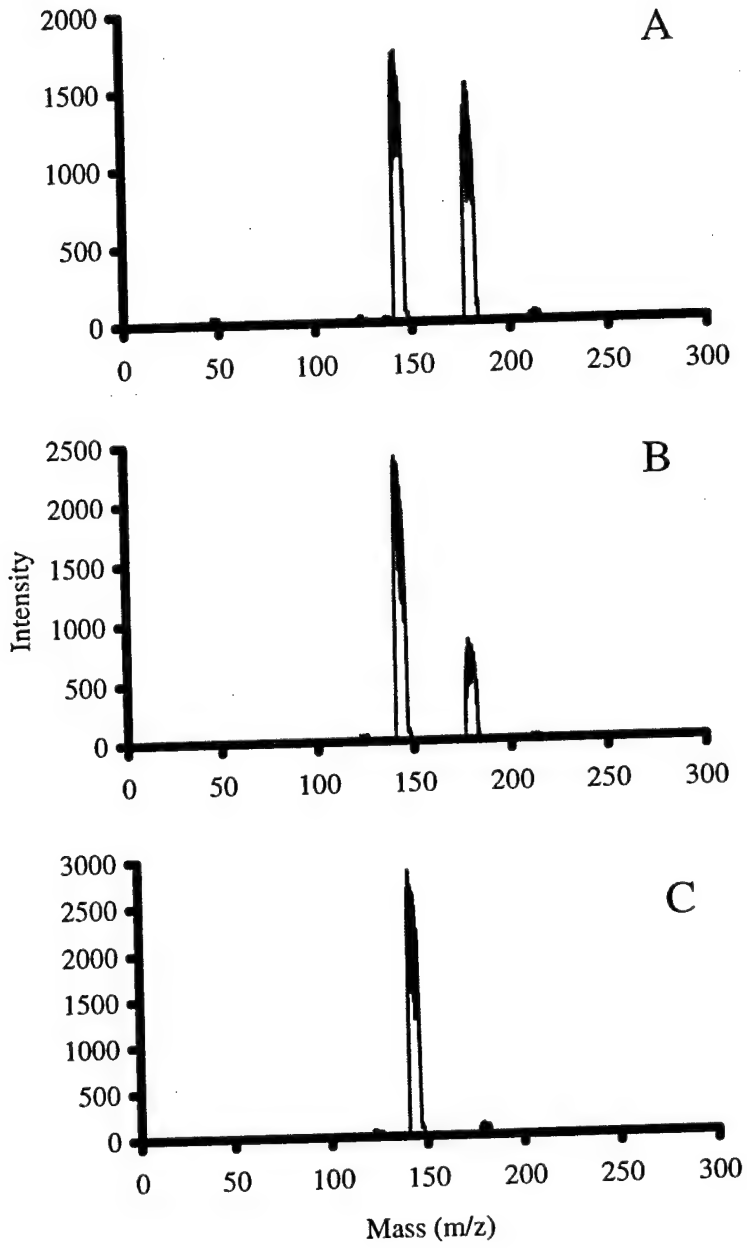

Figure 2-2. Mass spectra of benzophenone anion and SF_6^- at 3 torr. (A) T = 35°C, (B) T = 50°C, and (C) T = 75°C. The relative number density of the neutral benzophenone and SF_6 is the same in each spectra, but the temperature is different. Concentration of benzophenone ≈ 147 ppm , SF_6 ≈ 8.3 ppm (as a fraction of the buffer gas mixture).

Apparent Loss of BP^- to SF_6. As mentioned in Chapter 1, electron capture rates are believed to be insensitive to temperature in the range of this experiment. Therefore, the relative decrease in the benzophenone peak ($\frac{m}{z} = 182$) compared to the SF_6 peak ($\frac{m}{z} = 146$) as temperature increases is indicative of electron transfer as in Reaction 2-1.

$$BP^- + SF_6 \xrightarrow{k_{transfer}} BP + SF_6^- \qquad (2\text{-}1)$$

Time profiles often reveal if an ion is being consumed or produced, and Figure 2-3 contains the time profiles for the ions in Figure 2-2 (B).

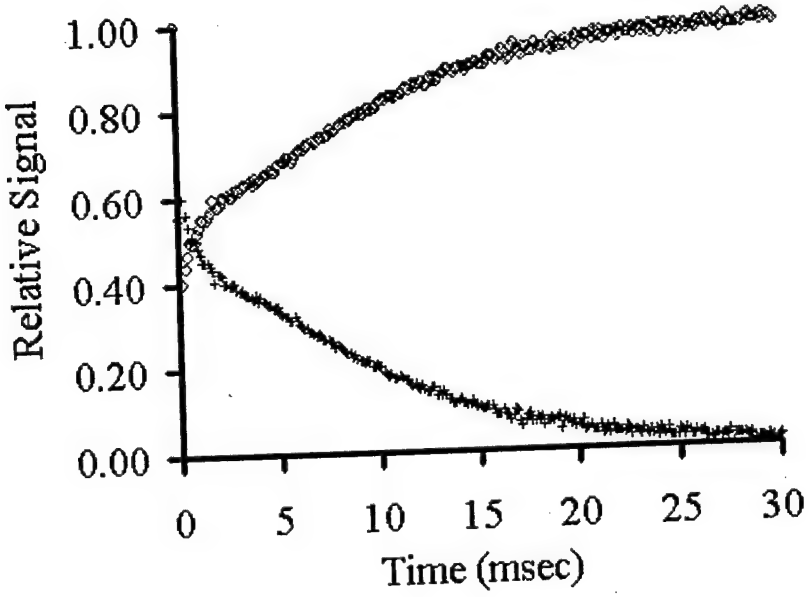

Figure 2-3. Normalized time profile of BP^- (+) and SF_6 (o) taken from data collected under the same conditions as the mass spectrum in Figure 2-2 (B). These data strongly suggest that BP^- is being lost while SF_6^- is being produced.

Recall from Chapter 1 that SF_6 was specifically chosen as a surrogate because of independent experimental evidence that it does not undergo Reaction 2-1. However, the time profiles in Figure 2-3 clearly indicate BP^- is being lost while SF_6^- is being produced. In order to verify if Reaction 2-1 was actually occurring or not, standard kinetic experiments were conducted by adding successive SF_6 injections to a given benzophenone concentration at a set ion source temperature. The first order loss of BP^- was calculated for each SF_6 concentration, and the second order $k_{transfer}$ rate constant was calculated as in Equation 2-2:

$$k_{transfer} = \frac{k'}{[SF_6]} \tag{2-2}$$

where k' is the psuedo first order loss of BP^-. For a brief mathematical review of psuedo first order kinetics, see Appendix B. The results, in Figure 2-4, indicate that the loss of BP^- to SF_6 is not a second order process. If it were second order, $k_{transfer}$ would be constant for all SF_6 concentrations. So, what is happening to the BP^- ? As shown in Reactions 1-1 and 1-7, electron capture is a reversible process. A detached electron can be recaptured by benzophenone (and re-detached ad infinitum), or it can be captured by SF_6. SF_6^- does not appear to detach electrons in the temperature range of these experiments. Therefore, once a detached electron is scavenged by SF_6, it is lost.

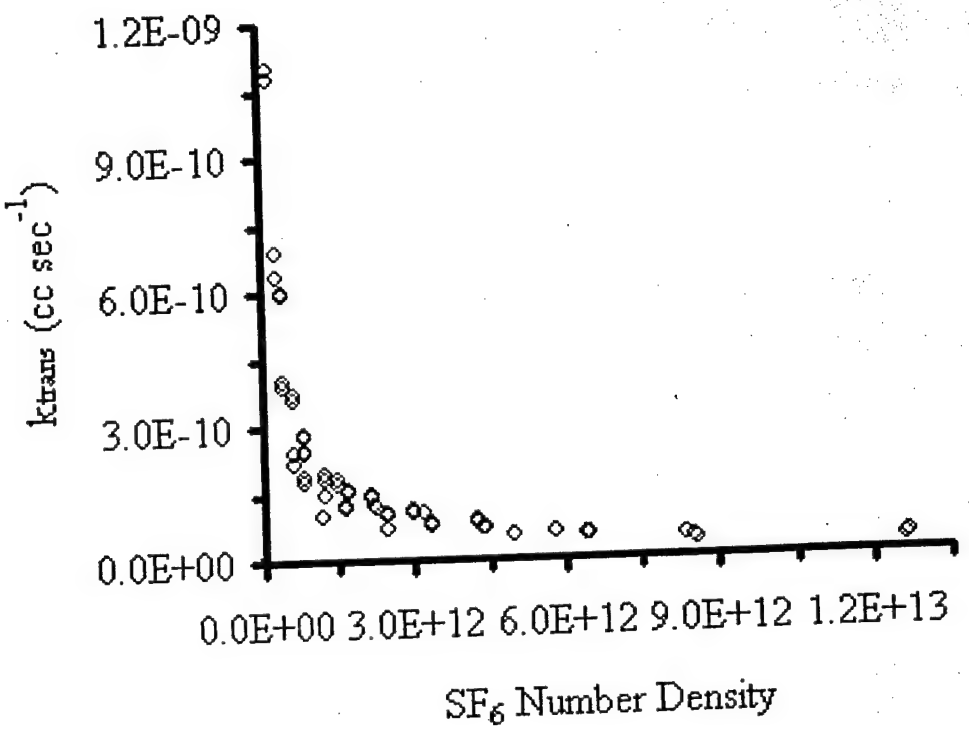

Figure 2-4. The calculated 2nd order rate constant for the direct electron transfer reaction $BP^- + SF_6 \rightleftharpoons BP + SF_6$ as a function of SF_6 number density. If this process were actually occurring, the 2nd order rate constant would not decrease with increasing SF_6 number density.

In this case, Reaction 2-3 correctly describes the chemistry:

$$BP^- \underset{k_{ec}}{\overset{k_{det}}{\rightleftharpoons}} BP + e^- \overset{k_a[SF_6]}{\rightharpoonup} SF_6^- \qquad (2\text{-}3)$$

where k_a is the electron capture rate constant for SF_6.

Time Profile Data and Differential Equations Model. The thermal electron detachment problem just described makes the mass spectra data almost worthless for

calculating the electron capture rate constant for benzophenone. However, examining the time profiles revealed a very interesting result as in Figure 2-5.

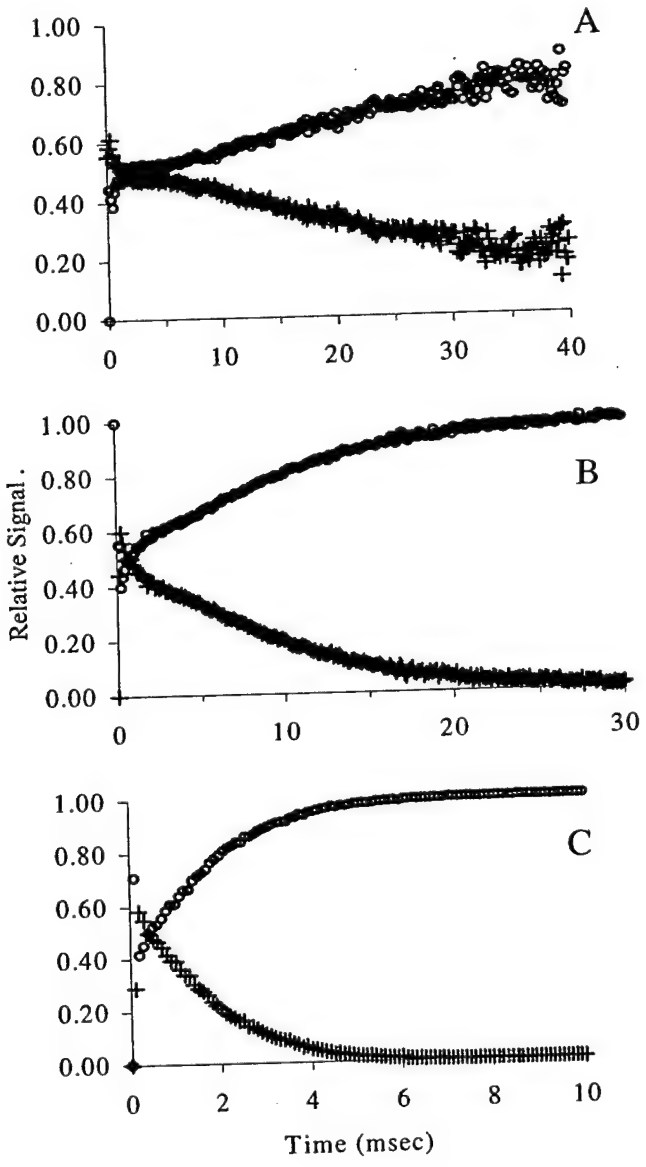

Figure 2-5. Time profiles of BP^- (+) and SF_6^- (o), taken under the same conditions as the mass spectra in figure 2-2. (A) T = 35°C, (B) T = 50°C, and (C) T = 75°C. Although the BP^- decays away faster at higher temperatures, the relative initial populations of BP^- and SF_6^- is not affected by temperature.

The initial concentrations of BP^- and SF_6^- are essentially not affected by the ion source temperature. But, the rate of Reaction 2-3 is affected by the temperature. At 35°C, the BP^- is not depleted after 40 msec. At 50°C, the BP^- population is depleted after 30 msec, and at 75°C, the BP^- population is depleted after 10 msec. This result is encouraging because the initial concentrations might be useful for calculating the electron capture rate constant using Equation 1-45.

To determine whether the result in Figure 2-5 was due to actual chemistry or just an artifact of the PHPMS instrument, the experiment was modeled with the IBM Kinetic Simulator. This software package is a stochastic differential equation solver. The diffusion rates for SF_6^- and BP^- were assumed to be the same. Table 2-1 shows the electron capture and thermal detachment rate constants required for the IBM Kinetic Simulator to match time profiles from the experimental data taken at 2 and 3 Torr and the temperatures indicated. The benzophenone concentration was ≈ 147 ppm, and the SF_6 concentration was ≈ 8.3 ppm (as a fraction of the buffer gas mixture).

Table 2-1. Parameters used for the IBM Kinetic Simulator

Temperature (°C)	k_{det} (sec^{-1})	k_{ec} ($cc\ sec^{-1}$)
40	50	1.50×10^{-8}
46	120	1.50×10^{-8}
51	200	1.50×10^{-8}
55	285	1.50×10^{-8}

Table 2-1 continued

Temperature (°C)	k_{det} (sec^{-1})	k_{ec} ($cc\ sec^{-1}$)
60	400	1.50×10^{-8}
65	575	1.50×10^{-8}
69	750	1.50×10^{-8}
75	1100	1.50×10^{-8}

In summary, the IBM kinetic simulation program showed that the initial populations of each ion were directly proportional to the product of the assigned electron capture rate constant and the number density of the neutral species. Therefore, the information from the early part of the time profiles about relative concentration can be used in Equation 1-45 to calculate the electron capture rate constant for benzophenone. The other lesson learned from these simulations is that the disappearance of BP^- is related to the thermal electron detachment rate constant and the relative amounts of SF_6 and benzophenone that are present.

As outlined in Chapter 1, in the first few msec of the ion time profiles, the plasma in the ion source is electron dominated. During this time, the negative ions are essentially bottled in the ion source (i.e. $k_{diff} \approx 0$) and the electrons are diffusing to the wall. Unfortunately, this early region in the time profile contains the data needed to calculate the electron capture rate constant. To overcome this problem, the initial populations of BP^- and SF_6^- were extrapolated from logarithmic time profiles as in Figure 2-6.

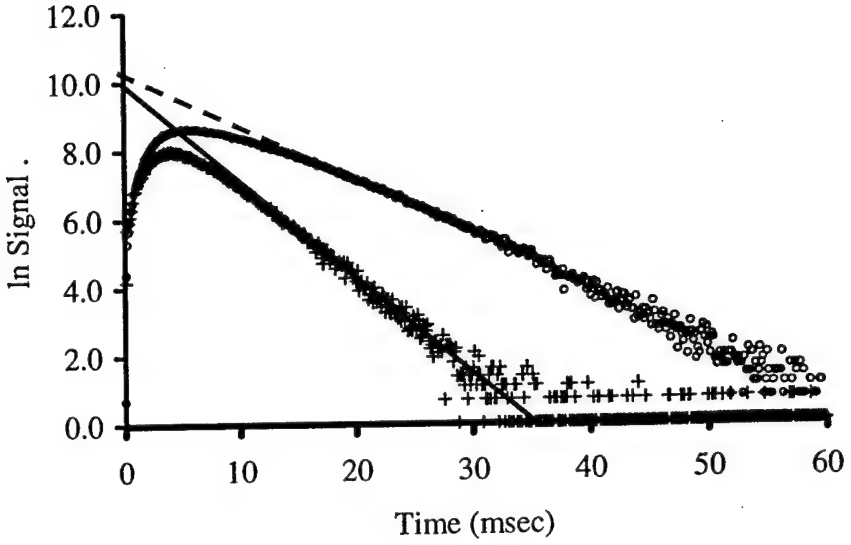

Figure 2-6. Logarithmic time profiles of BP^- (+) and SF_6^- (o) demonstrating the technique for extrapolating the initial number densities of each ion.

Experiments were then conducted at various temperatures, pressures and concentrations of SF_6 and benzophenone. The measured electron capture rate constants are in Figure 2-7.

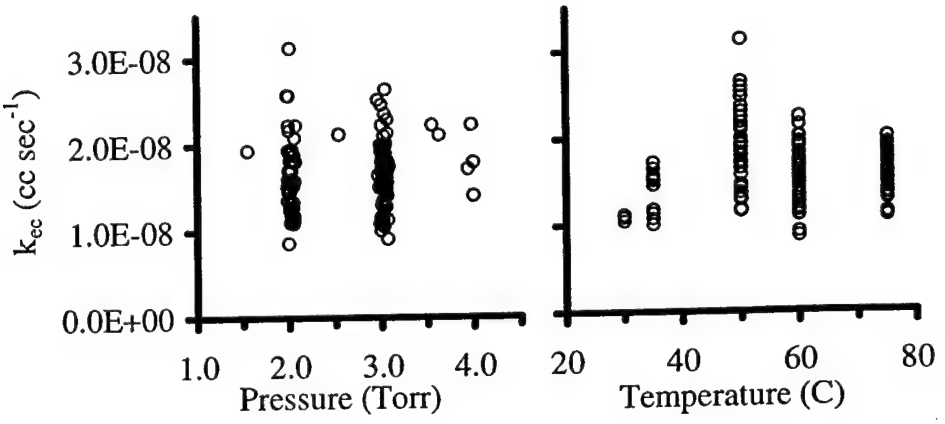

Figure 2-7. Measured electron capture rate constants for benzophenone. These data were collected at various temperatures, pressures, and relative concentrations of SF_6 and benzophenone.

The average resonance electron capture rate for benzophenone is 1.65×10^{-8} cc sec^{-1}. Note that the electron capture rate constant appears to be independent of temperature. It is also independent of pressure which indicates the experiments are being done in the high pressure limit. Further, k_{ec} values calculated from normalized time profile data were essentially the same as the values shown in Figure 2-7.

Failure of Model at Low Number Densities. The next experimental goal was to measure the thermal electron detachment rate at various pressures. Appendix C contains a detailed mathematical workup of the differential equations that describe BP^- and the electrons. Equation 2-4 is the result of integrating and algebraically manipulating the differential equation. Also, the following three assumptions were invoked: 1) the electrons are in a steady state, 2) no electrons are being lost to diffusions, and 3) no impurities are present.

$$-\left(\frac{\Delta ln[BP^-]}{\Delta t} + k_{diff}\right)^{-1} = \frac{k_{det}k_a}{k_{ec}}\frac{[M]}{[SF_6]} + \frac{1}{k_{det}} \qquad (2\text{-}4)$$

The term in the left hand side of this equation has experimental meaning. On a logarithimic plot of the time profile, $\frac{\Delta ln[BP^-]}{\Delta t}$ represents the slope of the line as in Figure 1-3. This observed first order loss is the result of BP^- both diffusing to the wall and being lost to thermal electron detachment followed by electron scavenging by SF_6 as

shown in reaction 2-3 above. So, the term $\frac{\Delta ln[BP^-]}{\Delta t} + k_{diff}$, represents the observed chemical loss of BP^-. To make Equation 2-4 less cumbersome the term k_{loss} has been invented as in Equations 2-5 and 2-6.

$$-\left(\frac{\Delta ln[BP^-]}{\Delta t} + k_{diff}\right) = k_{loss} \qquad (2\text{-}5)$$

$$(k_{loss})^{-1} = \frac{k_{det}k_a}{k_{ec}}\frac{[M]}{[SF_6]} + \frac{1}{k_{det}} \qquad (2\text{-}6)$$

This equation is convenient because it should be linear for a given temperature. Once the y intercept is established, it can be used in conjunction with the slope to calculate the electron capture rate constant, k_{ec}. Remember, k_a (2.6×10^{-7} cc sec^{-1}) is the electron capture rate constant for SF_6. Typical results are shown in Figure 2-8. The prediction line was created by using the average k_{ec} value measured in Figure 2-7, and estimations of k_{det} from the IBM Kinetic Simulator program. The data in Figure 2-8 are interesting for two reasons. First, at higher relative SF_6 concentrations, $\frac{[BP]}{[SF_6]} \leqslant 20$, the data match the prediction line. However, at lower SF_6 concentrations the observed k_{loss} is higher than

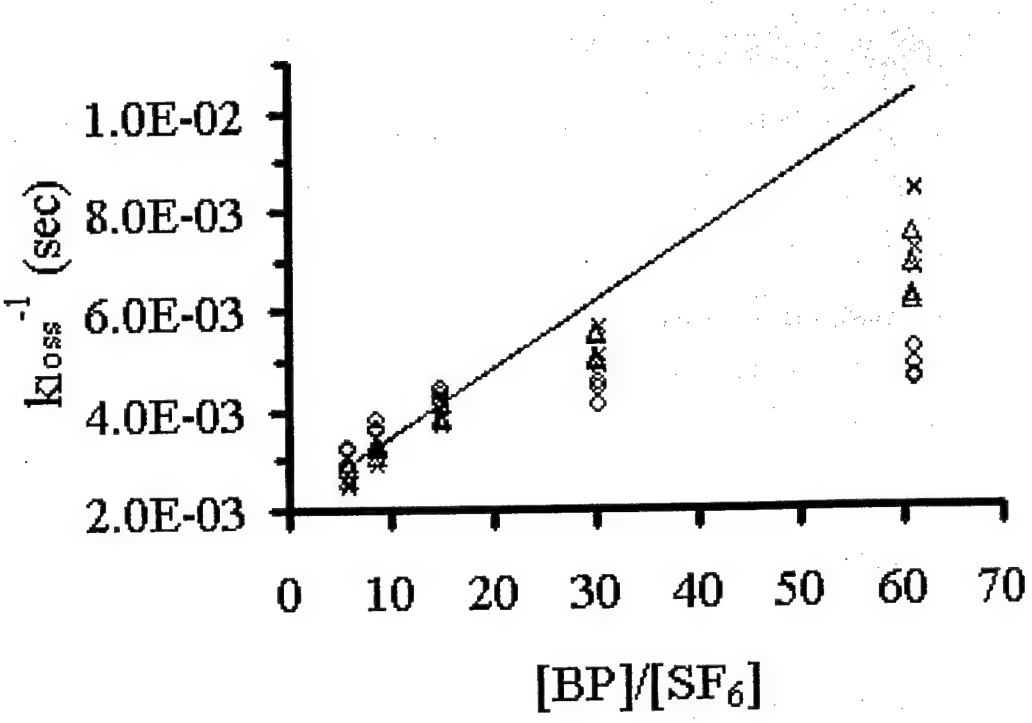

Figure 2-8. A plot of Equation 2-4. Data were collected at 60°C and 2 –3 Torr at various relative SF_6 and benzophenone concentrations as indicated on the graph. The line is predicted for $k_{ec} = 1.65 \times 10^{-8}$ cc sec^{-1} and $k_{det} = 450$. Benzophenone number densities (as a fraction of the buffer gas mixture) (o) 212 ppm, (Δ) 423 ppm, and (x) 843 ppm. SF_6 concentrations can be deduced by dividing the X axis value into the given benzophenone concentration.

predicted by Equation 2-6 (note that in Figure 2-8, the y axis is the inverse of k_{loss}). Second, the data represented by (Δ) and (x) represent experimental conditions where the total number densities of benzophenone and SF_6 are 2 times and 4 times greater than the experiment represented by (o). The (Δ) and (x) higher number density data are closer to the prediction line than the (o) lower number density data. This result suggests that one or more of the assumptions listed above are incorrect. For example, what if some of the electrons were being lost to diffusion? In this case, k_{loss} would be higher than predicted

especially in experimental conditions where the number density of electron capturing species was low.

The New Model with Electron Diffusion. While the linear model does not appear useful for presenting data, it was very useful for revealing this faulty assumption. Equation 2-7 is the complete integrated equation describing BP^- in time.

$$ln[M^-]_t = \left(\frac{k_{ec}k_{det}[M]}{k_{ec}[M] + k_{ediff} + k_a[SF_6]} - k_{det} - k_{diff} - k_{col}[X] \right) t + ln[M^-]_0 \quad (2\text{-}7)$$

This equation is also derived in Appendix C and involves a steady state treatment of the electrons. Equation 2-7 can be used to predict the slope of the logarithmic plot for a BP^- time profile. The only unknown parameters are the electron diffusion rate, k_{ediff}, and the concentration of high EA impurities, [X].

Attempts to rigorously measure the electron diffusion rate constant where not successful. However, using data from experiments with benzophenone and SF_6 at 60°C, and Equation 2-7, k_{ediff} was calculated for each data point. Figure 2-9 displays these results in a historgram. At 4 Torr and 60°C, k_{ediff} is probably between 1×10^4 and 1×10^5 sec^{-1}.

Figure 2-10 is a comparison of predicted values for the BP^- versus actual measured values. These experiments were done over a wide range of SF_6 and benzophenone concentrations.

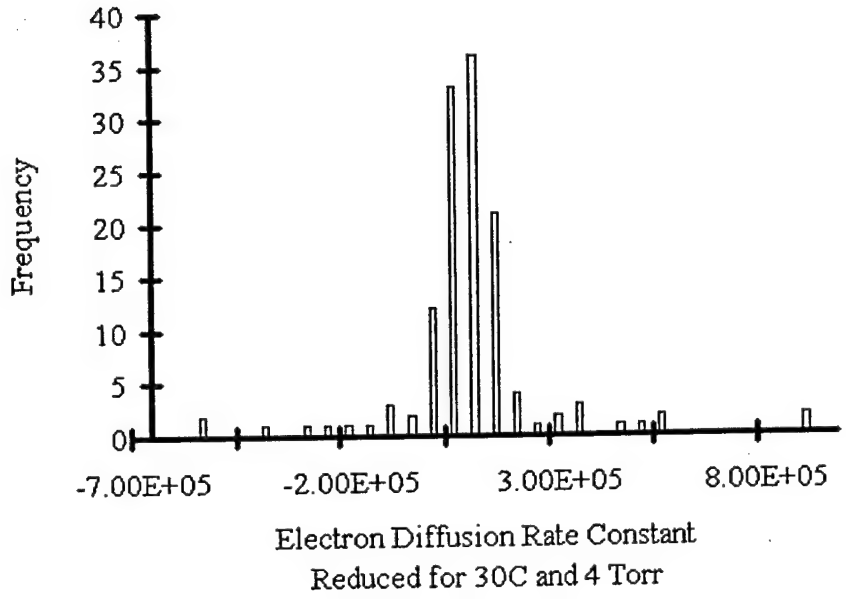

Figure 2-9. A histogram of reduced electron diffusion rate constants from experiments with benzophenone and SF_6 at 60°C.

Data were collected at buffer gas pressures of primarily 2 and 3 Torr. The temperature ranged from 35-75°C; k_{det} for each temperature was estimated from experiments where the number densities of SF_6 and benzophenone were high, and the linear model was approximately correct. The data points above 750 have significantly more spread than the points between 200 and 600. The >750 data were collected at 75°C where k_{det} is high. As a result, the number of linear data points on the logarithmic time profile is limited, and the uncertainty of measured slopes is higher than the lower temperature experiments. The k_{ediff} value was approximated to be 5×10^4 sec^{-1} (at 30°C and 4 Torr). Also, an impurity peak, probably from chlorobenzophenone, was noted at $\frac{m}{z} = 217$. To account for this peak, [X] was estimated to be $\approx 0.025\%$ of the benzophenone concentration.

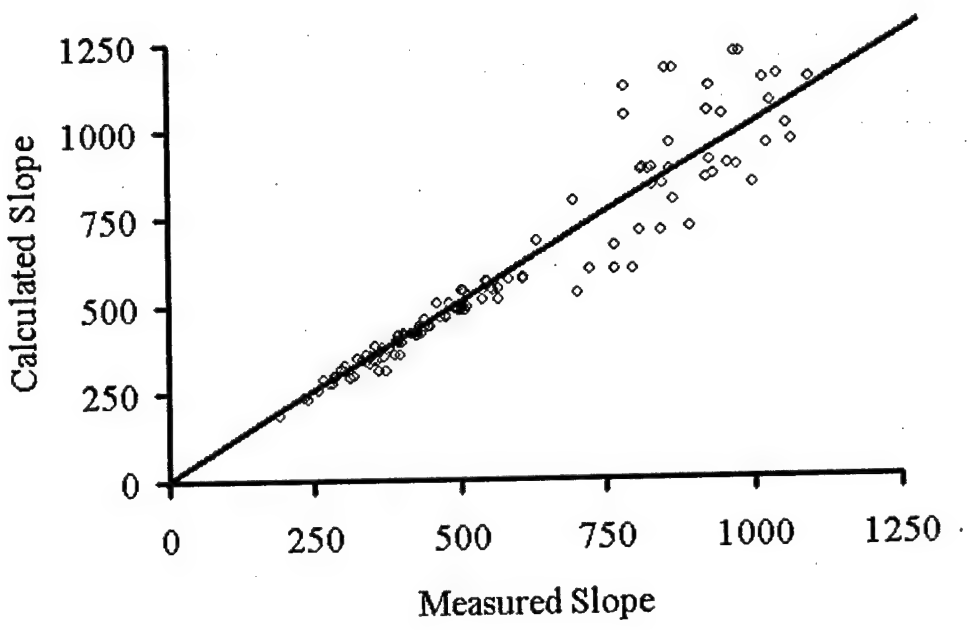

Figure 2-10. A comparison of benzophenone data versus calculated values of Equation 2-7 when the following parameters are used: kec = 1.65 x 10^{-8} cc sec^{-1}, k_{diff} = 92.7 sec^{-1} (4 torr, 30C), k_{ediff} = 5 x 10^{4} sec^{-1} (4 torr, 30°C). Data were collected from 35 -75°C and 2-3 Torr, k_{det} = 250, 450, 1200 was estimated for each data point based on previous experiments where SF_6 was in great excess. Electron transferring impurity ≈ 0.025% of the benzophenone number density.

Predictions of Thermal Detachment. Equation 1-34 put forth by Kebarle [55], and Equation 1-36 put forth by Miller [17, 56], can both be used to predict thermal electron detachment rate constants as a function of temperature. Table 2-2 shows the thermodynamic values used for the Miller and Kebarle equations to predict the data. Figure 2-11 compares measured thermal detachment rate constants to predicted values from both the Kebarle and the Miller equations.

Table 2-2. Thermodynamic and kinetic properties of benzophenone

Property	Value	Equation
Electron Affinity	0.61 eV = 58.9 kJ mol^{-1}	Both
k_{ec}	1.65 x 10^{-8} cc sec^{-1}	Both
$S_{anion} - S_{neutral}$	+38.5 J mol^{-1} K^{-1}	Miller
ΔS_{ni}	-3.3 J mol^{-1} K^{-1} (-.79 e.u.)	Kebarle

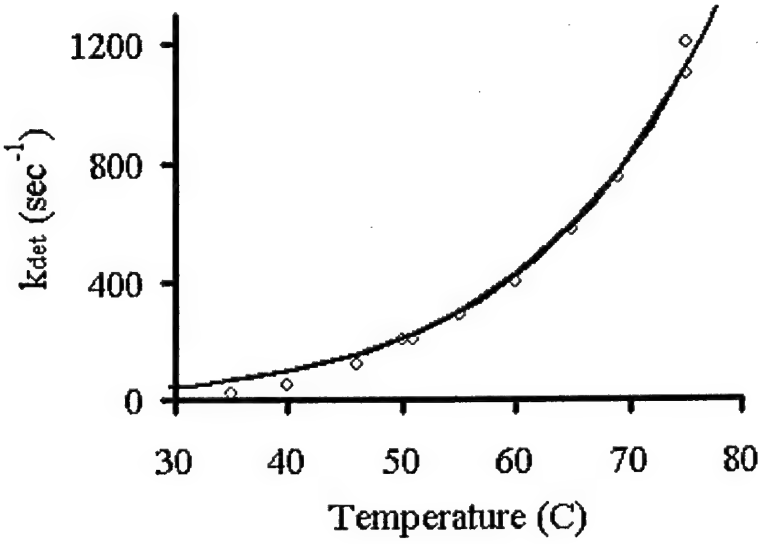

Figure 2-11. Thermal electron detachment predictions for BP^- using the Kebarle and Miller equations with the parameters in Table 2-2. (o) are measured data for BP^-. The solid lines which lie almost on top of each other are the predictions from each equation.

Efforts to Stabilize BP^- with SiF_4

Williamson et al has reported a clustering reaction between BP^- and SiF_4 as indicated in Reaction 2-8 [77].

$$BP^- + SiF_4 \rightleftharpoons (BP \bullet SiF_4)^- \qquad (2\text{-}8)$$

Williamson suggests that this reaction lies far enough to the right that it might stop thermal electron detachment. If this hypothesis is true, electron capture rate constants for benzophenone could be measured by comparing the $(BP \bullet SiF_4)^-$ peak ($\frac{m}{z} = 286$) with the SF_6 peak in typical mass spectra as in Figure 2-12. Comparing the spectra in Figure 2-12 A and B, shows that SiF_4 does protect BP^- from thermal electron detachment. But, comparing the spectra in Figure 2-12 B and C reveals that the $(BP \bullet SiF_4)^-$ peak is relatively larger at lower temperatures. This increased signal implies that Reaction 2-8 is not shifted completely to the right as suggested by Williamson. And while SiF_4 is useful for qualitatively detecting BP^- at high temperatures, it is not useful for quantitative electron capture rate constant determinations.

Quinoxaline

Quinoxaline has a reported electron affinity of 0.68 eV [76]. Throughout this chapter the quinoxaline anion will be abbreviated Qx^-. Quinoxaline has a mass of 130 amu, and its structure is depicted in Figure 2-13.

Experimental

The PHPMS was used for all experiments. The gas handling plant was prepared by injecting a solution of quinoxaline in toluene. Injection amounts ranged from 1.27 x 10^{-5} – 7.52 x 10^{-3} moles of quinoxaline which resulted in mixing ratios of 61 ppm – 36.8 ppt in the buffer gas.

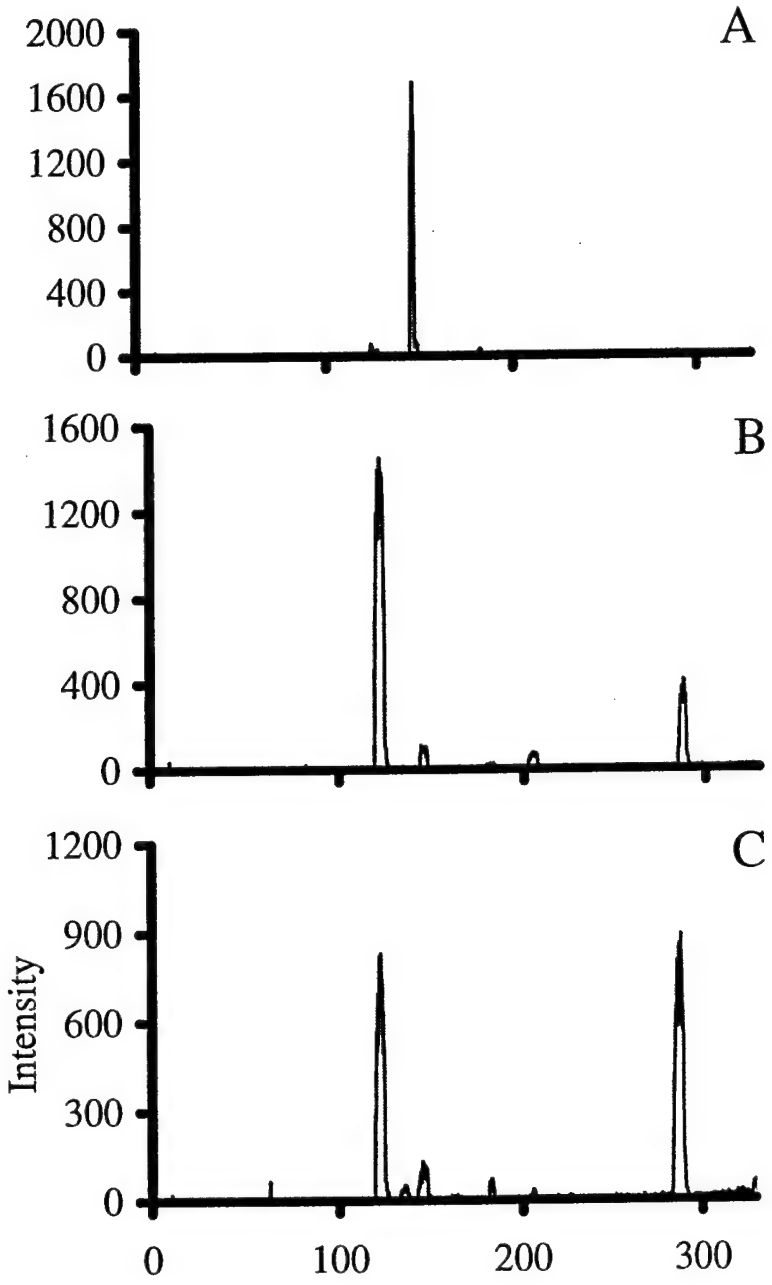

Figure 2-12. Mass spectra for the $(BP \bullet SiF_4)^-$ experiment. Spectrum A is at 90°C with 416 ppm benzophenone and 26 ppm SF_6. Spectrum B is the addition of 18.4 ppm SiF_4. Spectrum C is the same mixture at 61°C

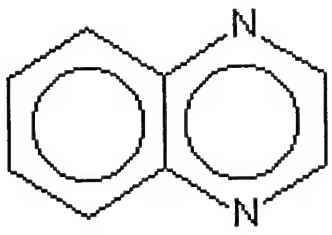

Figure 2-13. The molecular structure of quinoxaline.

The Clasius-Clapyeron equation was used to estimate vapor pressure limits for quinoxaline in the gas handling plant, transfer line, and the ion source; injection amounts were limited to stay below the vapor pressure limit. Pure SF_6 was injected in amounts ranging from $6.98 \times 10^{-7} - 1.85 \times 10^{-5}$ moles which resulted in mixing ratios of 0.3 – 94 ppm in the buffer gas. SF_6 injection amounts were generally governed by the goals of each individual experiment.

Data were collected at source pressures ranging from 2-4 torr. All experiments involved taking mass spectra to determine which ions were present. Then, time profiles were taken for each ion present. Two types of experiments were conducted. The first type involved setting the ion source temperature and the quinoxaline concentration and adding successive SF_6 injections. The second type involved setting the SF_6 and quinoxaline concentrations and varying the ion source temperature.

Results and Discussion

Similar to benzophenone, electron capture rate constants were calculated for quinoxaline by extrapolating the initial relative concentrations of Qx^- and SF_6^- from

logarithmic time profiles. Figure 2-14 shows the calculated rate constants versus pressure and temperature.

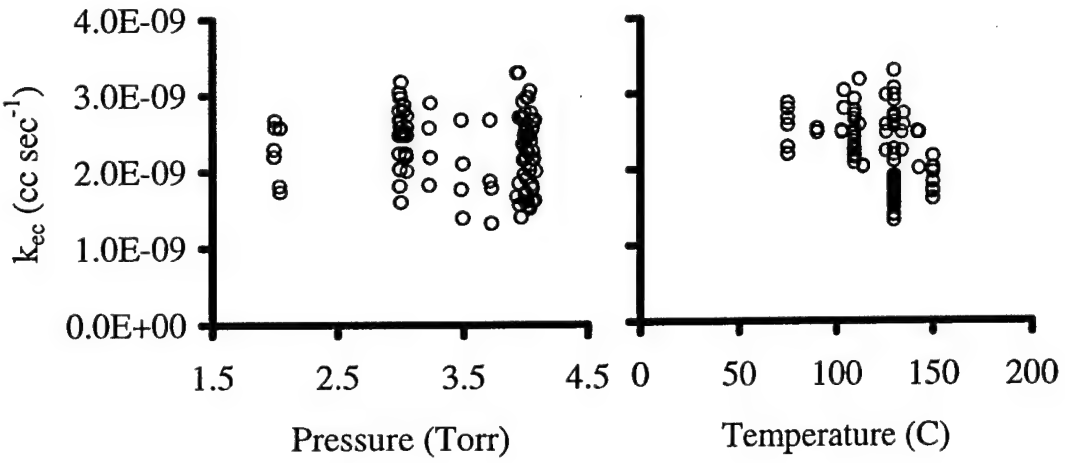

Figure 2-14. Measured electron capture rate constants for quinoxaline. These data were collected at various temperatures, pressures, and relative concentrations of SF_6 and quinoxaline.

Similar to benzophenone, the quinoxaline experiments appear to be in the high pressure limit, and the electron capture rate does not seem to vary with temperature. The average electron capture rate is 2.31×10^{-9} cc sec^{-1}. Even though the EA of quinoxaline is approximately 0.07 eV higher than benzophenone, quinoxaline captures electrons about seven times slower.

Equation 2-7 can also be used to compare the measured sloped of the Qx^- logarithmic time profiles to predicted values as shown in Figure 2-15. As might be expected, the same reduced electron diffusion rate constant used for the benzophenone experiments also works reasonable well to explain the quinoxaline data.

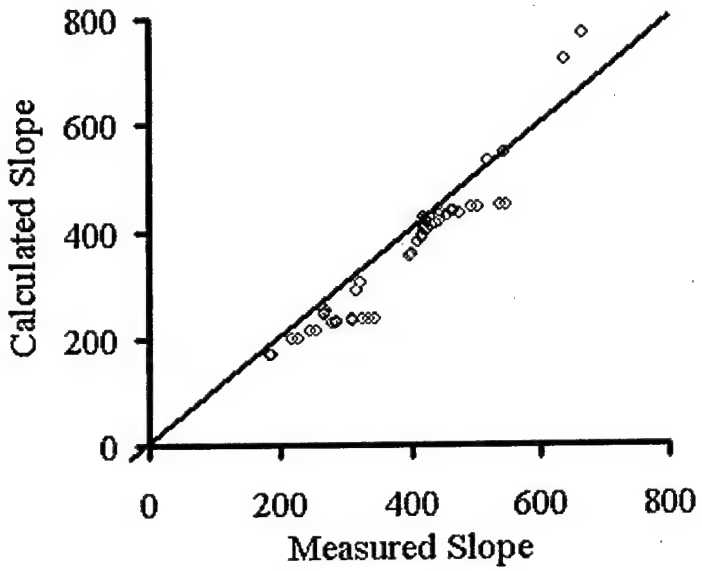

Figure 2-15. A comparison of the quinoxaline data versus calculated values of Equation 2-7 when the following parameters are used: $k_{ec} = 2.31 \times 10^{-9}$ cc sec^{-1}, $k_{diff} = 92.7$ sec^{-1} (4 torr, 30C), $k_{ediff} = 5 \times 10^{4}$ sec^{-1} (4 torr, 30C) Data were collected from 75°-145°C and 2-4 Torr, k_{det} was estimated for each data point based on previous experiments were SF_6 was in great excess.

The thermal electron detachment rate constants can also be calculated using the Kebarle or Miller equations, Equations 1-34 and 1-36 respectively, with the parameters in Table 2-3.

Table 2-3. Thermodynamic and kinetic properties of quinoxaline

Property	Value	Equation
Electron Affinity	0.68 eV = 65.6 kJ mol^{-1}	Both
k_{ec}	2.31×10^{-9} cc sec^{-1}	Both
$S_{anion} - S_{neutral}$	+39 J mol^{-1} K^{-1}	Miller
ΔS_{ni}	-3.0 J mol^{-1} K^{-1} (-0.72 e.u.)	Kebarle

Figure 2-16 compares measured thermal electron detachment rate constants with predictions from the Kebarle and Miller Equations.

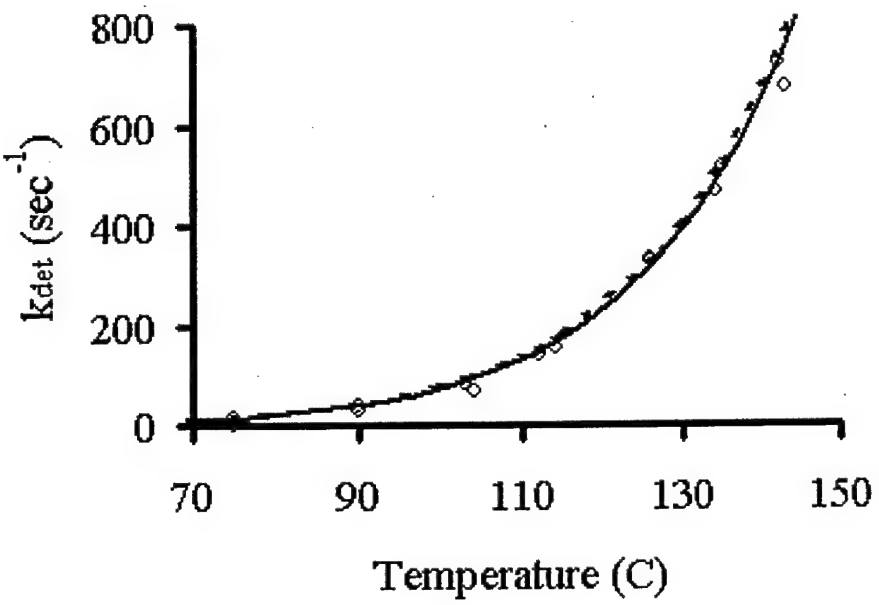

Figure 2-16. Thermal electron detachment predictions for Qx^- using the Kebarle and Miller equations with the parameters in Table 2-3. (o) are measrured data for Qx^-. The dashed line is from the Kebarle equation, and solid line is from the Miller equation

While quinoxaline captures electrons slower than benzophenone, comparing Figures 2-16 and 2-11 reveals that quinoxaline also detaches electrons much more slowly than benzophenone.

Anthracene

Anthracene has a reported electron affinity of 0.54 eV [76]. Throughout this chapter the anthracene anion will be abbreviated as A^-. Anthracene has a mass of 178 amu, and its structure is depicted in Figure 2-17.

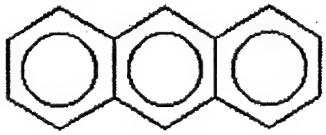

Figure 2-17. The molecular structure of anthracene.

Experimental

The PHPMS was used for all experiments. The gas handling plant was prepared by injecting a saturated solution of anthracene in toluene. Injection amounts ranged from $2.24 \times 10^{-6} - 3.59 \times 10^{-5}$ moles of anthracene which resulted in mixing ratios of 10.6 – 196.2 ppm in the buffer gas. The Clasius-Clapyeron equation was used to estimate vapor pressure limits for anthracene in the gas handling plant, transfer line, and the ion source; injection amounts were limited to stay below the vapor pressure limit. Pure SF_6 was injected in amounts ranging from $5.39 \times 10^{-8} - 7.02 \times 10^{-7}$ moles which resulted in mixing ratios of 0.3 – 3.6 ppm in the buffer gas. SF_6 injection amounts were generally governed by the goals of each individual experiment.

Data were collected at source pressures ranging from 2-4 torr. All experiments involved taking mass spectra to determine which ions were present. Then, time profiles were taken for each ion present. Experiments involved setting the SF_6 and anthracene concentrations and varying the ion source temperature.

Results and Discussion

Electron capture rate constants were measured in the same fashion as benzophenone and quinoxaline. However, the logarithmic time profiles of A^- appeared abnormal at higher pressure as shown in Figure 2-18.

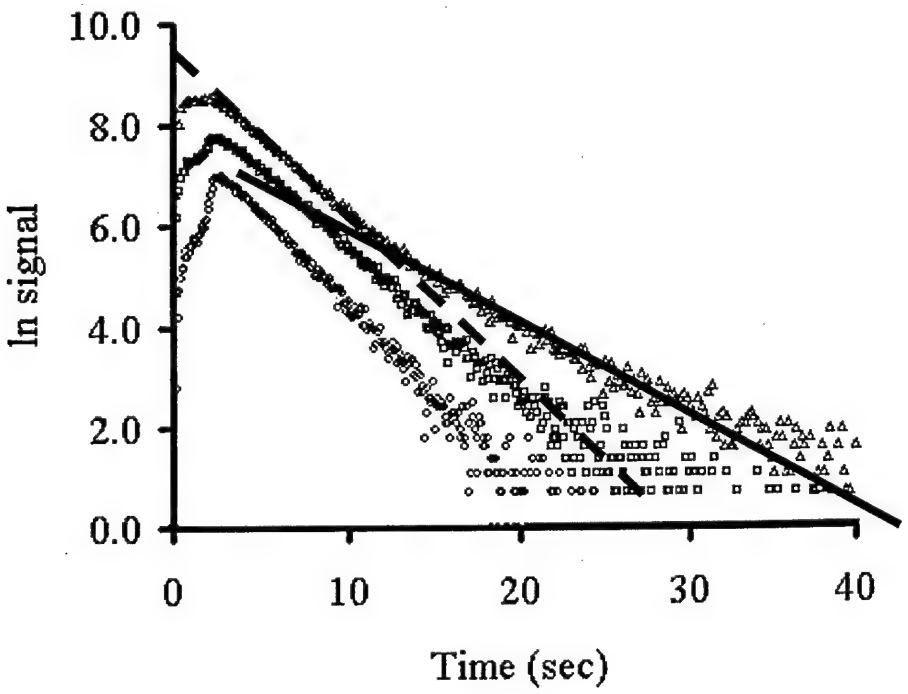

Figure 2-18. Time profiles of A^- at 2 Torr (o), 3 Torr ( ), and 4 Torr (Δ) demonstrating the non-linear behavior as pressure increases. The full and dashed lines show indicate how the 4 torr data might consist of time profiles from two different anions.

The time profiles in Figure 2-18, suggest that an impurity with the same unit mass as anthracene could be present in the sample.

Close examination of the 4 Torr data reveals that from about 5-10 msec the logarithmic time profile is linear with a slope given by the dashed line. After 15 msec, the logarithmic time profile is linear with a less steep slope given by the solid line. This flattening of the time profile lowers the extrapolated value for the initial concentration of A^-. Because this flattening is more prevalent at higher pressures, the measured electron capture rate constants appear to have a negative pressure dependence as shown in Figure 2-19.

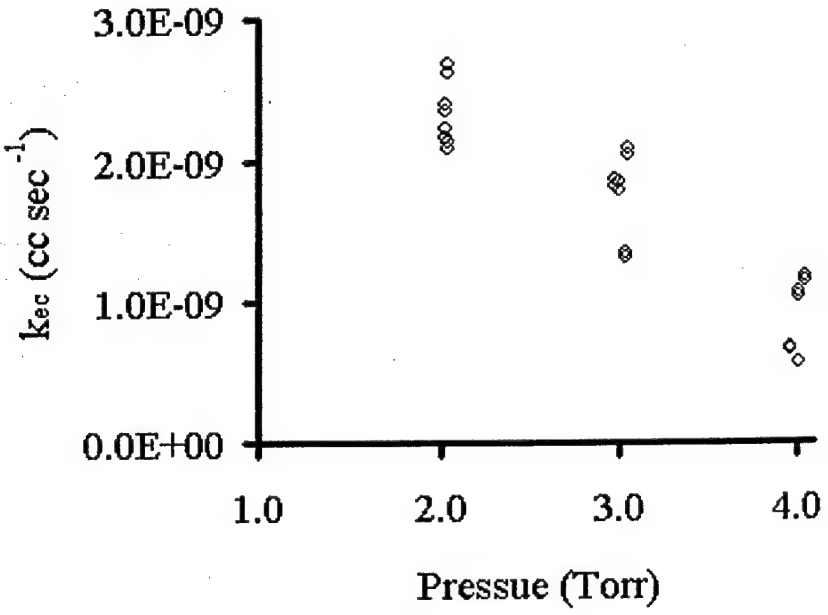

Figure 2-19. Calculated electron capture rate constants calculated from the logarithmic time profiles for anthracene.

Efforts were made to identify the phantom impurity. High resolution mass spectra revealed a peak at 179 amu, but this peak is explained by the carbon 13 isotope. The resolution of the PHPMS quadrupole mass spectrometer was not good enough to conduct more meaningful experiments.

As will be shown in Chapter 3, it is also possible for A^- to react with O_2 and H_2O to form various cluster products. These clustering reactions are reversible. So, another explanation for the non-linear behavior in Figure 2-18 is that the reverse cluster reactions are replenishing the A^- population. However, mass spectra for these experiments showed very low intensity signals for these cluster products.

In summary, extrapolating the initial concentrations of SF_6^- and A^- from the logarithmic time profiles does not appear to work for anthracene like it did for benzophenone and quinoxaline. To solve this problem, normalized time profiles for benzophenone and quinoxaline were compared with the logarithmic time profiles. And for both of these molecules the electron capture rate constants calculated from the logarithmic time profiles were in good agreement with those calculated from normalized time profiles. Normalized time profiles for anthracene from the same data that lead to Figure 2-19 were used to calculate the electron capture rate constants shown in Figure 2-20.

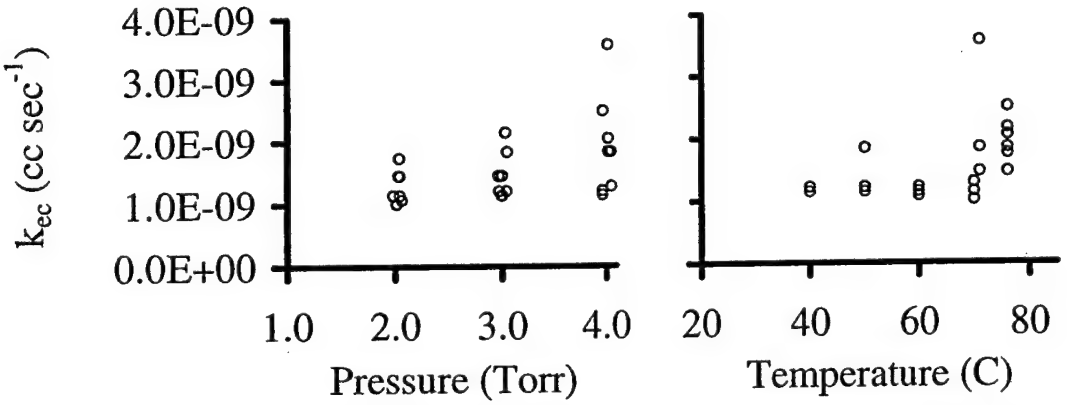

Figure 2-20. Measured electron capture rate constants for anthracene. These data were collected at various temperatures, pressures, and relative concentrations of SF_6 and anthracene.

As can be seen by comparing Figures 2-19 and 2-20 the normalized time profiles lead to more behaved electron capture rate constants. The average $k_{ec} = 2.09 \times 10^{-9}$ cc sec^{-1}. As with benzophenone and quinoxaline, Equation 2-7 can be used to predict the slope of the logarithmic time profiles for a given set of parameters as in Figure 2-21.

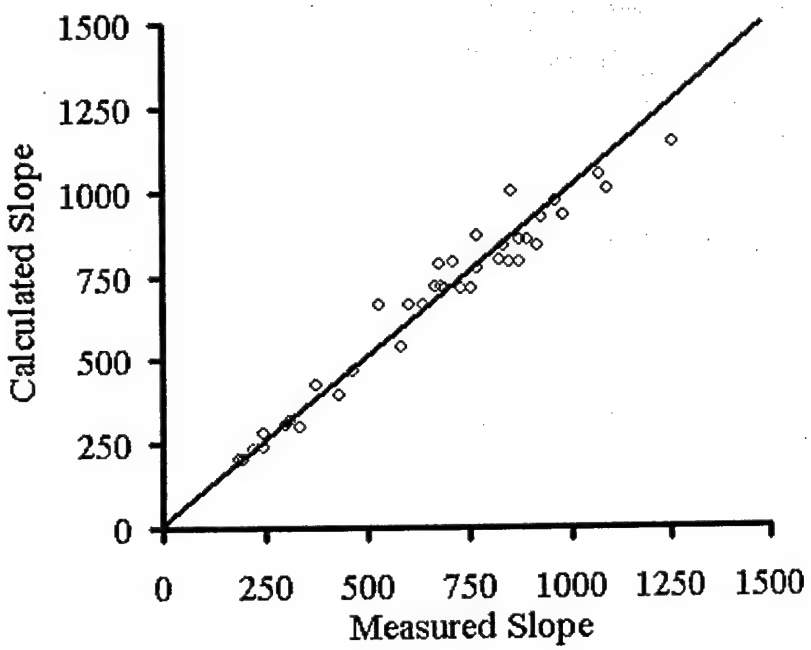

Figure 2-21. A comparison of anthracene data versus calculated values of Equation 2-7 when the following parameters are used: $k_{ec} = 2.09 \times 10^{-9}$ cc sec^{-1}, $k_{diff} = 92.7$ sec^{-1} (4 torr, 30C), $k_{ediff} = 5 \times 10^{4}$ sec^{-1} (4 torr, 30C) Data were collected from 40-81°C and 2-4 Torr, k_{det} was estimated for each data point similar to previous benzophenone and quinoxaline experiments.

Once again the same electron diffusion term used for the previous molecules explains the anthracene data.

The thermal electron detachment rate constants can also be predicted using the Kebarle or Miller equations, Equations 1-34 and 1-36 respectively, with the parameters in Table 2-4.

Table 2-4. Thermodynamic and kinetic properties of anthracene.

Property	Value	Equation
Electron Affinity	0.54 eV = 52.1 kJ mol^{-1}	Both
k_{ec}	2.09 x 10^{-9} cc sec^{-1}	Both
$S_{anion} - S_{neutral}$	+42 J mol^{-1} K^{-1}	Miller
ΔS_{ni}	0.0 J mol^{-1} K^{-1} (0.0 e.u.)	Kebarle

Figure 2-22 compares measured thermal electron detachment rate constants with predicted values from the Kebarle and Miller equations using the parameters in Table 2-4. One caution should be noted regarding the measured thermal electron detachment rate constants. These data are collected from the slope of the logarithmic time profiles. As mentioned earlier, these data, especially at high pressures, are suspect for anthracene. To be certain, the measured detachment rates are at least as high as they appear in Figure 2-22; they could, in fact, be higher.

Quinazoline

Quinazoline has a mass of 130 amu, and its EA has been reported at 0.56 eV [76]. Throughout this section the quinazoline anion will be abbreviated Qz^-.

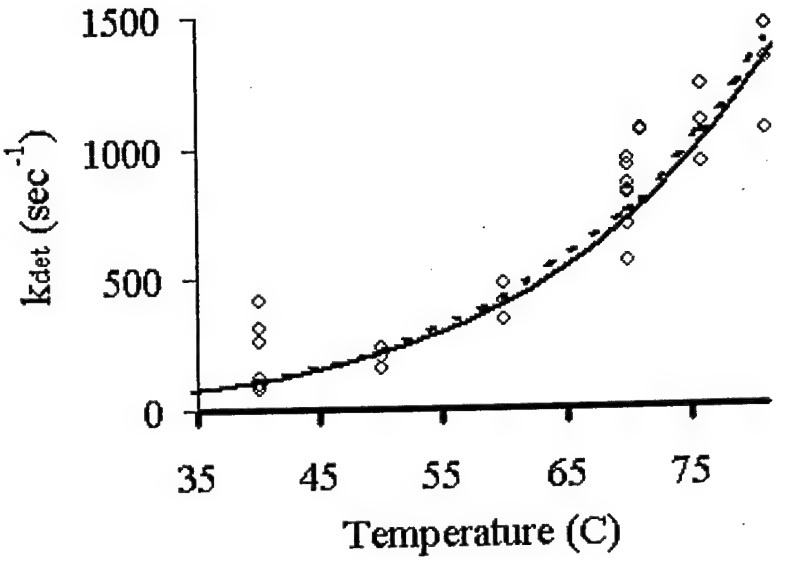

Figure 2-22. Thermal electron detachment predictions for A^- using the Kebarle and Miller equations with the parameters in Table 2-4. (o) are measrured data for A^-. The dashed line is from the Kebarle equation, and solid line is from the Miller equation.

It is the meta-substituted isomer of quinoxaline as shown in Figure 2-23.

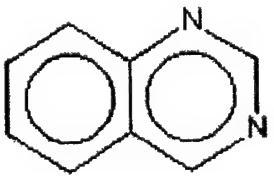

Figure 2-23. The molecular structure of quinazoline.

Experimental

The PHPMS was used for all experiments. The gas handling plant was prepared by injecting a solution of quinazoline in toluene. Injection amounts ranged from 1.38 x 10^{-5} – 2.27 x 10^{-5} moles of quinazoline which resulted in mixing ratios of 66 –102 ppm in

the buffer gas. The Clasius-Clapyeron equation was used to estimate vapor pressure limits for quinazoline in the gas handling plant, transfer line, and the ion source; injection amounts were limited to stay below the vapor pressure limit. Pure SF_6 was injected in amounts ranging from $1.05 \times 10^{-7} - 9.06 \times 10^{-7}$ moles which resulted in mixing ratios of 0.1 – 0.9 ppm in the buffer gas. SF_6 injection amounts were generally governed by the goals of each individual experiment.

Data were collected at source pressures ranging from 2-4 torr. All experiments involved taking mass spectra to determine which ions were present. Then, time profiles were taken for each ion present. Experiments involved setting the SF_6 and quinazoline concentrations and varying the ion source temperature.

Results and Discussion

Quinazoline immediately presented a problem as indicated in Figure 2-24. In this case, there are two peaks of almost equal intensity, the Qz^- peak at 130 amu and another peak at 162 amu. From the experiments in Chapter 3 it will be shown that 162 amu ion is the $(Qz \bullet O_2)^-$ cluster. However, no oxygen was added to produce this spectrum. The PHPMS is fitted with O_2 and H_2O traps, but background levels of these impurities are probably 1-5 ppm. This small amount of O_2 is responsible for signal at 162 amu as shown in Reactions 2-9.

$$Qz^- + O_2 \rightleftharpoons (Qz \bullet O_2)^- \rightleftharpoons ? \qquad (2\text{-}9)$$

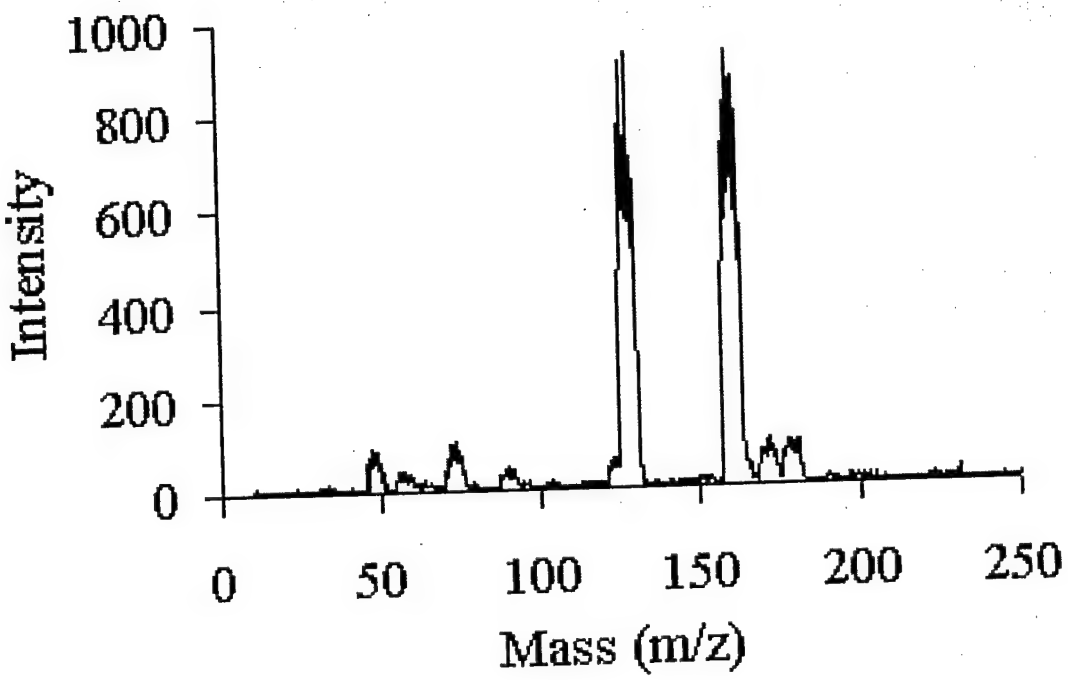

Figure 2-24. Typical mass spectrum for quinazoline taken at 3.0 Torr and 35°C. Quinazoline concentration was 102 ppm (as a fraction of the buffer gas).

The question mark in Reaction 2-9 is important. Again Chapter 3 will address how $(Qz \bullet O_2)^-$ reacts with H_2O. Further, the O_2 may not thermally detach electrons, or it might detach them much slower than Qz^- alone. The normalized time profiles showed that Reaction 2-9 did not reach a steady state equilibrium condition in the time scale of these experiments.

While Reaction 2-9 is obviously a complication, it occurs after the Qz^- is formed. So, it is conceivable that the initial concentrations of SF_6^- and Qz^- could still be used to measure the electron capture rate constant. Figure 2-25 shows measured electron capture rate contants from both the logarithmic and the normalized time profiles. The

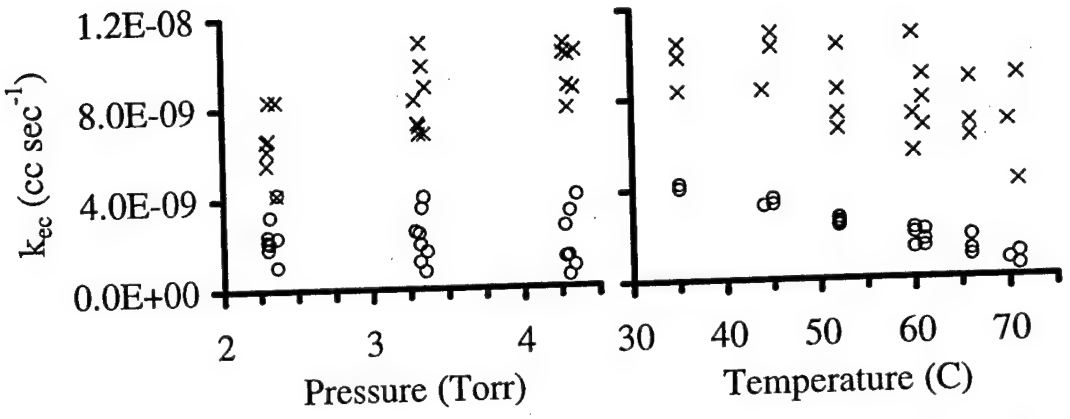

Figure 2-25. Measured electron capture rate constants for quinazoline. (o) were calculated from logarithmic time profiles. (x) were calculated from normalized time profiles.

results are interesting for two reasons. First the values calculated from the normalized time profiles (average $\approx 7.67 \times 10^{-9}$ cc sec^{-1}) are about 3.4 times larger than the values calculated by the logarithmic time profiles (average $\approx 2.23 \times 10^{-9}$ cc sec^{-1}). Second, the values calculated with logarithmic time profiles show a linear decrease with temperature ($R^2 \approx 0.94$). Treating the quinazoline data the same as the anthracene leads us to infer that the electron capture rate constant is $\approx 7.67 \times 10^{-9}$ cc sec^{-1}. However, uncertainty about the effects of the O_2 clustering reaction leads to greater uncertainty in this measurement than with the previous molecules.

Thermal electron detachment is also complicated by the O_2 clustering reaction. Although not explicitly stated in the literature, it is generally accepted that a cluster anion, like $(Qz \bullet O_2)^-$, does not directly detach electrons. Rather, it falls apart and then the molecular anion, Qz^-, detaches the electron. If this premise is true, the clustering reaction would have the effect of acting as a reservoir of protection against thermal detachment,

and, measured thermal electron detachment rate constants would be only a fraction of their true value. If the first half of Reaction 2-9 reached equilibrium, the steady state concentrations of Qz^- and $(Qz \bullet O_2)^-$ could be used with the equations in Appendix C to adjust the measured values. Unfortunately, Reaction 2-9 does not reach equilibrium in the time scale of these experiments.

Measured thermal electron rate constants shown here in Figure 2-26 represent a minimum for each temperature.

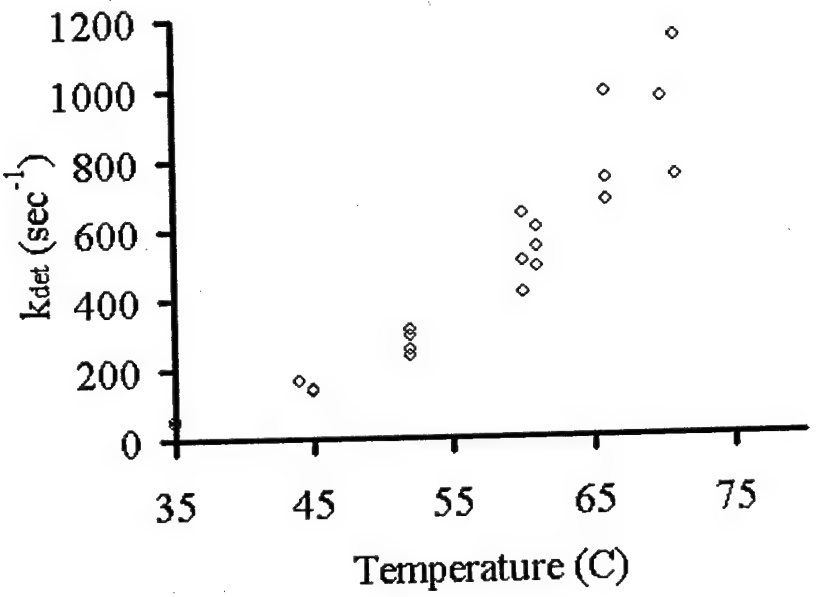

Figure 2-26. Observed loss of Qz^- to thermal electron detachment. The measured values have not been corrected for the effects of the O_2 clustering reaction.

The actual rate constants could be 2-5 times bigger.

Conclusion

Electron capture and thermal electron detachment rate constants were measured for benzophenone, quinoxaline and anthracene. In addition, the loss of electrons by diffusion was determined to be important in making these measurements, and the electron diffusion rate, in the plasma conditions present in the PHPMS, was determined to approximately 300 times greater than the diffusion rate for negative ions. Once the electron capture rate constant is known, predictive equations for thermal electron detachment, previously purposed by Kebarle and Miller can be used to calculate the thermal electron rate constant as a function of temperature. Table 2-5 summarizes the findings for each compound.

Table 2-5. Summary of kinetic and thermodynamic properties for each molecule

Compound	k_{ec} (cc sec^{-1})	EA (eV)	$S_{anion} - S_{nuetral}$ (J K^{-1} mol^{-1})	ΔS_{ni} (J K^{-1} mol^{-1})
Benzophenone	1.65×10^{-8}	0.61	+38.5	-3.3
Quinoxaline	2.31×10^{-9}	0.68	+39	-3.0
Anthracene	2.09×10^{-9}	0.54	+42	0.0
Quinazoline	$2.0 - 9.0 \times 10^{-9}$	0.56	not reported	not reported

Both anthracene and quinazoline produced complicated time profiles. Reactions with O_2 were demonstrable problematic for quinazoline, and O_2 may have contributed to the abnormal time profiles for anthracene. As will be explored in detail in Chapter 3, O_2

and another ever present impurity, H_2O, having been causing problems in the detection of anions from low EA molecules for the past 30 years.

FAILURE TO DETECT THESE ANIONS AT ATMOSPHERIC CONDITIONS

Introduction

In the environmental, biomedical and forensic sciences, an ever-increasing need exists for the trace detection and analysis of specific substances in complex samples. Everyday applications include finding a particular pollutant in a sample of lake water, determining Freon concentrations in the atmosphere, and searching for toxins in body fluids.

Some of the most promising methods that have been developed have been based on the gas phase negative ionization of compounds by the attachment of thermal-energy electrons as symbolized by Reaction 3-1[2, 78-81]:

$$e^- + M \rightleftharpoons M^- \qquad (3\text{-}1)$$

For compounds with a large positive EA, ≥ 1.0 eV, the second order forward rate constants, k_{ec}, is often very large, on the order of 10^{-7} cc sec^{-1} [20]. This fast reaction accounts for the extraordinarily high sensitivity that can be obtained by methods based on REC. The most common instruments are the electron capture detector (ECD) [82-84], the ion mobility spectrometer (IMS) [85], the atmospheric pressure ionization mass spectrometer (APIMS) [86], the ion mobility spectrometer with detection by mass spectrometry (IMS/MS) [87] , and the negative chemical ionization mass spectrometer (NCIMS) [79, 80].

Two problems have been encountered with these methods that rely on electron capture and the formation of negative ions. First, as indicated by the double arrow, Reaction 1 is reversible. This elementary step, also well detailed in the previous chapters, is called thermal electron detachment (TED). It is a particularly undesirable reaction since it completely destroys the molecular anions of interest and the associated response to the analyte, M. The rates of TED reactions increase strongly with increased temperature and decreased EA of M (this relationship is mathematically described by equation 1-32 and 1-34 in Chapter 1) so that, at commonly used ion source temperatures of about 150°C or greater, TED typically becomes unacceptably fast for compounds having EA values of less than about 0.78 eV [55, 58, 79]. Second, some classes of compounds react with trace levels of oxygen and water (both are commonly present in the buffer gas of an ion source). For example, the molecular anions of halogenated aromatic hydrocarbons are consumed in reactions with oxygen [88]. Molecular anions of perfluorinated aliphatic hydrocarbons also undergo fast side reactions with trace levels of water [89].

A recent report [77] demonstrated that the detrimental effects of the TED reaction on the REC mass spectra of some low electron affinity compounds (such as benzophenone) obtained at relatively high ion source temperatures could be overcome by the intentional addition of small amounts of silicon tetrafluoride to the ion source buffer gas. Due to a strong Lewis acid-base interaction between SiF_4 and the molecular anions of low-EA compounds that have a sterically unhindered Lewis base site, a strong molecular anion - SiF_4 complex is formed which prevented the TED reaction for low EA

compounds. As explained in the benzophenone section in Chapter 2, the SiF_4 reaction appears to be reversible. Therefore, TED is not stopped completely. Rather, a fraction of the parent anion is protected from TED while it is in the anion – SiF_4 complex. As a result, the addition of SiF_4 is useful only for qualitative detection of low EA compounds.

Another means of minimizing the TED reaction of low EA compounds is to simply lower the temperature of the ion source [80]. In this way, a point should be reached where the lifetime of the molecular anion against TED would be long relative to its lifetime against normal ion loss processes (either recombination with positive ions or diffusion to the walls) and the mass spectra thereby produced should include an intense molecular anion.

However, when using ion sources of relatively high pressure, as in APIMS or IMS, along with relatively low ion source temperatures, we have found great difficulty in observing molecular anions, as expected. For example, in spite of numerous attempts to observe and study the molecular anions of aromatic compounds of EA lower than about 0.7 eV (such as benzophenone, anthracene and azulene), we have observed a molecular anion only for the case of azulene [90], even with use of ion source temperatures as low as 20°C. It is interesting to note that this observation was also made some 25 years ago by Horning, Carrol and Dzidic [82], the first practitioners of APIMS.

In recent additional observations of our own by IMS/MS, we have also noted that when low EA compounds, such as benzophenone and anthracene, are added to the ion source at relatively low temperatures, the intensity of an ion at m/z = 50 is significantly increased (Figures 3-1).

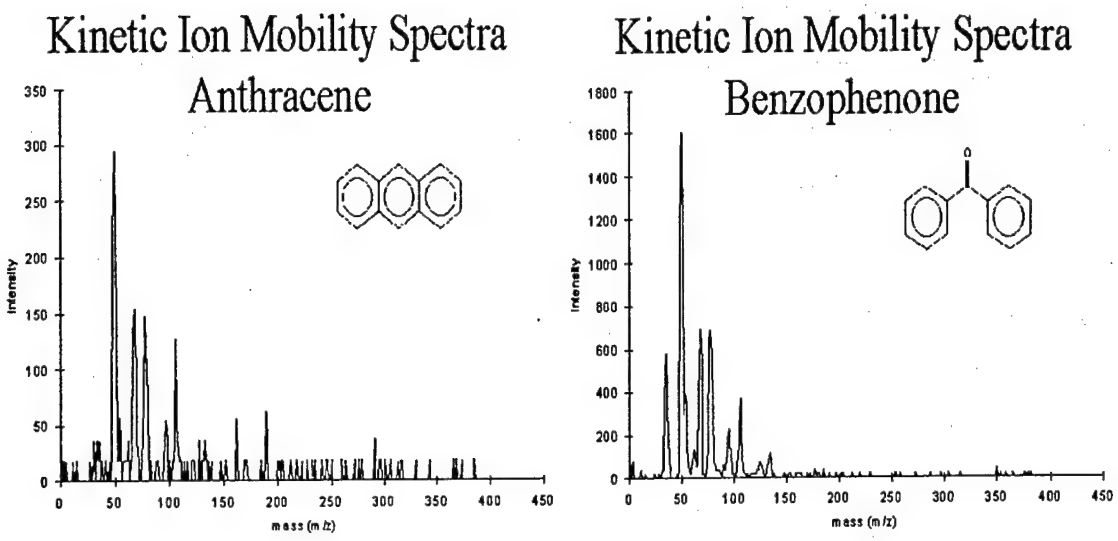

Figure 3-1. IMS spectra of anthracene demonstrating the absence of an M^- m/z = 178 peak and the presence of the m/z = 50 peak. IMS spectra of benzophenone demonstrating the absence of an M^- m/z = 182 peak and the presence of the m/z = 50 peak.

Since a likely assignment for the identity of this ion is $(O_2 \bullet H_2O)^-$, this observation suggests that if molecular anions are being produced in these cases, they are being rapidly destroyed by reactions involving trace levels of oxygen and water both of which commonly have partial pressures approaching the mTorr level in the buffer gases of one atmosphere total pressure. In the present study, this possibility is explored in detail and is, indeed, shown to explain the lack of REC responses to low EA compounds in high pressure ion sources at low ion source temperatures. This study also reveals a novel mechanism for the reaction of molecular anions with water and oxygen that is shown to be uniquely fast for low EA compounds. It is also shown that the new reaction processes revealed here offers a simple and reliable means for determining the EA of compounds having EAs less than about 0.7 eV.

Experimental

A pulsed high pressure mass spectrometer (PHPMS) was used for all experiments. The PHPMS was constructed in our laboratory and has been described in detail previously [77, 91]. Chapter 1 describes how the instrument is set up as well as summarizes the types of experiments and data that can be interrogated. For the present experiments, a gaseous mixture consisting of small quantities of water, oxygen, and the low EA compound of interest, M, were added to a methane buffer gas, in an associated gas handling plant. This mixture then flowed slowly through the ion source of the PHPMS. The ion source pressure was set to some constant value between 1 and 4 Torr. The ion source temperature was generally held constant at 50°C. A brief pulse (20 μs) of 3000 eV electrons produced positive ions and electrons within the ion source. In the methane buffer gas, these secondary electrons were rapidly thermalized and then captured primarily by the compound M (Reaction 3-1) to form molecular anions, M^-, which are also rapidly brought to thermal energy by collisions with the buffer gas. At the relatively low temperature used, the primary loss of these M^- ions will not be by their TED reactions, but will be shown to be by reactions with oxygen and water. The number density of ions within the source is sufficiently low so that the dominant loss of total negative charge is by diffusion to the ion source walls rather than by recombination with positive ions [8]. Relative ion abundances within the ion source are determined as a function of time after the electron pulse by measuring the relative ion wall currents; that is, by observing the ions that pass through a narrow slit on one wall of the ion source into

a vacuum chamber where the ions are mass analyzed (quadrupole mass filter), detected (ion-counting channeltron) and time analyzed (multichannel scaler).

Results and Discussion

In order to mimic the absolute concentrations of water and oxygen that might commonly be present in an ion source at one atmosphere pressure, small amounts of water (0.9 mTorr) and oxygen (0.5 mTorr) were added to the methane buffer gas (3.0 Torr) of our PHPMS. The negative ion mass spectrum thereby produced is shown in Figure 3-2. At the attenuation setting used for this mass spectrum, a very weak signal is noted at m/z = 50, presumed to be due to the negative ion, $(O_2 \bullet H_2O)^-$.

This ion was possibly formed by the REC reaction of O_2, followed by the hydration of the resulting O_2^- ion by water. The observed low intensity of this ion can be attributed to the very low rate constant for the REC reaction by oxygen. The pseudo second-order rate constant for the attachment of thermal energy electrons to oxygen at 50°C in nitrogen buffer gas at 3 Torr pressure is estimated to be only about 1×10^{-13} cm^3 s^{-1} [92], which is about 6 orders of magnitude slower than the rate constants of fast REC processes, for example, those of numerous substituted nitrobenzene compounds are known to exceed 1×10^{-7} cm^3 s^{-1} [20].

The mass spectrum shown in Figure 3-2 B was then obtained after adding 0.06 mTorr of anthracene to the same gas mixture that was used to produce the spectrum in Figure 3-2 A. Under these conditions, it is noted that only a small amount of the molecular anion, M^-, for anthracene at m/z = 178 is detected.

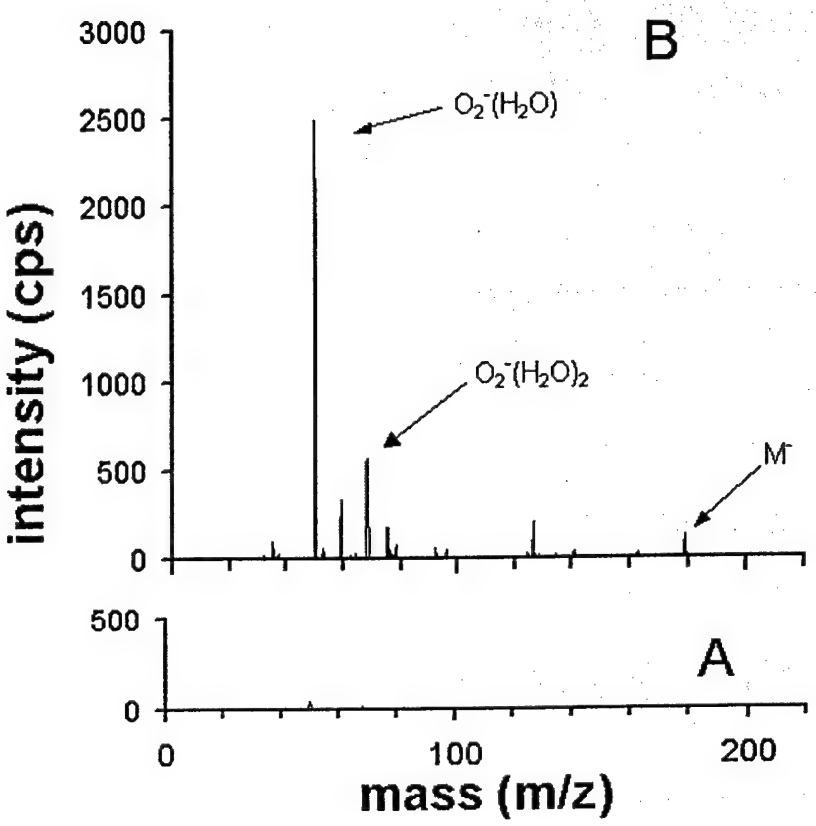

Figure 3-2. (A) The negative ion mass spectrum obtained with 0.5 mTorr oxygen and 0.9 mTorr water present in the methane buffer gas of the PHPMS ion source. The total pressure is 3.0 Torr and the ion source temperature is 50°C. (B) The negative ion spectrum obtained immediately after 0.06 mTorr anthracene was also added to the ion source mixture described in part A.

The much more important effects of anthracene's addition are noted for the ions of lower mass, which are not materially related to anthracene. The most abundant of these is the ion at m/z = 50, again thought to be $(O_2 \bullet H_2O)^-$, and the next most abundant ion at m/z = 68 is thought to be $(O_2 \bullet (H_2O)_2)^-$. An ion of low intensity at m/z = 60 is thought to be due to CO_3^- which is probably also formed from $(O_2 \bullet H_2O)^-$ by its reaction with trace levels of

CO_2 in the buffer gas. An ion of minor abundance at m/z = 126 is thought to be due to presence of an unknown impurity possibly introduced with anthracene. Finally, an ion at m/z = 210 is also invariably observed with anthracene and oxygen simultaneously present in the ion source, although the intensity of this ions is very low under the specific conditions of the experiment shown in Figure 3-2 B. This ion is thought to be due to an anthracene-oxygen adduct ion, $(M \bullet O_2)^-$. In summary, the spectra in Figure 3-2 are roughly those which we have been typically observed whenever anthracene or other compound of similarly low EA has been introduced to an atmospheric pressure ion source set to a relatively low temperature. Instead of observing an intense M^- ion, as expected, the intensity of the $(O_2 \bullet H_2O)^-$ ion is greatly increased.

Determination of the Mechanism

In order to obtain information concerning the dynamics of the reactions that produced the unexpected spectrum shown in Figure 3-2, measurements of relative ion intensities were also made as a function of time after the e-beam pulses. Again using the case of anthracene as an example, one set of measurements of this type is shown in Figure 3-3. Under the conditions of reagent concentrations used in this case, the molecular anion of anthracene, M^-, is the major ion initially formed by its REC reaction immediately after the e-beam pulse. However, within only about 2 ms after the pulse, the relative abundance of M^- has been decreased to a terminal level of about 0.30 and that of the $(O_2 \bullet H_2O)^-$ ion has increased to a terminal level of about 0.55.

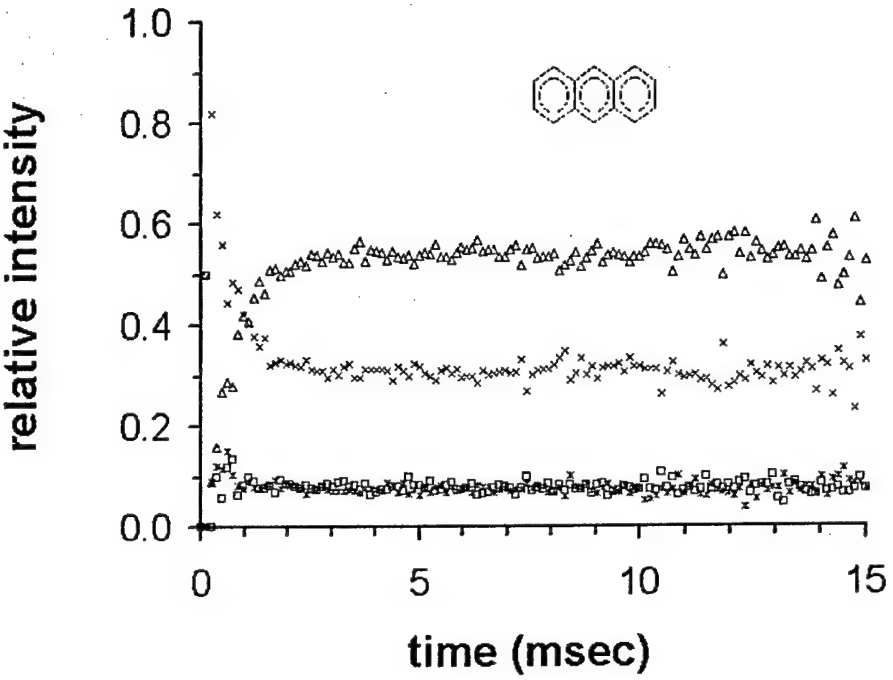

Figure 3-3. PHPMS measurements of the relative intensities of the major ions, M^- (x), O_2^- (*), $(M \bullet O_2)^-$ ( ) and $(O_2 \bullet H_2O)^-$ (Δ), observed as a function of time after the e-beam pulse with 0.80 mTorr oxygen, 0.050 mTorr water and 0.17 mTorr anthracene present in the ion source. The total methane buffer gas pressure is 3.0 Torr and the ion source temperature is 50°C.

Over this short period of time, an O_2^- ion and the anthracene-oxygen adduct ion, $(M \bullet O_2)^-$, have also each reached terminal levels of about 0.07. Over the entire period from about 2 ms to 10 ms after the pulse, either a state of chemical equilibrium or a steady dynamic state appears to have been reached in which the relative abundances of these four ions remain constant.

In attempting to identify the detailed reactions and mechanism that produced the spectrum in Figure 3-2 and the time dependencies shown in Figure 3-3, it is appropriate to first consider the most obvious candidate which is primarily based on well-known

negative ion-molecule reactions. This mechanism will be referred to here as Model A and consists of the series of reactions shown below:

$$M^- + O_2 \rightleftharpoons M + O_2^- \quad (3\text{-}2)$$

$$O_2^- + H_2O \rightleftharpoons (O_2 \bullet H_2O)^- \quad (3\text{-}3)$$

$$M^- + O_2 \rightleftharpoons (M \bullet O_2)^- \quad (3\text{-}4)$$

These reactions are assumed to occur immediately after the molecular anion, M^-, has been formed by the e-beam pulse and Reaction 3-1. Reaction 3-2 is a simple electron transfer from the molecular anion to oxygen. The rate constants for the forward and reverse directions can be readily estimated. The reverse reaction is expected to occur with collision frequency [93] and, therefore, will be about $k_{-2} = 2 \times 10^{-9}$ cc s^{-1}. The rate constant for the forward reaction can be estimated from k_{-2} and the equilibrium constant, $K_2 = k_2/k_{-2}$, expected for this reaction which can be deduced from $K_2 = \exp(-\Delta G^\circ_2 / RT)$. The standard free energy change, ΔG°_2, for Reaction 3-2 is adequately provided by the difference in the electron affinities of oxygen and anthracene [73]. Using a literature value of EAO2 = 0.45 eV [94, 95] and the EA of anthracene to be determined here, EA_M = 0.54 eV, an estimate of $k_2 = 8 \times 10^{-11}$ cc s^{-1} at 50°C is obtained. Rate constants for both the forward and reverse directions of Reaction 3-3 can be obtained from previous determinations of the third-order rate constant for the forward direction [96] and the total free energy change, $\Delta G^\circ_3 = -11.9$ kcal mol^{-1} for this reaction at 50°C [97]. From this information, a second order rate constant of about $k_3 = 2 \times 10^{-11}$ cc s^{-1} and a first order

rate constant of about $k_{-3} = 4\ s^{-1}$ are obtained under the present reaction conditions of 3.0 Torr total pressure and 50°C. The combination of Reaction 3-2 and 3-3 in Model A provide for the conversion of M^- to $(O_2 \bullet H_2O)^-$. Reaction 3-4 is included in Model A in order to account for the observed production of the adduct ion, $(M \bullet O_2)^-$, and as a side reaction, is envisioned to play no role in the conversion of M^- to $(O_2 \bullet H_2O)^-$ ions. In order to account for the position of equilibrium for Reaction 3-4 and the rapid achievement of this state observed in Figure 3-5, a near collisional second-order rate constant of $k_4 = 1 \times 10^{-9}$ cc s^{-1} and a first-order rate constant of $k_{-4} = 8 \times 10^4\ s^{-1}$ have been assigned to the forward and reverse directions of Reaction 3-4, respectively, in Model A. In order to determine whether Model A provides an adequate explanation of the dynamics of the anthracene reaction system, a computer simulation (using a deterministic differential equation problem solving routine) of the pulsed e-beam experiment based on Model A was created and is shown in Figure 3-4. In comparing this prediction with the experimental results shown in Figure 3-3, it is noted that the final equilibrium state predicted by Model A is, indeed, in good agreement with the experimental results. However, it is also noted that the time required to achieve this terminal state by Model A is about 200 times longer (0.4 s) than was required in the experiment (2 ms). Therefore, Model A does not adequately describe the processes by which the M^- ions of anthracene were converted to $(O_2 \bullet H_2O)^-$ ion in Figure 3-2.

Another candidate mechanism, which will be referred to here as Model B, can be envisioned simply by adding Reaction 3-5 to Reactions 3-2, 3-3 and 3-4 of Model A.

$$(M\bullet O_2)^- + O_2^- \rightleftharpoons (O_2\bullet H_2O)^- \qquad (3\text{-}5)$$

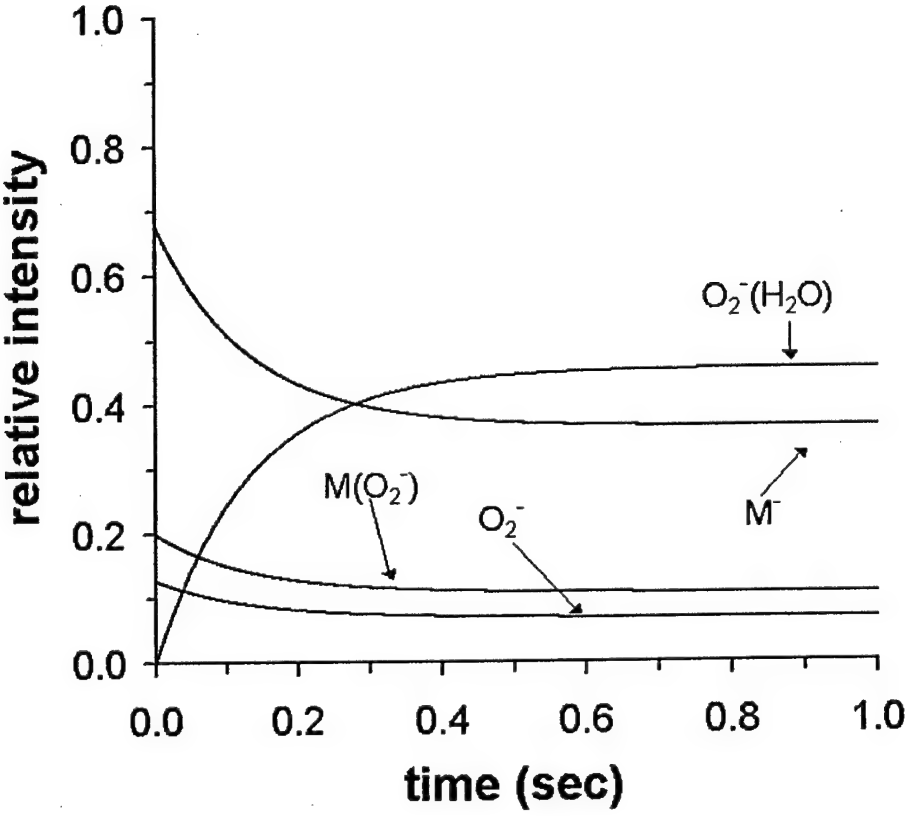

Figure 3-4. The relative intensities of the major ions, M^-, O_2^-, $(M\bullet O_2)^-$ and $(O_2\bullet H_2O)^-$ predicted by the candidate mechanism, Model A, as a function of time under the ion source conditions described in Figure 3-3.

In the new model thereby created, Reaction 3-4, which is very fast in the forward direction, along with Reaction 3-5 becomes the major means for conversion of M^- to $(O_2\bullet H_2O)^-$ ions. Reaction 3-5 might be viewed as a cluster exchange reaction in which a

water molecule replaces the molecule, M, in the MO_2^- complex ion. An interesting point concerning Reaction 3-5 is that if the center of negative charge density within the complex ion, $(M \bullet O_2)^-$, lies within the molecule M rather than O_2 (as might be expected from the fact that $EA_M > EA_{O2}$), then motion along the reaction coordinate towards the transition state for Reaction 3-5 would involve a shift in negative charge density from the M to O_2 molecules within the complex ion. Alternately, it is also possible that the center of negative charge within the $(M \bullet O_2)^-$ actually lies within the O_2 species, in spite of its lower EA, possibly due to the increased ion clustering potential of the molecule, M, over that of O_2.

In order to estimate rate constants for the forward and reverse directions of Reaction 3-5, the same procedure as was previously applied to Reaction 3-4 will be used. That is, it is assumed that the steady-state condition which is achieved by the intermediate ion, $(M \bullet O_2)^-$, and the product ion, $(O_2 \bullet H_2O)^-$, in Figure 3-3 is an equilibrium condition for Reaction 3-5. With this assumption, an equilibrium constant for Reaction 5, $K_5 = k_5 / k_{-5} = 25$, is determined from the measured ratio of $(M \bullet O_2)^-$ and $(O_2 \bullet H_2O)^-$ ion intensities in Figure 3-5 at any time after t = 2 ms and the known concentrations of H_2O and M within the ion source. The magnitudes of k_5 and k_{-5} were then varied until the model provided the best fit to the observed time dependencies of ion intensities. With estimates of $k_5 = 2 \times 10^{-9}$ cc s^{-1} and $k_{-5} = 8 \times 10^{-11}$ cc s^{-1}, and using the same rate constants as used in Model A for Reactions 3-2, 3-3 and 3-4, the time dependencies

predicted by Model B are shown in Figure 3-5 to be in very good agreement with the experimental results in Figure 3-3.

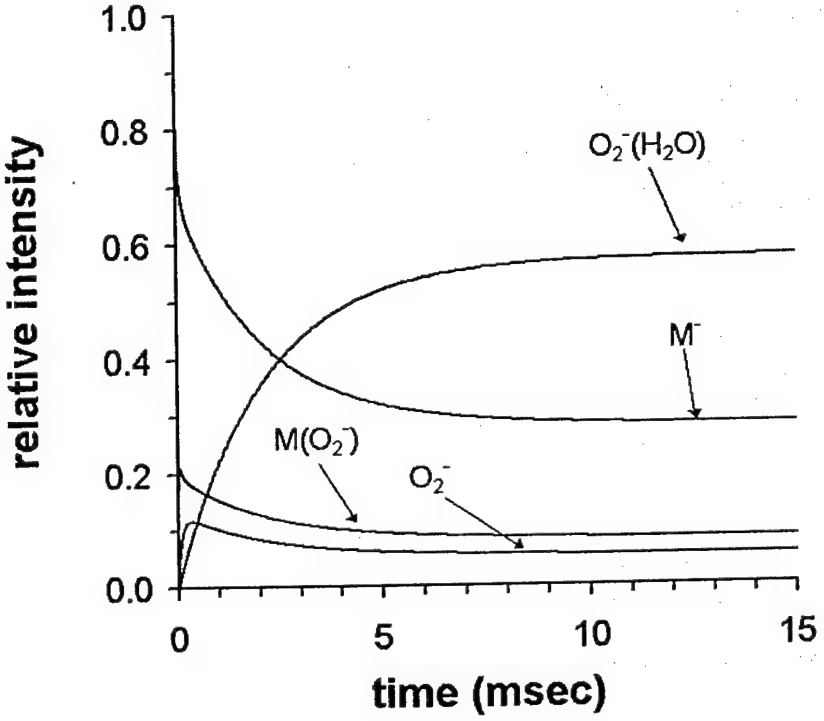

Figure 3-5. The relative intensities of the major ions, M^-, O_2^-, $(M \bullet O_2)^-$ and $(O_2 \bullet H_2O)^-$ predicted by the candidate mechanism, Model B, as a function of time under the ion source conditions described in Figure 3-3.

In summary, while Reactions 2 and 3 must be occurring and account for the steady-state abundance of O_2^- observed in this case, they are of minor importance in the observed fast conversion of M^- ions to $O_2^-(H_2O)$ ions. This is thought to be caused primarily by the sequence of Reactions 4 and 5, both of which are sufficiently fast in both directions as to cause the rapid achievement of a true equilibrium condition between these two ions.

In Figure 3-6, a PHPMS experiment is shown where quinazoline rather than anthracene was used as the low EA compound. relative intensity with the $(M\bullet O_2)^-$ ion being significantly more intense than it was for anthracene in Figure 3-3. For this reason, much less oxygen and much more water was used in order to have significant ion abundances of these three major ions throughout the period of measurement.

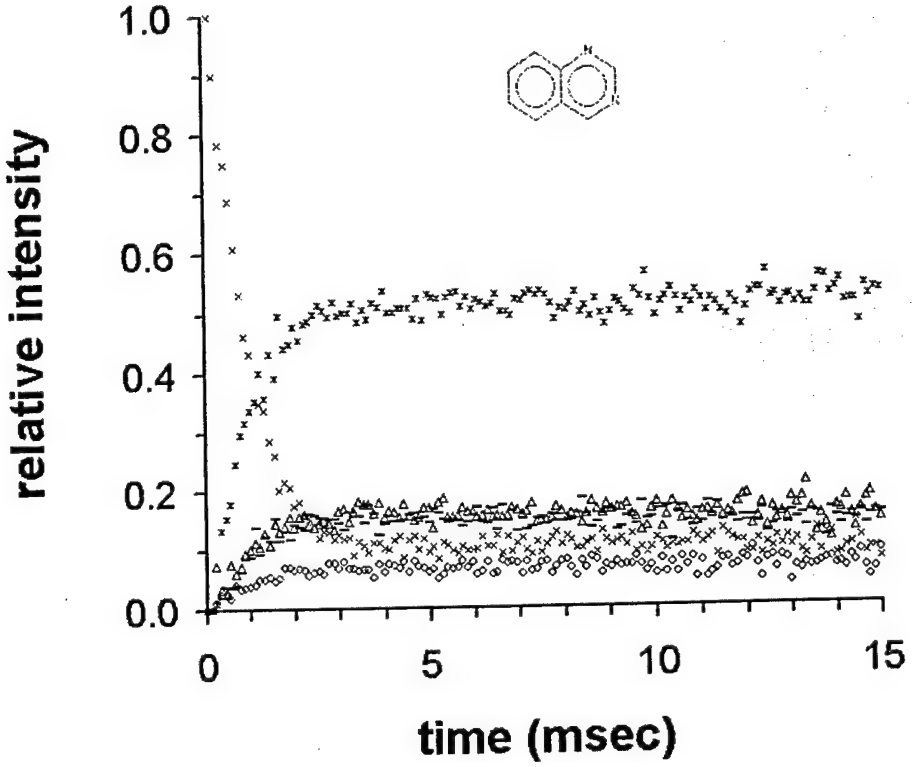

Figure 3-6. PHPMS measurements of the relative intensities of the major ions, M^- (x), $(M\bullet O_2)^-$ (⋆), $(M\bullet O_2\bullet H_2O)^-$ (-), $(O_2\bullet H_2O)^-$ (Δ), and $(O_2\bullet(H_2O)_2)^-$ (o), observed as a function of time after the e-beam pulse with 0.15 mTorr oxygen, 1.06 mTorr water and 0.38 mTorr quinazoline present in the ion source. The total methane buffer gas pressure is 3.0 Torr and the ion source temperature is 50°C.

Under these conditions, the ions M^-, $(M•O_2)^-$ and $(O_2•H_2O)^-$ again have significant Because a higher water concentration was used in this case, two higher-order water cluster ions, $(M•O_2•H_2O)^-$ and $(O_2•(H_2O)_2)^-$, also have significant relative intensities in Figure 3-6. The O_2^- ion does not have significant relative abundance because much less oxygen was used and because the rate constant, k_2, will be smaller than it was for anthracene due to the slightly greater EA for quinazoline (0.56 eV). Figure 3-6 also demonstrates that the time required for establishment of constant relative ion intensities is very short, about 2 msec. Application of Model A to this reaction system predicts that about 0.5 seconds would be required to achieve this terminal state and, therefore, Model A again fails to explain this reaction system. However, when Reaction 5 is also included in the mechanism for quinazoline, excellent agreement between the experimental results and those predicted by Model B are obtained when values of $k_5 = 2 \times 10^{-10}$ cm^3 s^{-1} and $k_{-5} = 2 \times 10^{-9}$ cm^3 s^{-1} are assigned. In order to account for the two higher order water cluster ions observed in this case, rate constants for the forward and reverse water clustering reactions were set to 4.6×10^{-11} cm^3 s^{-1} and 4.9×10^3 s^{-1}, respectively, values which have been previously determined specifically for the clustering reaction leading to $(O_2•(H_2O)_2)^-$ at 50°C [96].

In Figure 3-7, a PHPMS experiment using benzophenone (EA = 0.61 eV) as the low-EA compound is shown. In this case and under these experimental conditions, only the M^-, $(M•O_2)^-$ and $(O_2•H_2O)^-$ ions have major relative abundance. Again, a steady-state condition is achieved, within about 1 msec after the e-beam pulse, and this

observation cannot be explained in terms of Model A which predicted about 0.7 seconds to reach equilibrium.

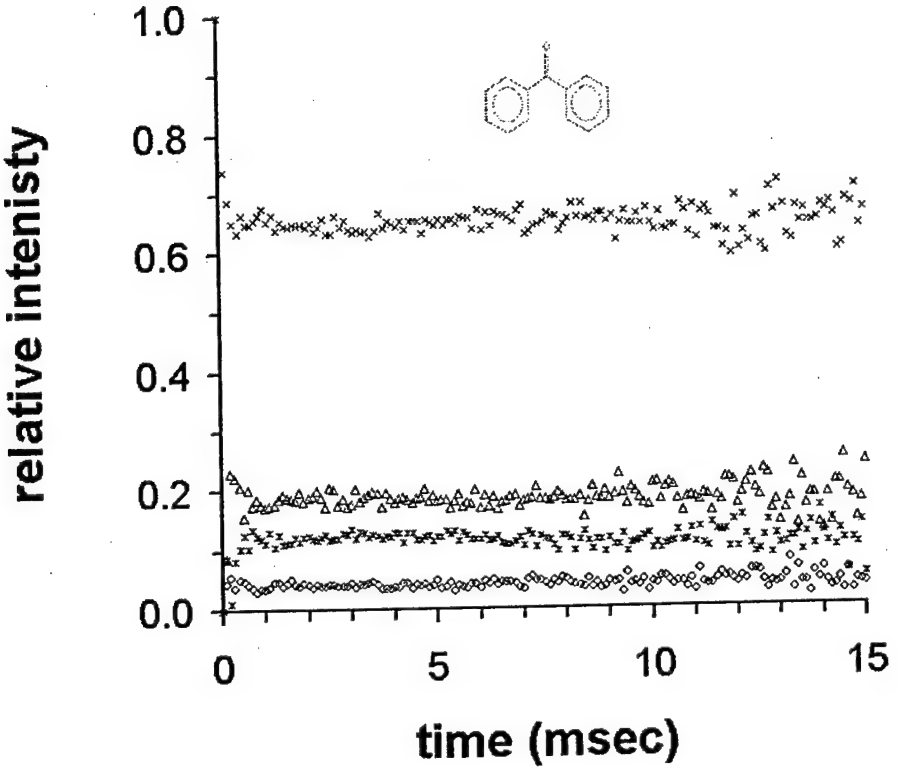

Figure 3-7. PHPMS measurements of the relative intensities of the major ions, M^- (x), $(M \bullet O_2)^-$ (⋆) $(O_2 \bullet H_2O)^-$ (Δ), and $(O_2 \bullet (H_2O)_2)^-$ (o), observed as a function of time after the e-beam pulse with 0.44 mTorr oxygen, 0.95 mTorr water and 0.86 mTorr benzophenone present in the ion source. The total methane buffer gas pressure is 3.0 Torr and the ion source temperature is 50°C.

However, the results in Figure 3-7 are also well explained by Model B when the appropriate forward and reverse rate constants, shown later, are assigned to Reactions 4 and 5. In Figure 3-8, a PHPMS experiment using quinoxaline, which has a significantly greater EA of 0.68 eV, is shown.

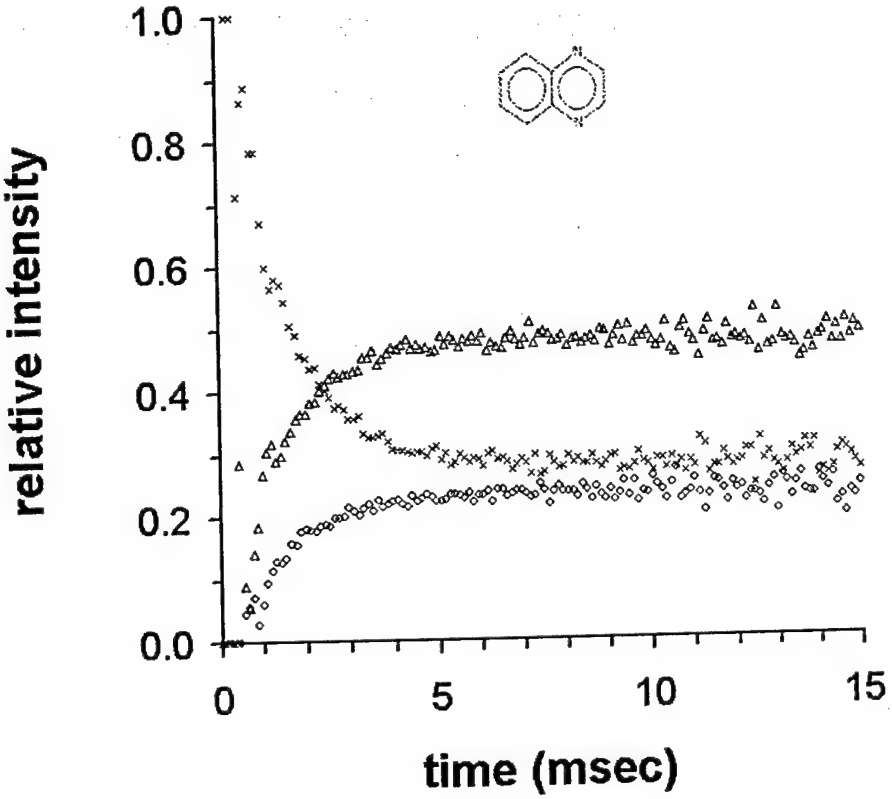

Figure 3-8. PHPMS measurements of the relative intensities of the major ions, M^- (x), $(O_2 \bullet H_2O)^-$ (Δ), and $(O_2 \bullet (H_2O)_2)^-$ (o), observed as a function of time after the e-beam pulse with 0.98 mTorr oxygen, 1.52 mTorr water and 0.040 mTorr quinoxaline present in the ion source. The total methane buffer gas pressure is 3.0 Torr and the ion source temperature is 50°C.

Even though relatively high concentrations of both oxygen and water were used, it is noted that $(O_2 \bullet H_2O)^-$ ions are formed somewhat slower than for they were with use of the three compounds of lower EA previously considered. In this case, the achievement of terminal ion abundance ratios required about 5 ms. Also, it is noted that the adduct ion, $(M \bullet O_2)^-$, does not have significant relative abundance in this case. The fact that O_2^- is not observed in this case is expected because quinoxaline's higher EA shifts the equilibrium

position of Reaction 3-2 far to the left. As with the cases previously considered, the time dependence of the ion intensities observed for quinoxaline can not be explained by Model A. Primarily because the magnitude of k_2 for this reaction system is exceedingly low, Model A predicts that about 0.6 seconds would be required to achieve the terminal state. Therefore, it appears that this reaction system also proceeds by a different mechanism, which might also be assumed to be Model B. In the case of quinoxaline, however, it was not possible to experimentally determine the magnitudes of the individual rate constants of the two elementary steps, Reaction 3-4 and 3-5, from PHPMS measurements as is was in the previous cases considered because the intermediate adduct ion, $(M\bullet O_2)^-$, does not have significantly high relative intensity as to provide a reliable estimate of the equilibrium constants, K_4 and K_5.

In Figure 3-9, a PHPMS experiment using azulene as the low EA compound is shown. Azulene also has a somewhat greater EA of 0.69 eV [98] and, in addition, is known to have an usually large entropy of negative ionization. $\Delta S^o_{ni} = 4.5$ cal K^{-1} mol^{-1} [98] which contributes about 0.08 eV additional free energy to its negative ionization at 50°C (as described in the previous sections on thermal electron detachment and statistical mechanics, this entropy term is not ΔS_{rxn}, it is strictly the entropy difference of the neutral molecule and its anion, or $S^0_{anion} - S^0_{neutral} = \Delta S^o_{ni}$). These experimental conditions

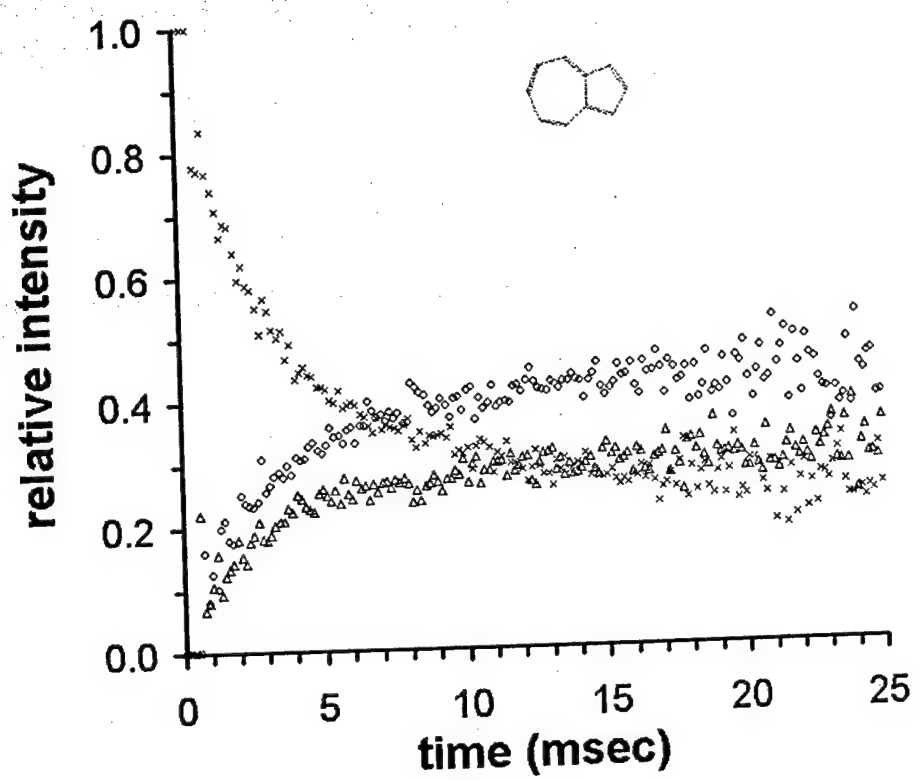

Figure 3-9. PHPMS measurements of the relative intensities of the major ions, M^- (x), $(M•O_2)^-$ (★) $(O_2•H_2O)^-$ (Δ), and $(O_2•(H_2O)_2)^-$ (o), observed as a function of time after the e-beam pulse with 4.8 mTorr oxygen, 4.0 mTorr water and 0.040 mTorr azulene present in the ion source. The total methane buffer gas pressure is 3.0 Torr and the ion source temperature is 50°C.

included very high concentrations of both oxygen and water. As a result, $(O_2•H_2O)^-$ ions were formed much more slowly than for they were for all four compounds of lower EA previously considered. After the 40-ms period of this experiment, a terminal steady-state condition was being approached but has not yet clearly been achieved. It is also noted that similar to the quinoxaline experiments, the adduct ion, $(M•O_2)^-$, does not have significant relative abundance. The fact that O_2^- is not observed is again expected due to

the higher EA and the ΔS°_{ni} of azulene, which shifts the equilibrium position of Reaction 3-2 far to the left. As with the other molecules previously considered, the time dependence of the ion intensities observed for azulene could not be explained in terms of Model A. Due primarily to the exceedingly small magnitude of k_2 (about 3×10^{-14} cm^3 s^{-1}) for this case, Model A predicts that the terminal state would take almost a full second to reach. Therefore, Model B may be required to explain the reaction dynamics associated with azulene. For this case, the rate constants for Reactions 3-4 and 3-5 again could not be individually estimated because the intermediate ion, $(M \bullet O_2)^-$, did not have significant relative intensity. The results shown here for azulene differ significantly from all of those previously considered here in that even though very high oxygen and water concentrations were used and the faster reaction dynamics of Model B were considered operative, the conversion of M^- ions to $(O_2 \bullet H_2O)^-$ ions proceeded too slowly to bring these reactions into equilibrium within the time of the experiment. These observations explains why in past studies of the electron capture reactions of low EA compounds in buffer gases of one atmospheric pressure containing trace levels of oxygen and water, the molecular anion of azulene has been easy to observe while those of compounds having slightly lower EA's have not been.

Determination of Electron Affinities

It has been shown above that the molecular anions, M^-, initially formed by resonance electron capture reactions and the $(O_2 \bullet H_2O)^-$ ions formed by subsequent reactions of M^- with oxygen and water can be brought into chemical equilibrium within

the time scale of the PHPMS experiments. The dominant processes by which this occurs has been shown to be Reactions 3-4 and Reaction 3-5 (Model B). Therefore, an overall expression for the equilibrium condition can be written by combining Reactions 3-4 and 3-5 as shown by Reaction 3-6 below:

$$M^- + O_2 + H_2O \rightleftharpoons (O_2 \bullet H_2O)^- + M \qquad (3\text{-}6)$$

Equilibrium constants K_6 (atm^{-1}) for this overall process can then be obtained from the PHPMS measurements and Equation 3-7:

$$K_6 = I_{O2\text{-}(H2O)} P_M / I_{M^-} P_{O2} P_{H2O} \qquad (3\text{-}7)$$

where I_i is the relative intensity of the ion, *i*, after equilibrium has been achieved and P_j is the partial pressure of the substance, *j*, within the ion source in units of atmospheres. An expression for the free energy change of Reaction 3-6, ΔG°_6, can be written in terms of the single step reactions in either candidate mechanism, Model A or Model B. Therefore, ΔG°_6 will be given by: $\Delta G^\circ_6 = \Delta G^\circ_2 + \Delta G^\circ_3$. For those cases except azulene where the ΔS°_{ni} of M is of negligible magnitude, ΔG°_2 will be well-approximated by the difference in electron affinities of oxygen and M; i.e., $\Delta G^\circ_2 = EA_M - EA_{O2}$. Since ΔG°_3 is known to be -11.9 kcal mol^{-1} (-0.52 eV) at 50°C [97] and EA_{O2} is known to be 0.45 eV [94, 95] the electron affinity of the low-EA compound can be determined from the PHPMS measurements of the equilibrium constant, K_6, and Equation 3-8:

$$EA_M = EA_{O2} - \Delta G^\circ_3 - RT \ln K_6 \qquad (3\text{-}8)$$

In Figure 3-10, the EA_M values determined in this way are shown for all four of the low-

EA compounds for which a state of chemical equilibrium was achieved within the time scale of the PHPMS experiments. For each compound, many determinations of this kind

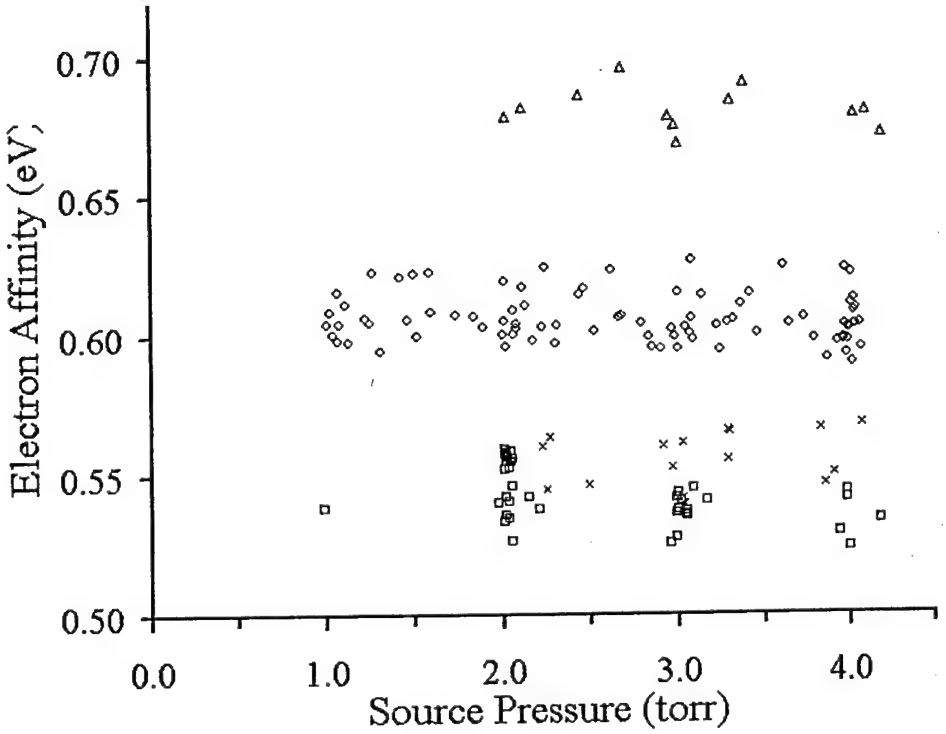

Figure 3-10. Electron affinity determinations for anthracene (□), benzophenone (o), quinoxaline (Δ), and quinazoline (x) by the PHPMS method described here. The individual measurements shown where obtained at 50° C using a variety of different reagent concentrations and total ion source pressures between 1 and 4 Torr.

were made using different combinations of concentrations for oxygen, water and the low EA compound. In addition, the total ion source pressure was also varied over the range from 1 to 4 Torr. As can be seen in Figure 3-10, the EA values thereby determined where relatively independent of these changes in experimental conditions.

EA values were determined for each molecule from the average of these measurements. These values of 0.54, 0.56, 0.61 and 0.68 eV for anthracene, quinazoline, benzophenone and quinoxaline, respectively, are shown to be in reasonably good agreement of the literature values (anthracene [99, 100],quinazoline [101], benzophenone [93, 94, 102],quinoxaline [101]).

The method of EA determination for low-EA compounds just described offers an advantage over the usual PHPMS method for EA determinations in which the equilibrium position of the electron transfer reaction of the compound of interest is measured against another compound of known and similar EA[93]. In such measurements, it is often difficult to arrange the concentration ratios so that significant ion intensities are observed for both molecular anions (as in the case of Reaction 3-2 in the present study). With the present method and the simultaneous use of two reference compounds, oxygen and water, a given change of the concentrations of both oxygen and water results in a much greater change in the ion intensity ratio, $I_{O2\text{-}(H2O)}/I_{M^-}$ (for example, lowering the concentrations of O_2 and H_2O by one order of magnitude causes an increase in the ion intensity ratio of two orders of magnitude). In addition, with use of the conventional method based on paired low EA compounds, the ubiquitous presence of trace oxygen and water in common buffer gas supplies give rise to the fast reactions described here which, of course, constitute unwanted side reactions in the conventional method.

Conclusions

In this study, we have discovered why molecular anions, M^-, for many low EA compounds, M, are not readily observed in electron capture ion sources operating under buffer gas conditions of near ambient conditions of pressure and temperature. This is because these molecular anions react rapidly with trace levels of oxygen and water to form the ion, $(O_2 \bullet H_2O)^-$. It has been shown that the conversion of M^- to $(O_2 \bullet H_2O)^-$ ions proceeds by way of a two-step mechanism in which the an intermediate ion complex of the type, $(M \bullet O_2)^-$, is first formed by the reaction of M^- with oxygen. Because forward and reverse rate constants for both of the elementary steps in this mechanism are relatively large, a state of chemical equilibrium is readily achieved for the overall process and this provides a convenient means for determining the electron affinities of the low EA compounds. By this method, the electron affinities of anthracene, quinazoline, benzophenone and quinoxaline are shown here to be equal to 0.54, 0.56, 0.61 and 0.68 eV, respectively.

REFERENCES CITED

REFERENCES CITED

1.Wolpert, L. and A. Richards, *Passionate minds : the inner world of scientists.* 1997, Oxford ; New York: Oxford University Press. vi, 240 p.

2. Horning, E.C., et al., *Electron capture : theory and practice in chromatography.* Journal of chromatography library, ed. A. Zlatkis, Poole, C. F. Vol. 20. 1981, Amsterdam ; New York: Elsevier Scientific Pub. Co. xii, 429.

3. Carson, R., *Silent spring*. 40th anniversary ed. 2002, Boston: Houghton Mifflin. xix, 378 p.

4. Christophorou, L.G., *Electron-molecule interactions and their applications.* 1984, New York: Academic Press.

5. *Gas Lasers*, in *Applied atomic collision physics Pure and applied physics; v. 43*, H.S.W. Massey, E.W. McDaniel, and B. Bederson, Editors. 1982, Academic Press: New York.

6. Manos, D.M. and D.L. Flamm, *Plasma etching : an introduction.* Plasma -- materials interactions. 1989, Boston: Academic Press. xii, 476 p.

7. Wayne, R.P., *Chemistry of atmospheres : an introduction to the chemistry of the atmospheres of earth, the planets, and their satellites.* 3rd ed. 2000, Oxford [England] ; New York: Oxford University Press. xxix, 775 p.

8. Kebarle, P., *Pulsed High Pressure Mass Spectrometer*, in *Techniques for the Study of Ion Molecule Reactions*, J.F.a.W.S. Jr., Editor. 1989, CRC Press: Boca Raton. p. 221-286.

9. Williamson, D.H., W.B. Knighton, and E.P. Grimsrud, *Effect of buffer gas alterations on the thermal electron attachment and detachment reactions of azulene by pulsed high pressure mass spectrometry.* International Journal of Mass Spectrometry, 2000. 196: p. 481-489.

10. Munson, M.S. and F.H. Field, *Chemical Ionization Mass Spectrometry.* Journal of the American Chemical Society, 1966. 88(12): p. 2621-30.

11. McDaniel, E.W. and E.A. Mason, *The mobility and diffusion of ions in gases.* 1973, New York,: Wiley. xi, 372 p.

12. Mason, E.A., *Ion mobility: its role in plasma chromatography*, in *Plasma chromatography*, T.W. Carr, Editor. 1984, Plenum Press: New York. p. 43-93.

13. Kregel, M.D., *Diffusion in Decaying Plasmas.* Journal of Applied Physics, 1970. 41(5): p. 1978-&.

14. McDaniel, E.W., *Collision phenomena in ionized gases.* Wiley series in plasma physics. 1964, New York,: Wiley. xxii, 775 p.

15. Fanklin, R.N., *Electronegative plasmas -- why are they so different?* Plasma Sources Science & Technology, 2002. 11(A): p. A31-A37.

16. Biondi, M.A., *Dissociate attachment of electrons in iodine. I. Microwave determination of the absolute cross section at 300K.* Physical Review, 1959. 109(6): p. 2005.

17. Miller, T.M., et al., *Observation of Thermal Electron Detachment from Cyclo-C_4F_8- in Falp Experiments.* International Journal of Mass Spectrometry and Ion Processes, 1994. 135(2-3): p. 195-205.

18. Rogoff, G.L., *Ambipolar Diffusion-Coefficients for Discharges in Attaching Gases.* Journal of Physics D-Applied Physics, 1985. 18(8): p. 1533-1545.

19. Lineberger, W.C. and L.J. Puckett, *Positive ions in nitric oxide afterglows.* Physical Review, 1969. 186(1): p. 116.

20. Knighton, W.B., et al., *Resonance Electron-Capture Rate Constants for Substituted Nitrobenzenes.* Journal of Physical Chemistry, 1994. 98(14): p. 3770-3776.

21. Vogt, E., Wannier, G.H., Physical Review, 1954. 95: p. 1190.

22. Dunning, F.B., *Electron-Molecule Collisions at Very-Low Electron Energies.* Journal of Physics B-Atomic Molecular and Optical Physics, 1995. 28(9): p. 1645-1672.

23. Klots, C.E., *Rate constants for unimolecular decomposition at threshhold.* Chemical Physics Letters, 1976. 38(1): p. 61.

24. Compton, R.N., et al., *Nondissociative electron capture in complex molecules and negative ion lifetimes.* The Journal of Chemical Physics, 1966. 45(12): p. 4634.

25. Hahndorf, I. and E. Illenberger, *Temperature dependence of electron attachment processes.* International Journal of Mass Spectrometry, 1997. 167/168: p. 87.

26. Christophorou, L.G. and J.K. Olthoff, *Electron interactions with SF_6.* Journal of Physical Chemistry Reference Data, 2000. 29(3): p. 267.

27. Takayanagi, K., *Introduction to electron-molecule collisions*, in *Electron-Molecule Collisions*, K. Takayanagi and I. Shimamura, Editors. 1984, Plenum: New York. p. 1-80.

28. Barsotti, S., M.W. Ruf, and H. Hotop, *Clear experimental evidence for p-wave attachment- Threshhold behavior in electron attachment to chlorine molecules.* Physical Review Letters, 2002. 89(8): p. 08201-1.

29. Reddish, T., *Electron and photoelectron spectroscopy*, in *Unpublished Class Notes Windsor University.*

30. Thoss, M. and W. Domcke, *Theory of vibrational relaxation processes in resonant collisions of low energy electrons with large molecules.* Journal of Chemical Physics, 1998. 109(16): p. 6577.

31. Dessent, C.E.H., J. Kim, and M.A. Johnson, *Spectroscopic observation of vibrational Feshbach resonances in near-threshold photoexcitation of X dot CH_3NO_2 (X- = I^- and Br^-).* Faraday Discussions, 2000(115): p. 395-406.

32. Leber, E., et al., *Vibrational Feshbach resonances in electron attachment to nitrous oxide clusters: decay inter heterogenous and homogeneous cluster anions.* Chemical Physics Letters, 2000. 325: p. 345.

33. Leber, E., et al., *Vibrational Feshbach resonances in electron attachment to carbon dioxide clusters.* European Physical Journal D, 2000. 12(1): p. 125-131.

34. Tulej, M., et al., *Feshbach states of the propadienylidene anion H_2CCC^-.* Physical Chemistry Chemical Physics, 2001. 3: p. 4674.

35. Miller, T.M., et al., *Electron attachment to SF_5CF_3 (296-563 K) and calculations of the neutral and anion thermochemistry.* Journal of Chemical Physics, 2002. 116(14): p. 6021-6027.

36. Miller, T.M., et al., *Electron attachment to PCl3 and POCl3, 296-552 K.* Journal of Chemical Physics, 1998. 109(2): p. 578-584.

37. Miller, T.M., et al., *Thermal Electron-Attachment to SF_4 and SF_6.* Journal of Chemical Physics, 1994. 100(12): p. 8841-8848.

38. Suess, L., R. Parathasarathy, and F.B. Dunning, *Nondissociative low energy electron attachment to SF_6, C_6F_6, $C_{10}F_8$, and c-C_7F_{14}: Negative ion lifetimes.* Journal of Chemical Physics, 2002. 117(24): p. 11222.

39. Michaud, M., M. Lepage, and L. Sanche, *Lifetime of negative ion resonances and the density of free electron states: O_2 isolated in an argon matrix.* Physical Review Letters, 1998. 81(13): p. 2807.

40. Naff, W.T. and C.D. Cooper, *Transient negative-ion states in alicyclic and aromatic fluorocarbon molecules.* The Journal of Chemical Physics, 1968. 49(6): p. 2784.

41. Klots, C.E., *Statistical aspects of autoinization lifetimes.* The Journal of Chemical Physics, 1967. 46(3): p. 1197.

42. Hadijiantoniou, A., L.G. Christophorou, and J.G. Carter, *Long-lived parent negative ions formed via nuclear-excited Feshbach resonances. Part 1-Benzene derivatives.* Journal of the Chemical Society. Faraday Transactions II, 1973. 69: p. 1691.

43. Hadijiantoniou, A., L.G. Christophorou, and J.G. Carter, *Long-lived parent negative ions formed via nuclear-excited Feshbach resonances. Part 2-Aromatic molecules other than benzene derivatives and non-aromatic organic structures.* Journal of the Chemical Society. Faraday Transactions II, 1973. 69: p. 1704.

44. Collins, P.M., et al., *Energy dependence of the electron attachment cross section and the transient negative ion lifetime for -benzoquinone and 1,4 -naphthoquinone.* Chemical Physical Letters, 1970. 4(10): p. 646.

45. Johnson, J.P., et al., *Long-lived parent negative ions formed via nuclear-excited Feshbach resonances. Part 4- Sytematic study of NO_2-containing benzene derivatives.* Journal of the Chemical Society. Faraday Transactions II, 1975: p. 1742.

46. Horacek, J., W. Domcke, and H. Nakamura, *Electron attachment and vibrational excitation in hydrogen iodide: calculations based on the nonlocal resonance model.* Zeitschrift, Fur Physik D, 1997. 42: p. 181.

47. Garrett, W.R., *Thermally stable negative ions of polar molecules.* Journal of Chemical Physics, 1978. 69(6): p. 2621.

48. Tobita, S., et al., *Polycyclic aromatic hydrocarbons: negative ion formation following low energy (0-15 eV) electron impact.* Chemical Physics, 1992. 161: p. 501.

49. Christophorou, L.G., A. Hadijiantoniou, and J.G. Carter, *Long-lived parent negative ions formed via nuclear-excited Feshbach resonances. Part 3-Variation of the autodetachment lifetime with incident electron energy.* Journal of the Chemical Society. Faraday Transactions II, 1973. 69: p. 1713.

50. Atkins, P.W. and J. De Paula, *Atkins' Physical chemistry.* 7th ed. 2002, Oxford ; New York: Oxford University Press. xxi, 1149 p.

51. Lindermann, F.A., et al., *Discussion on "The radiation theory of chemical action".* Transactions of the Faraday Soceity, 1922. 17: p. 598.

52. Slater, N.B., *Theory of unimolecular reactions.* 1959, Ithaca, N.Y.,: Cornell University Press. 230 p.

53. Cleve, P.T. *Les Prix Nobel.* 1992. Stockholm,: Imprimerie Royale.

54. Miller, T.M., *Detachment -- Personal Communication with Knighton,W.B.* 1999: Boston, MA.

55. Grimsrud, E.P., S. Chowdhury, and P. Kebarle, *Thermal energy electron detachment rate constants. The electron detachment from azulene$^-$ and the electron affinity of azulene.* Journal of Chemical Physics, 1985. 83(8): p. 3983-3989.

56. Van Doren, J.M., et al., *Electron Attachment to cyclo-$C_4F_4Cl_2$.* International Journal of Mass Spectrometry, 2003. Accepted but not yet published.

57. McQuarrie, D.A., *Statistical thermodynamics.* 1973, Mill Valley, Calif.: University Science Books. xi, 343 p.

58. Knighton, W.B., J.A. Bognar, and E.P. Grimsrud, *Thermal electron detachment rate constants of the molecular anion of perfluorobenzene.* Chemical Physics Letters, 1992. 192(5,6): p. 522.

59. Mock, R.S. and E.P. Grimsrud, *Thermal Electron Detachment Rate Constants for Azulene- at Atmospheric-Pressure by the Photodetachment-Modulated Electron-Capture Detector.* International Journal of Mass Spectrometry and Ion Processes, 1989. 94(3): p. 293-303.

60. Kestin, J. and J.R. Dorfman, *A course in statistical thermodynamics.* 1971, New York,: Academic Press. xv, 577 p.

61. Dow Chemical Company. Thermal Research Laboratory., *JANAF thermochemical tables.* 2d ed. 1971, Washington,: U.S. National Bureau of Standards; for sale by the Supt. of Docs., U.S. Govt. Print. Off. 1 v. (unpaged).

62. Chutjian, A., A. Garscadden, and J.M. Wadehra, *Electron Attachments to molecules at low elctron energies.* Physics Reports, 1996. 264: p. 393.

63. Fehsenfeld, F.C., *Electron Attachment to SF_6.* Journal of Chemical Physics, 1970. 53(5): p. 2000.

64. Alge, E., N.G. Adams, and D. Smith, *Rate coeffieients for the attachment reactions of electrons with c-C_7f_{14}, CH_3Br, CF_3Br, CH_2Br_2, and CH_3I determined between 200K and 600K using the FALP techniques.* Journal of Physics B - Atomic Molecular and Optical Physics, 1984. 17(18): p. 3827.

65. Alge, E., N.G. Adams, and D. Smith, *Rate coeffieients for the attachment reactions of electrons with CCl_4, CCl_3F, CCl_2F_2, $CHCl_3$, Cl_2 and SF_6 determined between 200K and 600K using the FALP techniques.* Journal of Physics B - Atomic Molecular and Optical Physics, 1984. 17: p. 461.

66. Spanel, P. and D. Smith, *Falp Studies of Electron-Attachment at Elevated Electron Temperatures - the Influence of Attachment on Electron-Energy Distributions.* International Journal of Mass Spectrometry and Ion Processes, 1993. 129: p. 193-203.

67. Smith, D. and P. Spanel, *Studies of Electron-Attachment at Thermal Energies Using the Flowing Afterglow Langmuir Probe Technique.* Advances in Atomic, Molecular, and Optical Physics, Vol 32, 1994. 32: p. 307-343.

68. Spanel, P., et al., *A coordinated flowing afterglow and crossed beam study of electron attachment to CCl3Br.* International Journal of Mass Spectrometry, 1997. 167: p. 1-12.

69. Hanstorp, D. and M. Gustafsson, *Determination of the Electron Affinity of Iodine.* Journal of Physics B, 1992: p. 1773.

70. Christophorou, L.G. and J.K. Olthoff, *Electron attachment cross sections and negative ion states of SF_6.* International Journal of Mass Spectrometry, 2001. 205(1-3): p. 27-41.

71. Smith, D., et al., *Formation of SF_5- in Electron-Attachment to SF_6 - Swarm and Beam Results Reconciled.* Chemical Physics Letters, 1995. 240(5-6): p. 481-488.

72. Culbertson, J.A. and E.P. Grimsrud, *Fates of the Molecular Anions of SF_6 and C_7F_{14} Upon Recombination with Positive-Ions.* International Journal of Mass Spectrometry and Ion Processes, 1995. 150: p. 87-98.

73. Kebarle, P. and S. Chowdhury, *Electron Affinities and Electron Transfer Reactions.* Chemical Reviews, 1987. 87: p. 513-534.

74. Grimsrud, E.P., S. Chowdhury, and P. Kebarle, *Electron-Affinity of SF_6 and Perfluoromethylcyclohexane - the Unusual Kinetics of Electron-Transfer Reactions a-+B=a+B-, Where a=SF_6 or Perfluorinated Cyclo-Alkanes.* Journal of Chemical Physics, 1985. 83(3): p. 1059-1068.

75. Neumaier, M., O. Hampe, and M.M. Kappes, *Electron Transfer Collisions of Fullerene Dianions and SF_6 in a Penning-Trap--Personal Communication with Salyards, M. J.* 2003: Bozeman, MT.

76. Salyards, M.J., W.B. Knighton, and E.P. Grimsrud, *Effects of oxygen and water on the resonance electron capture reactions of low electron affinity compounds.* International Journal of Mass Spectrometry, 2003. 222(1-3): p. 201-212.

77. Williamson, D.H., W.B. Knighton, and E.P. Grimsrud, *Lewis acid-base interactions of SiF_4 with molecular anions formed by electron capture reactions.* International Journal of Mass Spectrometry, 2001. 206(1-2): p. 53-61.

78. Stemmler, E.A. and R.A. Hites, *Electron capture negative ion mass spectra of environmental contaminants and related compounds.* 1988, New York: VCH Publishers. xvii, 390 p.

79. Sears, L.J., J.A. Campbell, and E.P. Grimsrud, *Ionization Dynamics within the High-Pressure Electron-Capture Mass-Spectrometer - the Unusual Spectra of Derivatized Polycyclic Aromatic-Amines and Perchlorinated Unsaturated-Hydrocarbons.* Biomedical and Environmental Mass Spectrometry, 1987. 14(8): p. 401-415.

80. Knighton, W.B., L.J. Sears, and E.P. Grimsrud, *High-pressure electron capture mass spectrometry.* Mass Spectrometry Reviews, 1995. 14(4-5): p. 327-343.

81. Dougherty, R.C., J. Dalton, and F.J. Biros, *Negative Chemical Ionization Mass-Spectra of Polycyclic Chlorinated Insecticides.* Organic Mass Spectrometry, 1972. 6(11): p. 1171.

82. E.C. Horning, D.I.C., I. Dzidic, R.N. Stillwell, *Electron capture : theory and practice in chromatography*, in *Journal of chromatography library ; v. 20*, C.F. Poole, Editor. 1981, Elsevier Scientific Pub. Co.: Amsterdam ; New York. p. xii, 429 p.

83. Dressler, M., *Selective gas chromatographic detectors.* Journal of chromatography library. Vol. 36. 1986, Amsterdam; New York New York, NY, U.S.A.: Elsevier; Distributors for the U.S. and Canada, Elsevier Science. xiii, 319.

84. Grimsrud, E.P., *Detectors for capillary chromatography*, in *Chemical analysis ; v. 121*, H.H. Hill and D.G. McMinn, Editors. 1992, Wiley: New York. p. xvii, 444 p.

85. Eiceman, G.A. and Z. Karpas, *Ion mobility spectrometry.* 1994, Boca Raton: CRC Press. 228 p.

86. Bruins, A.P., *Mass-Spectrometry with Ion Sources Operating at Atmospheric-Pressure.* Mass Spectrometry Reviews, 1991. 10(1): p. 53-77.

87. Giles, K. and E.P. Grimsrud, *The kinetic ion mobility mass-spectrometer - Measurements of ion molecule reaction rate constants at atmospheric pressure.* Journal of Physical Chemistry, 1992. 96(16): p. 6680-6687.

88. Knighton, W.B., J.A. Bognar, and E.P. Grimsrud, *Reactions of Selected Molecular Anions with Oxygen.* Journal of Mass Spectrometry, 1995. 30(4): p. 557-562.

89. Knighton, W.B., D.R. Zook, and E.P. Grimsrud, *Cluster-assisted decomposition reaction of the molecular anions of SF_6 and C_7F_{14}.* Journal of the American Society for Mass Spectrometry, 1990. 1(5): p. 372-381.

90. Sahlstrom, K.E., W.B. Knighton, and E.P. Grimsrud, *Thermal electron detachment of the molecular anion of azulene at elevated pressures by ion mobility spectrometry.* International Journal of Mass Spectrometry, 1998. 180: p. 117-127.

91. Knighton, W.B. and E.P. Grimsrud, *Gas-phase electron-transfer reactions between selected molecular anions and halogenated methanes.* Journal of the American Chemical Society, 1992. v114(n7): p. p2336(7).

92. Chanin, L.M., Phelps, A.V., Biondi, M.B., *Measurement of resonance electron capture rates constants for oxygen.* Physical Review, 1962. 128: p. 219.

93. Grimsrud, E.P., et al., *Electron-Affinities from Electron-Transfer Equilibria - a-+B=a+B-.* Journal of the American Chemical Society, 1985. 107(16): p. 4627-4634.

94. Chen, E.C.M. and W.E. Wentworth, *Determination of Molecular Electron-Affinities Using the Electron-Capture Detector in the Pulse Sampling Mode at Steady-State.* Journal of Physical Chemistry, 1983. 87(1): p. 45-49.

95. Travers, M.J., D.C. Cowles, and G.B. Ellison, *Reinvestigation of the electron affinities of O_2 an NO.* Chemical Physics Letters, 1989. 165(5): p. 449.

96. Payzant, J.D. and P. Kebarle, *Kinetics of Reactions leading to $O_2^-(H_2O)$ In Moist Oxygen.* Journal of Chemical Physics, 1972. 56((7)): p. 3482.

97. Arsahdi, M. and P. Kebarle, *Hydration of OH^- and O_2^- in gas phase - Comparative solvation of OH^- by water and hydrogen halides- Effects of acidity.* Journal of Physical Chemistry, 1970. 74(7): p. 1483.

98. Chowdhury, S., et al., *Entropy Changes and Electron-Affinities from Gas-Phase Electron-Transfer Equilibria - a-+B=a+B-.* Journal of Physical Chemistry, 1986. 90(12): p. 2747-2752.

99. Heins, T., Chowdhury, S., Kebarle P., *Electron-affinities of napthalene, anthracene and substituted napthalenes and anthracenes.* Organic Mass Spectrometry, 1993. 28(4): p. 358-365.

100. Schiedt, J. and R. Weinkauf, *Photodetachment photoelectron spectroscopy of mass selected anions: Anthracene and the anthracene-H2O cluster.* Chemical Physics Letters, 1997. 266(1-2): p. 201-205.

101. Dillow, G.W. and P. Kebarle, *Electron-affinities of aza-substituted polycyclic aromatic-hydrocarbons.* Canadian Journal Of Chemistry-Revue Canadienne De Chimie, 1989. 67(10): p. 1628-1631.

102. Huh, C., et al., *Thermodynamic stabilities and resonance demand of aromatic radical anions in the gas phase.* Bulletin Of The Chemical Society Of Japan, 1999. 72(5): p. 1083-1091.

APPENDICIES

APPENDIX A

HIGH PRESSURE LIMIT EQUATIONS

From Reaction 1-7:

$$M + e^- \underset{k_{-1}}{\overset{k_1}{\rightleftharpoons}} M^{*-} \underset{k_{-2}[B]}{\overset{k_2[B]}{\rightleftharpoons}} M^-$$

$$\frac{d[M]}{dt} = k_{-1}[M^{*-}] - k_1[M][e^-]$$

$$\frac{d[M^{*-}]}{dt} = k_1[M][e^-] + k_{-2}[B][M^-] - k_{-1}[M^{*-}] - k_2[B][M^{*-}]$$

Steady state assumption: $\frac{d[M^{*-}]}{dt} = 0$

$$[M^{*-}] = \frac{k_1[M][e^-] + k_{-2}[B][M^-]}{k_{-1} + k_2[B]}$$

Substitute in $[M^{*-}]$

$$\frac{d[M]}{dt} = \frac{k_{-1}k_1[M][e^-] + k_{-1}k_{-2}[B][M^-]}{k_{-1} + k_2[B]} - k_1[M][e^-]$$

Common denominator and related algebra follows.

$$\frac{d[M]}{dt} = \frac{k_{-1}k_1[M][e^-] + k_{-1}k_{-2}[B][M^-] - k_{-1}k_1[M][e^-] - k_2[B]k_1[M][e^-]}{k_{-1} + k_2[B]}$$

$$\frac{d[M]}{dt} = \frac{k_{-1}k_{-2}[B][M^-] - k_2[B]k_1[M][e^-]}{k_{-1} + k_2[B]}$$

Let the pressure of B be infinitely high for the high pressure limit

$$\lim_{[B]\to\infty} \frac{k_{-1}k_{-2}[B][M^-] - k_2[B]k_1[M][e^-]}{k_{-1} + k_2[B]} = \frac{k_{-1}k_{-2}[M^-] - k_2k_1[M][e^-]}{k_2}$$

So, in the high pressure limit:

$$\frac{d[M]}{dt} = -k_1[M][e^-] + k_{-1}\frac{k_{-2}}{k_2}[M^-]$$

From the simplest Reaction 1-1:

$$M + e^- \underset{k_{det}}{\overset{k_{ec}}{\rightleftharpoons}} M^-$$

$$k_{ec} = k_1$$

$$k_{\text{det}} = k_{-1}\frac{k_{-2}}{k_2}$$

where k_1 is a function of σ_{cap}, the electron capture cross section, and $\frac{k_{-2}}{k_2}$ is a Maxwell-Boltzman function of temperature. It does not matter if the initial rate equation is written in terms of [M$^-$] instead [M]; the final relationships are unchanged.

APPENDIX B

REVIEW OF PSUEDO 1ST ORDER KINETICS

$$\frac{d[BP^-]}{dt} = k_{trans}[SF_6][BP^-]$$

$$k_{trans}[SF_6] = k'$$

$$\int \frac{1}{[BP^-]} dBP^- = \int k'[SF_6]dt$$

$$\frac{\Delta ln[BP^-]}{\Delta t} = k'$$

$$k_{trans} = \frac{k'}{[SF_6]}$$

APPENDIX C

MODELING WITH DIFFERENTIAL EQUATIONS

$$\frac{d[M^-]}{dt} = k_{ec}[M][e^-] - k_{\det}[M^-] - k_{diff}[M^-] - k_{col}[X][M^-]$$

$$\frac{d[e^-]}{dt} = k_{\det}[M^-] - k_{ec}[M][e^-] - k_{ediff}[e^-] - k_a[SF_6][e^-]$$

where k_{ec} is the electron capture rate constant for M, k_{det} is the thermal detachment rate constant, k_{diff} is the diffusion rate constant, k_{col} is the Langevan collisional rate constant $\approx$ 2.0×10^{-9} cc sec^{-1}, X is the concentration of any electron transferring impurities, k_{ediff} is the elctron diffusion rate constant, and k_a is the electron capture rate constant for SF_6.

We assume that $[e^-]$ is steady state so $\frac{d[e^-]}{dt} = 0$ and can solve for $[e^-]$

$$[e^-] = \frac{k_{\det}[M^-]}{k_{ec}[M] + k_{ediff} + k_a[SF_6]}$$

Substitute in for $[e^-]$:

$$\frac{d[M^-]}{dt} = k_{ec}[M]\left(\frac{k_{\det}[M^-]}{k_{ec}[M] + k_{ediff} + k_a[SF_6]}\right) - k_{\det}[M^-] - k_{diff}[M^-] - k_{col}[X][M^-]$$

Collect terms:

$$\frac{d[M^-]}{dt} = [M^-]\left(\frac{k_{ec}k_{\det}[M]}{k_{ec}[M] + k_{ediff} + k_a[SF_6]} - k_{\det} - k_{diff} - k_{col}[X] \right)$$

Separate variables and integrate:

$$\int_0^t \frac{1}{[M^-]} d[M^-] = \int_0^t \frac{k_{ec}k_{det}[M]}{k_{ec}[M] + k_{ediff} + k_a[SF_6]} - k_{det} - k_{diff} - k_{col}[X]dt$$

$$ln[M^-]_t = \left(\frac{k_{ec}k_{det}[M]}{k_{ec}[M] + k_{ediff} + k_a[SF_6]} - k_{det} - k_{diff} - k_{col}[X] \right) t + ln[M^-]_0$$

Assume electron diffusion is not happening and no impurities are present (i.e. $k_{ediff} = 0$, and $[X] = 0$).

$$\frac{\Delta ln[M^-]}{\Delta t} + k_{diff} = \frac{k_{det}k_{ec}[M]}{k_{ec}[M] + k_a[SF_6]} - k_{det}$$

Common denominator and related algebra:

$$\frac{\Delta ln[M^-]}{\Delta t} + k_{diff} = \frac{-k_{det}k_a[SF_6]}{k_{ec}[M] + k_a[SF_6]}$$

Invert both sides:

$$\left(\frac{\Delta ln[M^-]}{\Delta t} + k_{diff} \right)^{-1} = -\frac{k_{ec}[M] + k_a[SF_6]}{k_{det}k_a[SF_6]}$$

Rearrange by dividing each term on the right side by k_{ec}:

$$\left(\frac{\Delta ln[M^-]}{\Delta t} + k_{diff} \right)^{-1} = -\frac{[M] + \frac{k_a}{k_{ec}}[SF_6]}{\frac{k_{det}k_a}{k_{ec}}[SF_6]}$$

Rearrange into a linear equation:

$$-\left(\frac{\Delta ln[M^-]}{\Delta t} + k_{diff} \right)^{-1} = \left(\frac{k_{det}k_a}{k_{ec}} \right)\left(\frac{[M]}{[SF_6]} \right) + \frac{1}{k_{det}}$$

$$y = mx + b$$